The Role Of The Periaxonal Space In Sustained Impulse Conduction

A thesis submitted for the degree of Doctor of Philosophy at University College London

João **Diogo** Geada **Trigo** Calheiros de Figueiredo

Department of Neuroinflammation,

The Institute of Neurology,

UCL

2013

Disclaimer

I, João Diogo Geada Trigo Calheiros de Figueiredo, confirm that the work presented in this thesis is my own, except for the processing of the tissue to be imaged under bright-field and electron microscope (including resin embedding, staining and cutting), which was performed by Dr. Daniel Morrison.

Where information has been derived from other sources, I confirm that this has been indicated in the thesis.

Abstract

The axonal ability to sustain impulse conduction highlights the mystery regarding the return pathway of sodium ions after entering the axoplasm, as the axolemmal sodium pump must extrude these ions into the periaxonal space, rather than returning them to the nodal gap. We have explored the pathway taken by these ions using *in vivo* confocal microscopy to observe axons during sustained impulse activity.

Mice transgenically expressing yellow fluorescent protein in some axons were stimulated electrically at physiological frequencies or pharmacologically while observing their axonal structure by confocal imaging. A series of morphological changes ensued, starting with an expansion of the periaxonal space, separating the axolemma from the Schwann cell and compressing the axoplasm. The increase in axoplasmic pressure caused an inflation of the axonal morphology at the paranodes and a herniation of the enclosed axoplasm on either side of the nodal membrane, directed back over the outside of the axon, displacing the paranodes and widening the nodal gap. Concurrently, the fluid in the expanded periaxonal space accumulated into droplets that travelled to the paranode where they escaped by apparently parting the axolemmal attachment of the paranodal loops of myelin. These alterations occurred in virtually all axons, and none occurred in axons treated with sodium channel or sodium pump inhibitors. All these changes reversed spontaneously, and impulse conduction continued throughout.

We conclude that the sodium ions entering the axon during impulse activity are pumped into the periaxonal space that swells osmotically, compressing the axon. This causes an inflation of the axon at the paranodes and an axoplasmic extrusion. The sodium rich periaxonal fluid then escapes to the extracellular space through the nodal gap. These changes appear to highlight an overlooked part of the normal physiological repertoire of nerve fibres, revealing the pathway taken by sodium ions during sustained impulse conduction.

Acknowledgments

A lot of people have directly or indirectly contributed to the elaboration of this thesis and should be acknowledged. First of all I would like to thank my supervisor, Prof. Ken Smith, for taking me in as a student. He helped me to design my project and provided me with the tools required to tackle it, offering me his valued guidance on the direction of my studies. I also thank him for all the knowledge that he shared with me, allowing me to grow greatly as a scientist.

I would like to thank Dr. Andrew Davies, first for all the help with electrophysiology, and secondly for all the friendship, support, advice and helping hand that he always offered; Dr. Angelina Mosley and Dr. Maria Sajic for teaching me how to use the confocal microscope; Dr. Daniel Morrison and Dr. Roshni Desai for all the advice and friendship; all the present and former staff and students in the laboratory for their kind support and valuable input.

I would also like to thank the GABBA Program for providing me with this opportunity, and Catarina Carona for all her guidance and help with the bureaucracy. I would specially like to thank the 12th edition of the GABBA Program, namely André, António, Bernardo and Bruno, for all those late night *douradinho* research updates.

To my parents and siblings, for all that they have taught me, for all the support and for being present at all the important moments. To Joana, for

having dealt with the toughest years of our life and still having been able to help and encourage me to get to where I am now.

Table of contents

List of figures

1 Introduction

2 *In vivo* evoked stimulation

3 Modulation of nerve stimulation: a chemical approach

4 Mitochondria and axonal ionic homeostasis

1 Introduction

1.1 The myelinated axon

Myelin was first described over 100 years ago by Ramón y Cajal and it is now known to be a multi-lamellar structure that surrounds axons, functioning to increase internodal resistance and to decrease internodal capacitance (Hodgkin and Huxley, 1952, a). These electrical considerations allow for rapid, saltatory nerve conduction, by restricting sodium currents to nodes of Ranvier and reducing the loss of internodal current. The myelinating role is performed by Schwann cells in the peripheral nervous system (PNS), and by oligodendrocytes in the central nervous system (CNS). In both locations the myelin has a similar function and structure, consisting mostly of compact sheaths of myelin membrane (Robertson, 1959, Williams and Hall, 1970), but following different scheme of myelination in each situation.

In the PNS, the myelinating Schwann cells are highly differentiated and polarized cells that establishing-to-one association with the axon. Each Schwann cell defines a single internode, so that there is one Schwann cell nucleus per internode. It is the association with the axon that upregulates the expression of myelin-related genes in undifferentiated pre-myelinating Schwann cells (Martini, et al. 1994). In contrast to the CNS, a well-defined basal lamina is present outside of the myelinating Schwann cell, apposed to its abaxonal surface, whilst the glial adaxonal membrane is connected to the axolemma (Bunge, et al. 1986). The basal lamina contains the B1 and B2 laminin chains (Ehrig, et al. 1990, Sanes, et al. 1990), fibronectin, type IV collagen, entactinhidogen (Lorimier, et al. 1992), and the proteoglycans N-

syndecan and glypican (Tona, et al. 1993). The positioning of the Schwann cell between the basal lamina and the axon is the first step of the myelinating process, providing spatial cues for the establishment of polarity(Wood, et al. 1990, Court, et al. 2006). Apical-basolateral polarity is initiated at the onset of myelination by recruitment of the complex Par-3, a component of the Par polarity complex, for the inner glial membrane adjacent to the axon(Chan, et al. 2006). Cell adhesion molecules of the nectin-like family further mediate the connection of glial membrane to the axolemma(Spiegel, et al. 2007, Maurel, et al. 2007). This association is accompanied by the downregulation of some cell adhesion molecules, such as the L1 adhesion molecule, highly expressed during the initial stages of Schwann cell ensheathing (Martini, et al. 1994), and upregulation of others, such as the myelin-associated glycoprotein (MAG) (Martini and Schachner, 1986). Part of this myelinating phenotype is regulated by the axon, as its signals drive glial organizational and molecular transitions(Jessen andMirsky 2002). The loosely spiralled glial membranes are then compacted, extruding the Schwann cell cytoplasm from the myelin layers (except at the edges of the myelin sheath), resulting in a multilamellar organization centred on the axon (Bunge, et al. 1989).

In the CNS, unlike Schwann cells, each oligodendrocyte spreads a large network of branching processes (Kirby, et al. 2006)that myelinate several internodes, almost invariably on different axons(Butt and Berry, 2000). Oligodendrocyte precursors originally migrate from the neural crest as oligodendrocyte progenitor cells (OPCs) into the future white matter, where they will initiate the myelinating process(Colognato and ffrench-Constant 2004).

Despite these differences, the axonal membranes of the PNS and CNS are similarly organized. Both cases require a continuous myelinating route along the axolemma, expanding and specializing both longitudinally and radially as development proceeds (Salzer 2003). The myelinating cell delivers myelin-membrane components to the axonal contact site by polarizing the glial secretory pathways for membrane transport towards the axon (Simons, et al. 2000). This intimate relationship is reciprocal, since the connection established with the myelinating cell modulates nerve fibres development, which in turn promotes the myelinating phenotype(Barres and Raff, 1999, Jessen and Mirsky, 2002), being actually necessary to maintain it (Pham and Gupta, 2009). Axonal outgrowth is also paired with gliogenesis, so that the axonal length is matched by the glial presence (Barres and Raff, 1999, Mirsky, et al. 2002). Cell-adhesion molecules, ion channels and associated cytoskeletal proteins are initially homogeneously distributed along the axon (Martini and Schachner, 1986), both in the CNS (Rasband, et al. 1999) and the PNS (Arroyo, et al. 1999). It is the interaction with the glial cells that drives the axonal polarization, namely by promoting the clustering of sodium and potassium channels at the node and juxtaparanode (Arroyo, et al. 1999, Rasband, et al. 1999). The myelinating glia is also capable of influencing axonal diameter (Aguayo, et al. 1979) and transport (de Waegh and Brady 1990, Kirkpatrick, et al. 2001).

In the mature myelinated axon, voltage-gated Na^+ and K^+ channels are clustered into distinct domains. The paranodal junction complex is the structure that separates the node, where Na^+ channels are clustered, and the juxtaparanode, where K^+ channels are clustered. This separation requires a

longitudinal polarization of the myelin segments, centred on the nodes of Ranvier: in the PNS, microvilli project from the edge of the Schwann cell, apposing the nodal axolemma (Ichimura and Ellisman 1991), while in the CNS, perinodal processes of specialized glia project to many nodes in a manner similar to the microvilli(Butt, et al. 1999). In addition to the longitudinal polarization, the myelin is also radially polarized. In the PNS, the outer abaxonal membrane expresses extracellular-matrix receptors (Previtali, et al. 2001), whereas in the adaxonal membrane the main cell adhesion molecules are the ones mediating axonal interactions (Trapp, et al. 1990). In the CNS, myelin sheaths are similarly organized, with distinct proteins present in the abaxonal and inner glial membranes (Scherer, et al. 1995).

In the PNS, the mature myelin sheath consists of various wraps of compacted Schwann cell membrane, in a number proportionate to the axon calibre (Smith, et al. 1982),surrounding a discrete portion of the axon, the internode, with a small collar of cytoplasm present in the abaxonal compartment and another one in the adaxonal compartment (Salzer 2003). The inner myelin lamella is separated from the axolemma by a minimal (circa 200 Å) space(Hirano and Dembitzer, 1969), the periaxonal space (PAS) (Shrager, et al. 1983), since adhesion molecules that mediate interactions with the axon, notably the myelin-associated glycoprotein (MAG), are especially enriched in the innermost layer of the myelin sheath (Trapp 1990).

The myelin sheath can be divided into two types, compact and non-compact. The bulk of the myelin sheath consists of compact myelin, which results from the fusion of adjacent layers of myelin plasma membrane, whereas non-

compact myelin can be found in particular locations such as the paranodes (the lateral borders of the myelin sheath, neighbouring the nodes of Ranvier), the Schmidt Lanterman incisures (Schwann cell cytoplasm not displaced from the myelin during its development) and the inner and outer edges of the myelin (Peles and Salzer, 2000).

Compact myelin in the PNS is mostly composed of lipids, cholesterol and sphingolipids such as galactocerebroside and sulfatide(Suter and Snipes, 1995), but it also has a protein content, including the usually called "P zero protein" (P_0), peripheral myelin protein 22 kDa (PMP22), and myelin basic protein (MBP). P_0 has an immunoglobulin-like domain, and is the most abundant myelin protein, its main role being myelin stabilisation (Lemke and Axel, 1985). PMP-22 has four transmembrane domains, and is essential in the maintenance of the myelinating phenotype, as point mutations cause dysmyelination (Chance and Pleasure, 1993). MBP is not a membrane protein, but a cytoplasmic protein(Davison and Cuzner, 1977) that interacts with PMP-22 (D'Urso, et al. 1999). In the CNS the principal compact myelin proteins are the proteolipid protein (PLP) and MBP (Deber and Reynolds, 1991).

P_0, PMP-22 and MBP are not found in non-compact myelin(Davison and Cuzner, 1977). Instead, in the PNS, the most abundant protein in the Schmidt Lantermann incisures and paranodes is the myelin-associated glycoprotein (MAG) (Trapp and Quarles, 1984). MAG is a transmembrane protein with five immunoglobulin-like domains, which plays a critical role in

stabilizing apposed Schwann cell membranes in the incisures and at the paranodes (Montag, et al. 1994).

1.2 The axonal domains

The internodes, as previously mentioned, correspond to the myelin segments extending from node to node, and measure approximately 100 times the axon diameter(Hess and Young, 1952). Probably due to its insulated nature, unlike other axonal locations, the internodal axonal membrane does not appear to be particularly specialized. Other than paranodal and juxtaparanodal components, such as Caspr, contactin or K_v channels (see below)spirally extending into the internode (Arroyo, et al. 1999), no proteins are known to be specifically enriched in the internode, with the exception of the sodium, potassium ATPase (sodium pump), whose location is discussed in section 1.6.

In the PNS, virtually every internode is subdivided into several cylindrico-conical segments, whose boundaries are delimited by the Schmidt-Lanterman incisures. These are conical-shaped cytoplasmic inclusions of non-compacted myelin that spiral through the myelin, providing a conduit across the myelin sheath (Scherer, et al. 1995). Differing from the longitudinal cytoplasmic microtubules normally found in the Schwann cell cytoplasm, in both the incisures and the nodes of Ranvier the microtubules are found to run circumferentially, acting as cytoskeletal components that stabilize the cytoplasmic spiral.

The Schmidt-Lanterman incisures follow a helical course analogous to that of the myelin spiralling around the axon, and they allow the Schwann cell to connect the inner and outer cytoplasmic edges of the glial cell. Electron microscopy studies (Sandri, et al. 1977), later confirmed by dye injection

studies (Balice-Gordon, et al. 1998), indicated that in the Schwann cells reflexive gap junctions connect the adjacent loops of non-compacted myelin (at incisures and paranodes). Immunohistochemical analysis of connexin distribution further suggests that the connexins Cx32 or Cx29 (Altevogt, et al. 2002)may be constituents of these gap junctions, providing a shorter diffusion pathway through the myelin sheath than that taken when spiralling down the wrapped sheath. This continuity between the inner and outer compartments of the Schwann cell cytoplasm, and between the extracellular and the periaxonal space, was shown to be accessible to ions, such as lanthanum, added to the extracellular medium (Hall and Williams, 1971). Even though these tracers were later considered not to be inert and with the potential to modify the structures of interest, a similar result was obtained when fluorescent dextrans, considered to be biologically inert, were used(Mierzwa, et al. 2010, a, Mierzwa, et al. 2010, b).

Being so, incisures may very well contribute to the transport of materials across the sheath. Additionally, the Schmidt-Lanterman incisures may grant a degree of elasticity and fortification of the nerve from mechanical stress during stretching and contraction (Singer and Bryant 1969). The same paranodal and juxtaparanodal components that are extended into the internode, such as Caspr, contactin or K_v channels, can also be found proximal to the Schmidt Lanterman incisures (Einheber, et al. 1997, Arroyo, et al. 1999, Tait, et al. 2000). Membrane-bound dense bodies and primary lysosomes are sometimes found included within the outer turns of the incisural spiral (Hall and Williams, 1970).

The nodes of Ranvier are unmyelinated gaps of about 1 μm located along the axon between each myelin segment in which the axoplasm is more exposed to the extracellular environment (Hess and Young, 1952). Ranvier originally observed a dark "cross of Ranvier" in nerves immersed in silver nitrate solution, which he considered that was due to a ring of 'cement-like' material surrounding the node. This strengthened his notion that the node was the point of contact between neighbouring Schwann cells. Nageotte, who also acknowledged the presence of strands of Schwann cell cytoplasm surrounding the node by observing the indentations between the myelin ridges, named them the "marginal protoplasmic network". By staining the fibres with acid fuchsine, he also observed the bracelet of Nageotte, a series of circular crests with curved spines surrounding the contracted portion of the axon, which he indicated as the attachment point of the myelin leaflets. It was later recognised that the 'cement-like' material was composed of fibrous protein material continuous with the Schwann cell membrane playing a role in the trafficking to and from the perinodal space(Hess and Young, 1952), and that similarly the bracelet of Nageotte corresponded to a fibrous protein constituent of the myelin (Hall and Williams, 1970).

The nodal cytoskeleton forms a dense axoplasmic undercoating (Salzer 2003), flanked on either side by the lateral edges of the myelinating glia, whose compact myelin lamellae open up into a series of cytoplasmic loops that spiral around. These glial edges enclose a belt of cytoplasm that forms a unique junction with the axon, establishing a series of tightly spiralled loops that closely appose and invaginate the axolemma. As a result, a continuous circumferential collar of cytoplasm rich with mitochondria is found adjacent to

the node (Rydmark, et al. 1998). The smooth external convexity of the terminal myelin sheath helps narrowing the perinodal space. It is in this location that the nerve fibre alters its internodal shape of a smooth-walled cylinder of stable dimensions, expanding into a paranodal bulb, before contracting at the nodal gap to a diameter considerably smaller than that of the internode, at least in larger diameter fibres (Robertson 1959).

In the PNS the Schwann cell cytoplasm extends beyond the outer border of the myelin sheath, with a system of finger-like processes projecting into the nodal space, interdigitating with their complements from the neighbouring paranode. Following changes to the environment of the fibre or to the Schwann cell-axon association, exploratory processes are protruded (Ballin and Thomas 1969). These closely appose the axon, forming a series of junctions with the axonal undercoating and its intramembranous particles (Quick and Waxman 1977). As a result, continuity is established between the Schwann cell and the axonal cytoskeleton (Ichimura and Ellisman 1991). These microvilli are structurally similar to those found on other cell types, with a diameter of 70-80 nm containing 4-6 internal filaments each, oriented inwards and ending as a regularly spaced hexagonal array (Rydmark and Berthold, 1983). Surrounding each Schwann cell and uninterrupted at the nodes of Ranvier is a continuous layer of basal lamina (Bunge, et al. 1986). The nodal gap is hence the name given to the space beneath the basal lamina between the two neighbouring Schwann cells. The neural cell adhesion molecule L1/Ng-CAM, and cytoactin/tenascin (Daniloff, et al. 1989, Mege, et al. 1992) are associated with the nodal basal laminas, where they help to stabilize the nodal structure.

Arguably, the most characteristic feature of the node is its enrichment of voltage-gated Na^+(Na_v) channels, notably $Na_{v1.6}$(Caldwell, et al. 2000), which are responsible for triggering the action potential by initiating inward current flow (discussed in more detail in section 1.3). The interaction with the extracellular matrix molecules tenascin-C, in the PNS, and tenascin-R, in the CNS, is suggested to help the segregation of Na_v channel clusters (Xiao, et al. 1999). Additionally, nodes of Ranvier contain two alternatively spliced isoforms of the Na_v binding protein ankyrin$_G$, ankyrin$_G$ 480 and 270 kDa (Kordeli, et al. 1990, Kordeli, et al. 1995), containing a membrane-binding domain, a spectrin-binding domain (Koenig and Repasky 1985), and a serine/threonine-rich domain (Zhang and Bennett 1996). These domains allow them to interact with the cytoplasmic domains of other cell-adhesion molecules such as the Nr-cell adhesion molecule Nr-Cam (Davis and Bennett, 1994, Davis, et al. 1996), and the 186 kDa isoform of Neurofascin (NF186), both members of the L1 family of CAMs. NF186 coordinates the organization and assembly of several transmembrane and cytoskeletal proteins in the nodal region (Thaxton, et al. 2011), and its genetic ablation causes paranodal and nodal disorganization (Sherman and Brophy 2005). Both NF186 and Nr-CAM interact with other CAMs on the Schwann microvilli (Davis, et al. 1996, Lambert, et al. 1997), supporting the notion of microvilli tethering to the nodal axolemma. Neurofascin and Nr-CAM are found in future nodes before the presence of ankyrin$_g$ and Na_v channels (Lambert, et al. 1997). Ankyrin$_G$ hence plays a critical role in the linking the cytoplasmic domains of neurofascin, Nr-CAM, and Na_v channels (Davis and Bennett, 1994) to the spectrin cytoskeleton.

In the CNS the node is also composed by some gangliosides and other glycoconjugates, and phosphacan (Sheikh, et al. 1999), and in both the PNS and the CNS its organelle content differs little from that of the juxtaparanode or the internode (Fabricius, et al. 1993).

As above stated, at the end of each internode the compact myelin lamellae open up into a series of cytoplasmic loops, the paranodal loops (Peles and Salzer, 2000). The paranodes are the locations where the axolemma and the membrane of the myelinating glial cell can have the closest interaction (Williams and Landon, 1963). Periodic intercellular concentrations known as transverse bands or septate-like bands (due to morphological similarities to invertebrate septate junctions) are present between each paranodal loop and the axon (Ichimura and Ellisman, 1991). Their main role is the axonal anchoring of myelin loops, which forms a lateral diffusion barrier that partially limits and controls diffusion into the periaxonal space, segregating nodal Na_v channels from juxtaparanodal voltage gated potassium (K_v) channels (Dupree, et al. 1999, Bhat, et al. 2001, Pillai, et al. 2009). The maintenance of these clusters is dependent on the myelin galactolipidsulfatide (Ishibashi, et al. 2002). The cell-adhesion molecule contactin and the axonal protein Caspr (that has the potential of binding to the actin cytoskeleton) are enriched in the paranodal axolemma (Peles, et al. 1997). These proteins form heterodimers in both the PNS (Einheber, et al. 1997) and the CNS (Rios, et al. 2000), and co-localize with an isoform of neurofascin, NF155 (Tait, et al. 2000). These dimers are thought to be components of the septate-like junctions, as their absence results in the loss of the junctions (Boyle, et al. 2001).
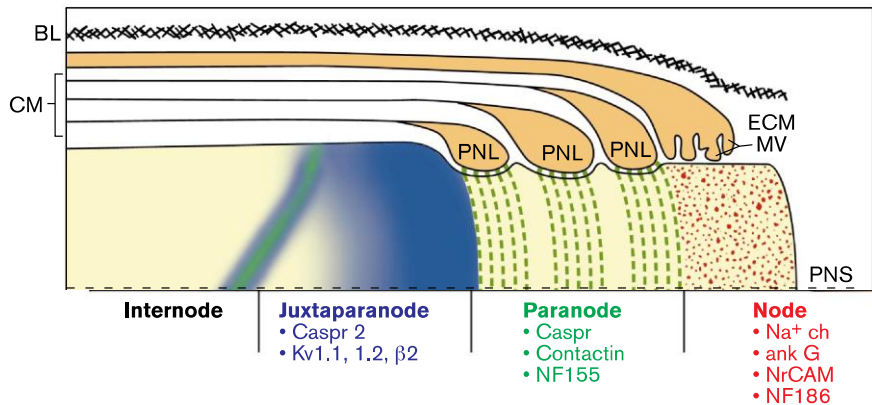
Figure 1 – Longitudinal section through the nodal region.

Schematic representation of the axon and the Schwann cell. Both cells are surrounded by a basal lamina (**BL**) and only a portion of the internode, located beneath the myelin (**CM**), is illustrated. A spiral of paranodal (green) and juxtaparanodal (blue) proteins extends into the internode. The juxtaparanodal region is enriched in Kv channels and Caspr2. At the paranode, where caspr, contactin and neurofascin 155 are found, the compact myelin opens up into a series of paranodal loops (**PNL**) that closely appose the axon. At the node of Ranvier, microvilli (**MV**) projecting from the Schwann cell contact the axolemma. The node is enriched in Na_v channels, ankyring (**ank G**) and the NrCAM and neurofascin 186 (**NF186**). Adapted (Peles and Salzer, 2000).

If the terminals of the myelin sheath flanking each node were not properly sealed to the node, part of the current generated there would take a short-circuit route under the myelin sheath, and less current would reach the next adjacent node (Rosenbluth 2009). This being said, the seal between the myelin sheath and the axolemma at the paranode is not tight, since although blocking the diffusion of larger molecules, it still provides delayed access to the periaxonal space for small molecules (Hall and Williams, 1971) and water soluble tracers (Hirano and Dembitzer, 1969, Rosenbluth, et al. 2006, Mierzwa, et al. 2010). These junctions are then likely to modulate saltatory

conduction by regulating ionic diffusion away not only from the node, but also the periaxonal space (Rosenbluth 2009). On the other hand, such a circuit would allow slow diffusion between the extracellular space and the periaxonal space to occur (Mierzwa, et al. 2010), providing a faster axonal access to water-soluble molecules such as glucose or similar metabolites, which may be harder to traffic across the myelin sheath (Rosenbluth 2009).

The columns of Schwann cytoplasm surrounding the node form a collar of cytoplasm from which finger-like protrusions project and surround the node (Quick and Waxman, 1977), providing a possible transference route for biological compounds. In some PNS nerve fibres, proximal to the nodes of Ranvier, the Schwann cell protrusions are found to form complexes of variable complexity of interdigitating axoplasm encircled by thin ridges of Schwann cell cytoplasm (Spencer and Thomas 1974, Gatzinsky, et al. 1988, Gatzinsky, et al. 1991). This complex, called the axon-Schwann cell network (ASN), is mainly located in the paranodal longitudinal crests (Gatzinsky, et al. 1988), and has been suggested to result from a dynamic interaction between the adaxonal Schwann cell cytoplasm and the axon. Furthermore, the perinuclear Schwann cell cytoplasm is rich in numerous components such as polyribosomes, microtubules and microfilaments (Kidd, et al. 1994), consistent with active biosynthetic pathways.
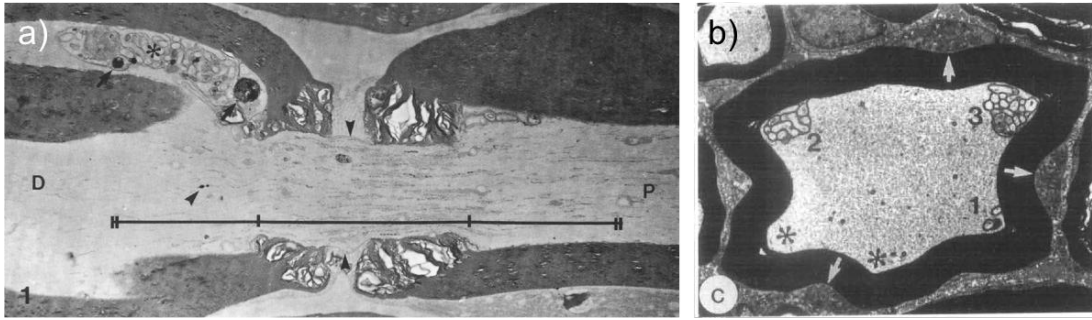
Figure 2a-b – The axon-Schwann cell network.

Longitudinal (**a**) and transverse (**b**) electron micrographs of a ventral root. Several acid-phosphatase positive bodies (an enzyme associated with lysosomes) are associated with the axon-Schwann cell network (**asterisk**, **a**). Arrows point atacid-phosphatase positive bodies associated with the network, larger than 0.2 µm in size. x 8000. Adapted (Gatzinsky and Berthold, 1990). In b, five axon crests are present 7.5 µm distal to the nodal midlevel. Of these, three show ASN complexes (denoted 1-3 according to increasing size). Asterisks indicate axon crests without ASN contents. Arrows point at mitochondrion-rich cords of Schwann cell cytoplasm occupying the myelin sheath furrows. x 5500. Adapted (Gatzinsky, et al. 1991).

Since the ASN is often enriched in vesicles, lamellar and dense inclusion bodies, lysosomes and constituents reminiscent of degenerated mitochondria (Gatzinsky, et al. 1988), the Schwann cell has been proposed to partially disintegrate and reconstruct portions of the axon (Spencer and Thomas 1974), maintaining axonal integrity by sequestrating and transporting material being degraded (Spencer and Thomas 1974, Gatzinsky, et al. 1988). The inclusion bodies could also be debris accumulated from the products of Schwann cell metabolism (Spencer and Thomas, 1974), namely the remodelling of the myelin sheath (Gatzinsky and Berthold, 1990), as they are most frequently seen in periods of myelin synthesis or regeneration (Payer 1979, Lee, et al. 2011).

In the PNS, in addition to septate-like junctions, both incisures and paranodes have tight junctions, gap junctions and adherens junctions. The gap junction protein Connexin32 is present in both the paranodes and the incisures of myelinating Schwann cells (Bergoffen, et al. 1993). Also present is the cell adhesion molecule e-cadherin, a component of adherens junctions whose suspected function is the binding of adjacent Schwann cell lamellae (Fannon, et al. 1995). Additionally, both paranodal and incisural tight and adherens junctions are associated with several cytoskeletal proteins such as spectrin and actin (Koch and Franke 1994). Also localized to the paranodes are two gangliosides, GD_{1b} and GQ_{1b}, which are believed to act as surface markers, playing a role in immunoregulation (Chiba, et al. 1993, Kusunoki, et al. 1993).

The region extending 10-15 um from the most internal paranodal junction is named the juxtaparanode, and is located under the compact myelin sheath. Its most characteristic feature is the presence of clusters of delayed rectifying K^+ channels, namely $K_{v1.1}$ and $K_{v1.2}$ (Chiu and Ritchie, 1982), that promote repolarization and help maintain the internodal resting potential (Vabnick, et al. 1999). A member of the Caspr family protein, Caspr2, is found in the juxtaparanodes, co-localized with $K_{v1.1/1.2}$ (Poliak, et al. 1999). Both $K_{v1.1/1.2}$ and Caspr2 have an intracellular domain, allowing them to complex, and Caspr2 has also been suggested to help connecting the juxtaparanodal axolemma to the glial cell membrane (Peles and Salzer, 2000).

The endoneurium is the layer of connective tissue enclosing the myelin sheath of a nerve fibre (Mizisin and Weerasuriya, 2011) that separates the

vascular space from the endoneurial space. These fibres are bundled together into groups named the nerve fascicles, enclosed by the perineurium, a protective connective tissue that separates the extracellular space from the endoneurial space(Sanes, et al. 1990). The epineurium is the name given to the outermost layer of connective tissue around the nerve (Mizisin and Weerasuriya, 2011) that both surrounds mono-fascicular nerves and loosely binds fascicles of multi-fascicular nerves together.

The specialized endoneurial microenvironment is delimited by the endothelium of endoneurial vessels and the multi-layered perineurium, within which peripheral nerve cells operate (Lorimier, et al. 1992). Homeostatic mechanisms located at the blood-nerve interface regulate the composition of the endoneurial fluid and its physical properties by controlling material exchange between the endoneurial microenvironment and the extracellular space, driven by the hydrostatic gradient (Mizisin and Weerasuriya, 2011). Due to the protective nature of this envelope, the endoneurial space, together with the central nervous system, is one of the only extracellular spaces that is under positive hydrostatic pressure and does not have lymphatic drainage (Sunderland 1946). The endoneurial fluid content of sodium, potassium and chloride is typically iso-osmotic with serum concentrations (Mizisin, et al. 1986, Mizisin, et al. 1988), and is not likely to exert an interstitial osmotic pressure (Mizisin and Weerasuriya, 2011).

1.3 Axonal ionic channels

It has long been known that ionic channels define the electrical properties of the axon, providing the membrane with voltage-dependent characteristics (Rothenberg 1950). Indeed, the crucial roles of voltage-gated sodium and potassium channels in the generation and propagation of action potentials were originally established in the squid giant axon by Hodgkin and Huxley (Hodgkin, and Huxley, 1952, b).

Voltage-gated ion channels are transmembrane ion-conducting pores that are sensitive to changes in membrane potential, opening (activating) or closing (inactivating) in response to alterations in this membrane potential (Waxman, 1995, Leibowitz, et al. 1986, Peles and Salzer, 2000). Rapidly activating and inactivating channels contribute to the depolarization of action potential, while delayed rectifiers with slower activation and inactivation influence later stages of the action potential, such as repolarization (Hodgkin and Huxley, 1952, c, Bergman 1970).

Electron microscopy studies have long suggested the presence of an exclusive cytoplasmic undercoating of the nodal axolemma, predicting its unique characteristics, compared with the rest of the axon (Peters 1966). Cytochemical findings supported the notion of structural distinctions between nodal and internodal axolemma (Quick and Waxman 1977), and associated with intra-axonal recordings (Waxman and Bennett, 1972) it was suggested that these structural distinctions corresponded to clusters of Na_v channels in the nodal axolemma (Quick and Waxman, 1977, Waxman and Quick, 1977, Waxman and Quick, 1978). Freeze-fracture studies revealed that the nodal

axolemma was indeed enriched with large particles (Rosenbluth 1976, Kristol, et al. 1978, Black, et al. 1982), suggested to correspond to clusters of Na$_v$ channels (Rosenbluth 1976). Immunocytochemical studies against Na$_v$ channels showed a similar pattern of distribution, with immunostaining at the axolemma at nodes of Ranvier and with no detectable immunoreactivity in the paranodal and internodal axolemma (Black, et al. 1989, Ritchie, et al. 1990).

Pharmacological techniques were also employed to assess the distribution of voltage gated sodium channels along the axon, using ligands that specifically bind to Na$_v$ channels. By binding saxitoxin (STX) in mammalian peripheral nerves, the Na$_v$ channel density in the nodal axolemma was suggested to be 12000/μm^2, much higher than the internodal density (<100/μm^2) (Ritchie and Rogart, 1977). This estimate assumed that the nodal axolemma, but not the myelin-coated axolemma, was accessible to externally applied STX, and that STX binding to non-neuronal cells did not occur. However, further studies demonstrated that a significant binding of STX to Na$_v$ channels in Schwann and glial cells occurs (Ritchie 1988), which led to an updating of the estimated Na$_v$ channel density at the node to 1000-2000/μm^2 (Howe and Ritchie, 1990). The density of Na$_v$ channels in non-myelinated axons is estimated to be 200/μm^2, both when measured pharmacologically (Pellegrino, et al. 1984), and when simulated to maximize conduction velocity (Hodgkin 1975).

The clustering of Na$_v$ channels at the node of Ranvier has additionally been confirmed by voltage-clamp studies. Electrophysiological studies have

indicated an average of 21000 Na_v channels per node in the rat sciatic nerve (Neumcke and Stämpfli, 1982) and a maximal density of $1500/\mu m^2$ (Chiu and Schwarz, 1987), a value concordant with that obtained with pharmacological studies (Howe and Ritchie, 1990). Na_v channel densities in the nodal axolemma are currently estimated to be 30 times the internodal axolemma density (Chiu and Schwarz, 1987).

One of the earliest theories about the mechanism of Na_v channels anchoring to the axolemma was the hypothetical action of the paranodal junction as a physical barrier, preventing channel diffusion along the axolemma (Rosenbluth 1976). However, the presence of Na_v channel clusters in transition nodes (i.e. demyelinated on one end) up to 5 months after demyelination (Shrager 1987, Shrager 1988) indicates that the Na_v channels clusters must be anchored by other mechanisms. More recently, due to the observation of the linkage of Na_v channels to cytoskeletal components (Angelides, et al. 1988, Srinivasan, et al. 1988)and the binding of the cytoplasmic domain of Na_v channels to ankyrin (Srinivasan, et al. 1988) (see above), cytoskeletal anchoring of Na_v channels has been accepted as the probable clustering mechanism (Waxman and Quick, 1978, Peles and Salzer, 2000, Rasband and Trimmer, 2001).

In myelinated axons, Na_v channels are responsible for action potential initiation at the axonal initial segment (the axonal 20-40 µm proximal to the cell body, located after the axon hillock) (Hedstrom and Rasband 2006) and the nodes of Ranvier (Vabnick, et al. 1996) and play the similar role of action potential propagation along unmyelinated axons (Waxman and Ritchie, 1993,

Goldin 2001). Ten different mammalian Na_v α-subunits ($Na_{v1.1-1.9}$ and an atypical Na_x) have been identified, and, in studies conducted with tetrodoxin (TTX), a specific Na_v channel blocker, the sub-types have been divided into TTX sensitive ($Na_{v1.1}$, $Na_{v1.2}$, $Na_{v1.3}$, $Na_{v1.4}$, $N_{av1.6}$ and $Na_{v1.7}$) and TTX resistant ($Na_{v1.5}$, $Na_{v1.8}$ and $Na_{v1.9}$) (Goldin 2001)channels. Of these, the main Na_v channels found in the nodes of Ranvier are $Na_{v1.2}$ and $Na_{v1.6}$ (Caldwell, et al. 2000, Boiko, et al. 2001).

It has been suggested that two types of sodium currents are present in the peripheral nerves. The first is a transient Na^+ current rapidly activated by membrane depolarization and then inactivated, so that further Na^+ ions can no longer pass through the channel irrespectively of how much the membrane is depolarized. This is believed to be the behaviour of about 98% of the Na^+ current (Waxman 1995, Vabnick, et al. 1996, Baker and Bostock, 1998). The second is a persistent Na^+ current, activated equally rapidly but at more negative membrane potential with minimal inactivation, which gives rise to a persistent inward flow of Na^+ ions at the resting potential (Baker and Bostock, 1998, Tokuno, et al. 2003).

Forty different mammalian α-subunits have been identified for K_v channels. These are grouped into twelve families known as K_{v1} to K_{v12} (Miller 2000, Yellen 2002, Lai and Jan 2006). The drug 4–aminopyridine (4-AP), a selective blocker of members of the K_{v1} family, has been used to study the distribution of K_v channels along the axon. Since the effect of 4-AP on action potential duration was greater in axons with incomplete myelination than in fully myelinated axons, K_{v1} channels were considered to be located in the

axolemmal regions normally located under myelin sheath (Foster, et al. 1982, Kocsis, et al. 1982, Ritchie 1982, Eng, et al. 1988). The fact that 4-AP does not affect the action potential in myelinated axons, has been interpreted as showing that myelin shields the K^+ channels in healthy fibres, with the channels only becoming exposed to 4-AP following myelin damage.

Since the blocking of exposed K^+ channels by 4-AP in incompletely myelinated axons results in a delay in action potential repolarization (Kocsis, et al. 1982), these channels were suggested to mediate repolarization. Due to their rapid activation during the rising phase of the action potential, they have hence been termed as fast potassium channels (Kocsis, et al. 1987).

Studies of paranodal disruption of ionic channels resulted in an augmented potassium conductance, but unaltered sodium conductance (Smith and Schauf, 1981). This data suggests the segregation of sodium and potassium channels, with the Na_v channels concentrated at the nodal axolemma surrounded by paranodal clusters of K^+ channels. Voltage-clamp studies also consider the density of fast K_v channels as maximal in the paranode, up to six times that of the node and internode (Roper and Schwarz 1989). Integrating the different studies, evidence strongly indicates that in the mammalian nervous system, K_{v1} and $K_{v1.2}$ channels are partly electrically isolated due to their location under the myelin sheath at juxtaparanodal regions of myelinated axons (Rosenbluth 1999).

Upon depolarization, paranodal K_v channels are activated, leading to a K^+ outflux from the axon into the juxtaparanodal periaxonal space, helping to modulate action potential propagation (Rosenbluth 1999, Vabnick, et al.

1999, Rasband and Trimmer, 2001). The segregation of many potassium channels within the juxtaparanode in myelinated fibres results in the spatial confinement of the released potassium ions during saltatory conduction, hence conserving the extracellular potassium in a local compartment, perhaps ready for transport back into the axon. Such a scheme would reduce the demand for energy to transport the potassium over longer distances, although it may increase the possibility of potassium-induced depolarization and spontaneous activity (Kapoor, et al. 1993, Rosenbluth 2009). In the absence of myelin, an increase in potassium ion concentration has been observed in the parenchyma upon raised impulse activity in myelin-deficient rats (Young, et al. 1989).

Recent studies have also described the presence of KCNQ (K_{v7}) channels in the node of Ranvier in the PNS (Devaux, et al. 2004, Lai and Jan 2006, Pan 2006). These channels coordinate with nodal Na_v channels, allowing currents that spread from one node to initiate an action potential (Schwarz, et al. 2006), acting as slow delayed rectifiers activated at sub-threshold levels and maintaining the resting potential and reducing excitability (Devaux, et al. 2004).

Summarizing, in the mammalian PNS, myelinated axons are complex structures in which the distribution of ionic channels is spatially organized. Na_v channels are found in the axonal initial segment, nodes of Ranvier and presynaptic terminals (Caldwell, et al. 2000). At the nodes of Ranvier, Na_v and KCNQ channels allow ion flow across the axolemma, allowing the travelling of the action potential from one node to the next one(Schwarz, et

al. 2006). K_{v1} channels are found at the juxtaparanodes and presynaptic terminals and increase the fidelity of the action potential at the nodes (Rosenbluth 2009).

1.4 Action potential

The action potential is a momentary polarity reversal of the membrane potential in excitable cells, such as neurons. It can propagate along axons, where it propagates from its point of initiation until it reaches the axonal terminal, and it constitutes the basic unit of information that allows communication in the nervous system (Hodgkin and Huxley, 1939). Most neurotransmission is characteristically initiated with the triggering of an action potential near the soma of the presynaptic cell and its propagation along the axon towards the presynaptic terminals, where activation of voltage-gated calcium (Ca_v) channels causes calcium influx culminating in neurotransmitter release (Olivera, et al. 1994).

In the case of myelinated axons, action potentials are not continuously propagated as waves, but instead recur at successive nodes of Ranvier (Ritchie and Rogart, 1977). At each node, the membrane potential is brought to the threshold potential to initiate an action potential, and the saltatory conduction is facilitated by the fact that whilst the axoplasm is electrically conductive, charge leakage through the axolemma is inhibited by the myelin sheath (Vizoso and Young, 1948). Being so, depolarization of one node of Ranvier is sufficient to increase the voltage at a neighbouring node, allowing for the voltage to extend spatially between sequential nodes of Ranvier.

This propagation of the action potential is monodirectional due to a temporary (a few milliseconds) inactivation of the sodium channels at the previous node of Ranvier (Hodgkin and Huxley, 1952, d). The period of time

following an action potential during which a subsequent action potential is unable to fire is thus termed the refractory period (Rushton 1951).

Once the membrane potential of the cell repolarizes, following the falling phase of the action potential, this inactivation is removed, allowing the channels to be reactivated for the next action potential (Raman and Bean, 1997). Even though the case has been made for a low resistance myelin sheath (Barrett and Barrett, 1982), the myelin is widely assumed to have very low electric capacity and very high resistance (Vizoso and Young 1948), thus shielding the internodal axolemma. The travelling of the action potential happens faster in this 'saltatory' way than it would be able to in unmyelinated axons. It was thought that 1 µm was the critical diameter above which conduction would occur more rapidly in myelinated than in non-myelinated axons (Rushton 1951), but further studies considering an internodal geometry that maximized conduction velocity have actually updated this value to 0.2 µm (Waxman and Bennett, 1972).

Unlike most electrical signals, that feature a unidirectional electron flow down a metal wire, neuronal signal conduction depends on the permeability of the axonal membrane to the ionic flow between intra- and extracellular fluids (Hodgkin and Huxley, 1952, b).

The action potential is initiated when a neuron, receiving multiple excitatory and inhibitory inputs in the somatodendritic region, integrates it in a way that triggers alterations in the membrane potential, which is the difference in electrical potential between the internal and external ion solutions (Coombs, et al. 1957, Fatt 1957, Fuortes, et al. 1957).

The resting membrane potential is indispensable for the normal functioning of the neuron and it is maintained through an uneven ionic distribution across the axolemma. Typically, in a resting condition, the membrane potential has a value of approximately -60 mV (Hodgkin and Huxley, 1939). The axolemma is permeable to several ions, meaning that the resting potential lies between the equilibrium potentials for the different ions. Energy consuming pumps, most notably the sodium, potassium ATPase (see below), maintain the equilibrium between the different ion concentrations (Skou 1957, Koester and Siegelbaum, 1991).

The action potential is normally initiated in the axonal initial segment, where voltage-gated sodium channels (Nav) are highly concentrated (Vabnick, et al. 1996), and together with certain voltage-gated potassium (Kv) channels, determine the threshold for firing an action potential (Kole, et al. 2008). The initial phase of the action potential, the depolarization period, happens in less than 1 millisecond, during which the membrane potential rises to about +30 mV (Bezanilla 2006).

The triggering of the action potential was demonstrated to require the presence of extracellular Na^+ ions (Hodgkin and Katz, 1949), suggesting that the increase in membrane conductance observed during the rising phase of the action potential was selective to these ions, and that such shift of membrane charge should produce a transient current (Hodgkin and Huxley, 1952, d). Indeed, the notion that discrete single sodium channels could produce the sodium ionic currents (Sigworth and Neher, 1980) was confirmed by patch-clamp studies (Neher and Sakmann, 1976, Hamill, et al.

1981). It is now acknowledged that the vast majority of action potentials depend on tetrodoxin-sensitive fast Na_v channels (Blair and Bean, 2003). Incomplete closing of some sodium channels can result in a persistent Na^+ current, and such has been detected in many neurons (Brown, et al. 1994, Taddese and Bean, 2002).

The activation of Na_v channels occurs with membrane depolarization, allowing the influx of sodium ions that will further depolarize the membrane (Grossman, et al. 1979, Neumcke and Stämpfli, 1982). During the action potential, the depolarization phase of the membrane potential is followed by a second phase in which the membrane potential returns to the resting values, i.e. it repolarizes (Hodgkin and Huxley, 1952, c).

In the squid giant axon the delayed rectifier potassium current (so named since it was largely detectable at depolarized membrane potentials and activated after a delay) drives the repolarization current (Hodgkin and Huxley, 1952, b). The main function of the delayed rectifier current during the action potential is then the speedy repolarization of the membrane potential, to minimize the inactivation period of the fast sodium channels (Baranauskas 2006).

In mammalian axons potassium channels modulate the resting membrane potential, the action potential threshold, and the afterhyperpolarization and interspike interval, and, along with inactivation of sodium channels, the gating of potassium channels participates in the downstroke of the action potential (Kress and Mennerick, 2009).

The third phase of the action potential is a slowly recovering overshoot of the resting potential, named the after-hyperpolarisation (Frankenhauser and Hodgkin, 1956) produced by the voltage-dependent potassium conductance activated during the spike, which transiently hyperpolarizes the membrane (Adelman and Palti, 1969).

One remarkable characteristic of the action potential is that even though it allows signal conduction through distances that can go up to many meters (Hodgkin and Huxley, 1939), since the majority of molecular movement during its conduction is the flow of electronically charged ions through dedicated channels driven by the potential gradient, material exchange is essentially local and short-ranged. However, this flow leads necessarily to a transient accumulation of displaced ions along the axolemma, which must be repaired locally by means of intra-/extracellular transport mechanisms, acting over the entire length of the axon.

1.5 Schwann cell mediated transport

At the node of Ranvier, the endoneurium is uninterrupted and continues straight along to encircle the following Schwann cell, delimiting a perinodal space around the axon (Hess and Young, 1952) where ionic interchanges take place (Rydmark and Berthold, 1983). Specifically, the Schwann cell has been suggested to actively control both the Na^+ and K^+ concentrations at the extracellular space of the nodal gap (Seneviratne, et al. 1972, Rydmark and Berthold, 1983). Indeed, since the myelinated axon is such a restricted biological construct (Vizoso and Young, 1948), an efficient distribution of molecules and solutes through its different domains must require dedicated channels (Hirano 1982, Einheber, et al. 1997, Mierzwa, et al. 2010), especially given that the conduction of the action potential is so dependent on ionic movement (Hodgkin and Huxley, 1952, b).

In addition to the ion channels present in the axon (see section 1.3), a wide variety is also expressed in Schwann cells (Chiu 1991, Ritchie 1992). Voltage-gated sodium channels seem to be uniformly present in both the cell membrane (Elmer 1990) and the cytoplasm (Ritchie, et al. 1990), which led to the suggestion of intercellular channel transfer, due to the high turnover rate of sodium channels and the apposition of Schwann cell to the node of Ranvier (Ritchie 1988).

The ion channel complement of Schwann cells includes both voltage-gated and inwardly rectifying potassium channels. Thus potassium channels such as $K_{v1.1}$, $K_{v1.2}$, and $K_{v1.5}$ have been found in myelinating Schwann cells (Chiu, et al. 1994, Mi, et al. 1994), namely in the paranodal region (Wilson and Chiu

1990). Since extracellular potassium can have a profound influence on excitability (Kapoor, et al. 1993, Brazhe, et al. 2011), efficient potassium clearance is crucial for correct nerve functioning (Kofuji and Newman, 2004). A spatial buffering mechanism has been suggested (Orkand, et al. 1966), in which potassium enters the Schwann cell in local regions of high extracellular potassium, flowing intracellularly across gap junctions to other regions. However, this mechanism has been questioned due to the low resting membrane potential of Schwann cells (Brunder and Lieberman 1988). Since the inner mesaxon and the Schmidt-Lanterman incisures are electrically isolated from the node (Chiu 1991), the function of the potassium channels located here (Poliak, et al. 1999) has remained unclear, except for the suggestion that the channels are involved in the scavenging of excess potassium ions from the periaxonal space(Baker 2002).

It should be noted, however, that channel mediated buffering is just one of the possible means of Schwann cell potassium homeostasis. Connexin29 (Cx29), present in Schwann cells and associated with axonal potassium channels (Altevogt, et al. 2002), has been suggested to constitute a pathway for the removal of K^+ accumulating in the periaxonal space during action potential conduction (Konishi 1990, Chiu 1991). This notion is further supported by the freeze-fracture finding of particle clusters in juxtaparanode, inner mesaxon and incisures (Stolinski, et al. 1985) that could correspond to Cx29 (Konishi 1990).

The elevated lipid content of the compact myelin restricts the diffusion of aqueous solutes (Deber and Reynolds, 1991). This fact raises the issue of

internodal accessibility to biologically important water-soluble molecules, such as nutrients (Rosenbluth 2009). As above stated, the paranodal myelin lamellae terminate as a series of cytoplasmic loops that spiral around and form a specialized junction with the axon (Bhat 2003). This junction attaches the myelin sheath to the axon, effectively isolating the electrical activity at the node from the internode and limiting the lateral diffusion of membrane components (Peles and Salzer, 2000), and it has been suggested to function as a signalling site between the axon and the myelinating glial cell (Edgar and Garbern, 2004).

The presence of a 10–20 nm periaxonal space within the paranodal junction space (Robertson 1959) questioned the permeability of the junction. However, for many years the myelinating cell and the axon were considered too closely apposed to allow any material circulation, such as ionic exchange, through their separation (Bunge 1968). Eventually, low molecular weight substances such as lanthanum ions (Hall and Williams, 1971, Hirano and Dembitzer, 1981) and fluorescent dextrans (Mierzwa, et al. 2010) were shown to permeate the periaxonal space, proximal to the node of Ranvier. Since the tracer flow was the same in live and fixed nerves, at a rate consistent with motion through a long pathway, the periaxonal space has been indicated as a relatively low-resistance pathway for the passive movement of water and solutes (Mierzwa, et al. 2010). Nonetheless, this diffusion is not assumed to be totally free, as the myelinating cell should actively influence the constitution of the periaxonal space (Mierzwa, et al. 2010). Electrophysiological (Frankenhauser and Hodgkin 1956) and voltage clamp pulse (Adelman and Palti, 1969) studies have actually demonstrated

that the periaxonal space can be overloaded with potassium during the repetitive conduction of nerve impulses, suggesting that diffusion of at least some ions through the paranodal junction is limited. The leakage of longitudinal current flow through the paranodal junction is then a theoretical possibility, considering the accumulation of K_v channels in the juxtaparanodal axolemma (Wang, et al. 1993) that could be activated by nodal action currents (Rosenbluth 2009), but no conclusive results have been presented yet.

As described above, the compact myelin in the PNS is interrupted by the Schmidt-Lanterman incisures (Scherer, et al. 1995). The biological importance of these incisures became clearer with the observation that the X-linked form of Charcot-Marie-Tooth disease (CMTX) (Suter and Snipes 1995) was caused by mutations in the Connexin32 (Cx32) gene (Bergoffen, et al. 1993). Since the Cx32-mediated communication pathway is based on the movement of ions and small molecules through Schwann cell gap junctions (Abrams, et al. 2000), these mutations are believed to affect the function of these junctions by interrupting the radial diffusion of small molecules across the myelin sheath (Scherer, et al. 1995). The Schmidt-Lanterman incisures are then thought to function as a communication and transport pathway connecting the periaxonal to the extracellular space. Dye diffusion studies indeed suggest that the gap junctions found in paranodes and incisures allow the trafficking of ions and other small molecules between the outer and inner cytoplasm of the Schwann cell through an intracellular pathway (Balice-Gordon, et al. 1998). This pathway allows the radial diffusion of ions and small molecules, directly traversing the myelin sheath,

instead of circumferentially through the Schwann cell cytoplasm (Scherer, et al. 1995). Due to its wrapped geometry, this pathway can be over a thousand-fold shorter than travelling spirally along the cytoplasm (Friede and Bischhausen, 1980).

Gap junctions consist in two half channels formed by a cluster of connexins (mainly connexin32) (Scherer, et al. 1995) crossing two plasma membranes, and play an additional structural role in the integrity of peripheral myelin sheaths (Scherer and Arroyo, 2002).

The paranodal loops are sealed off from the periaxonal space by tight junctions (Farquhar and Palade, 1963), specialized cell-cell contact sites that maintain a selective permeability and restrict the movement of lipids and proteins between membrane domains (Mizisin and Weerasuriya, 2011). These junctions are also present in the inner and outer mesaxon and the incisures (Mugnaini and Schnapp 1974, Sandri, et al. 1977, Tetzlaff 1982), where they follow the membrane spiral around the internode (Sandri, et al. 1977). Tight junctions are constituted by rows of inter-membranous particles between adjacent Schwann cell membranes (Mitic and Anderson 1998), and have been suggested to link adjacent membranes, increasing their mechanical strength, and to separate the glial outer membrane from the compact myelin membrane (Gow, et al. 1999).

The paranodal loops are also connected among themselves by several autotypic adherens junctions (Spiegel and Peles, 2002), which provide supplementary structural integrity. Adherens junctions are also present in the incisures where, due to the organization of the myelin sheath, they form a

series of multi-layered radially arranged junctions (Balice-Gordon, et al. 1998). These junctions contain E-cadherin and the cytoplasmic protein β-catenin, which links E-cadherin (Trapp, et al. 1989, Gumbiner 2000) to the actin cytoskeleton (Nagafuchi, et al. 1993). The adherens junctions are proposed to mediate rapid intracellular signalling (Fannon, et al. 1995), again by bypassing the longer course around the cytoplasmic spiral turns.

1.6 Axonal homeostasis

One of the main functions of axonal mitochondria is providing the ATP essential to impulse activity (Skou 1957), but due to the length of the axon, ATP might not be uniformly available along the axoplasm (Saks, et al. 2006). This fact indicates that axonal energy homeostasis might depend on the intracellular distribution of mitochondria (Chada and Hollenbeck 2003). In the PNS, axonal mitochondria are transported (Berthold and Mellström, 1982, Armstrong, et al. 1987, Gatzinsky and Berthold, 1990) associated with microtubules and neurofilaments (Perkins, et al. 2008). *In vitro* studies of mitochondria localisation have suggested that this transport slows down upon reaching the nodal/paranodal region (Misgeld, et al. 2007), where its density is higher than at the internode (Berthold, et al. 1993, Fabricius, et al. 1993, Perkins and Ellisman, 2011). It has been speculated that this slowing is caused by a checkpoint mechanism or an active recruitment of mitochondria to this region due to a high metabolic demand (Edgar, et al. 2008), caused by the possible activity of the sodium, potassium adenosine triphosphatase (sodium pump), indicated in some studies to be located in the nodal region (Vorbrodt, et al. 1982, Mrsulja, et al. 1985, Gerbi, et al. 1999). It should however be noted that *in vitro* studies are limited by the fact that cultured neurites normally continue to develop and grow during examination (Snow, et al. 1990, Piret, et al. 2013), meaning that mitochondrial trafficking must reflect these influences. Additionally, excised nerves are typically unmyelinated, and even though they may contain myelinated axons, these typically lack cell bodies and are therefore mandatorily undergoing

degeneration, and obviously have no perfused vasculature providing oxygen and nutrients.

The collar of Schwann cell cytoplasm neighbouring the node is rich in mitochondrial content, whose function is not entirely known. These mitochondria have been suggested to act as an energy source to be used by the surface membrane of the axon at the node (Williams and Landon, 1963). This notion has been supported by the observation that adenosine-5'-triphosphate (ATP) can be transported between different cells (Stone 1981). However, if the nodal/paranodal structure were indeed so often remodelled as the debris presence suggests (Gatzinsky and Berthold, 1990)(see above), another possible function of these mitochondria would be supplying the energy required to maintain the restructuring Schwann cell structure.

It has also been described above that the propagation of an action potential along myelinated axons involves an influx of sodium ions through nodal sodium channels (Ritchie 1982) and a subsequent efflux of potassium through voltage-gated potassium channels located within the internode and juxtaparanode (Baker and Bostock, 1998). In fact, in mammalian axons it is now known that the repolarisation due to potassium efflux does not act at the level of individual action potentials, but rather over time to maintain the axonal resting potential (Brismar 1980, Smith and Schauf, 1981, Ritchie 1982, Baker, et al. 1985, Smith and McDonald, 1999). However, surprisingly, several fundamental aspects of impulse conduction remain unknown, including the pathway(s) taken by the dislocated sodium and potassium ions. This knowledge is relevant since, for example, ion movements can have

osmotic consequences and these may be responsible for some axonopathies, especially if normal ionic homeostasis has been disrupted by metabolic disturbances.

With regard to sodium ions, it has been known for over 60 years that these ions enter the axon via voltage-gated sodium channels (Na_V) located in the nodal axolemma (Hodgkin and Katz, 1949), but what path they take afterwards remains a mystery.

With regard to potassium ions, it is now known that potassium channels are largely expressed beneath the myelin, at the juxtaparanodes and along the internodes (Baker, et al. 1985, Baker and Bostock, 1998, Altevogt, et al. 2002), and so it has been suggested that K^+ efflux will result in its accumulation in the periaxonal space (PAS) (Baker and Bostock, 1998, Altevogt, et al. 2002); being so, it follows that repetitive propagation of action potential leads to potassium build-up in the PAS. Indeed, in the short term, such accumulation can result in changes in axonal excitability (Kapoor, et al. 1993).

The sodium pump is the transmembrane enzyme that couples the energy generated from the hydrolysis of ATP with the translocation of Na^+ and K^+ ions across the membrane (Skou 1957). It is a complex of two polypeptides, alpha and beta, and a large number of aggregated lipids (Béguin, et al. 1998). The sodium pump not only works as a compensatory mechanism for the dissipation of ionic gradients, but it also plays a key function in cell metabolism and neuronal excitability, the exchange of substances between

the cell and its surroundings, and transepithelial transport (Ernst 1972, Skou and Esmann, 1992).

Arguably, the sodium pump performs the most important role in axonal ion homeostasis, but there are conflicting reports with regard to the location(s) of its different isoforms along the axon. The initial notion that it was located in the nodal axolemma was confounded by the later realisation that reports associating this pump exclusively with the node of Ranvier (Vorbrodt, et al. 1982, Mrsulja, et al. 1985, Gerbi, et al. 1999) could result from non-specific signal or an insufficient antibody access to the internodal axolemma. Indeed, more recent immunohistochemical (Mata, et al. 1991, McGrail, et al. 1991, Young, et al. 2008) and substrate (Alberti, et al. 2007) studies indicate a mainly (or perhaps exclusively) internodal (i.e. beneath the myelin sheath) expression of the α_1, α_3 and β_1 isoforms of the sodium pump.
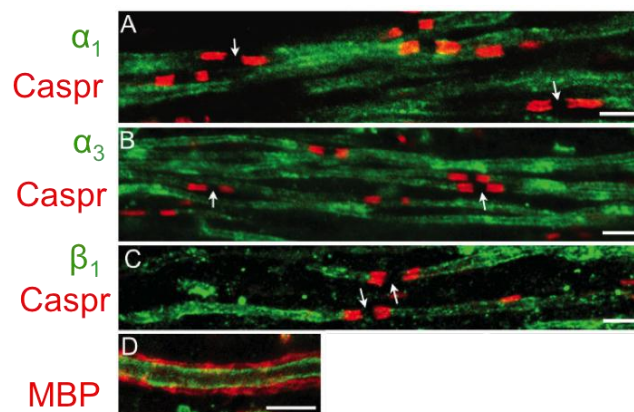
Figure 3a-d – The axonal distribution of the sodium pump.

The sodium, potassium ATPase (sodium pump) is enriched in the internodal axolemma of myelinated axons in the adult human brain. The sodium pump subunits α1, (**a**, **green**) α3 (**b**, **green**) and β1 (**c**, **green**) are located at the axolemma of myelinated axons, enriched in the internodal axon and not detected in the

nodal/paranodal axolemma (**a-c**, **arrows**), as demarcated by the paranodal marker Caspr (**a-c**, **red**). The sodium pump was expressed below myelin sheaths stained with myelin basic protein antibodies (**d**, **red**). Scale bars are 5 μm. Adapted (Young, et al. 2008).

Being so, it follows the assumption that Na$^+$ ions extruded from the axon by the sodium pump must travel first into the periaxonal space and then somehow navigate the myelin sheath before regaining position in the extracellular space. The most immediate pathway would be through the junctions located in the Schmitt-Lanterman incisures, but since these incisures are absent in the central nervous system the doubt persists that this might not be the most common pathway, or at least not a universal one. As previously mentioned, because several adhesion molecules tightly bind the axolemma and the glial membrane to each other, ion diffusion from the PAS seems to be limited (Frankenhauser and Hodgkin, 1956, Adelman and Palti, 1969). The presence of the sodium pump along the internodal axolemma would cause transport of K$^+$ ions from the periaxonal space back into the axoplasm, which, together with the alternative of being taken up by the glial cell through gap junctions (Rash 2010)or potassium channels (Chiu, et al. 1994, Mi, et al. 1994), poses much less of a problem. Evidence indicates that sodium ions entering the axon accumulate near the inner surface of the nodal membrane, and although the axon might have a means to cope with intense variations in Na$^+$ concentration, their mode of action is still very poorly understood (Bergman 1970).

At high frequencies of sustained stimulation the axon must manage a persistent influx of Na$^+$ ions. If this rate is greater than that which can be

counteracted by the sodium pump, Na^+ will accumulate intra-axonally, and then new mechanisms can operate to try to restore homeostasis. One theoretical mechanism is the reversal of the direction of the electrochemically-driven Na^+/Ca^{2+} exchanger (Waxman 1995, Stys and Lopachin, 1998). Little is known about how such an ionic disruption *in vivo* may affect the physiological properties of axons, including effects on volume resulting from changes in osmotic pressure. Changes in volume and osmotic stress in axons that may be tightly constrained by their individual basal lamina may have consequences that are rarely considered.

The different functions played by the sodium pump imply that it must also play a pivotal role in cell volume regulation. Due to the permeability of the cell membranes to water molecules, the cell volume is not constant. All metabolites dissolved in the extra- and intra-cellular fluids, such as glucose, amino acids, free fatty acids, and electrolytes, can cause osmotic pressure at the cell membrane. If the osmolarity between these fluids is different, water molecules will diffuse across the plasma membrane (Macknight and Leaf, 1977). Proteins and other macromolecules present in cells can cause a similar effect. This means that the maintenance of the cell volume within a physiological limit requires a precise volume-regulatory mechanism such as the activity of the sodium pump controlling the distribution of small ions between the cells and the extracellular fluid (Flores, et al. 1972).

As previously mentioned, the sodium pump uses the energy from ATP hydrolysis to extrude sodium from the cell, accumulating potassium, which means that a metabolic or oxygen supply reduction severely impairs volume

regulation of the cell(Flores, et al. 1972, Tranum-Jensen, et al. 1981). The cell metabolism and its osmotic regulation are further associated. The metabolism of glucose, which is eventually broken down into CO_2 and H_2O, is one of the main sources of energy of the axon(Magnani, et al. 1996). In addition to providing the cell with metabolic energy, glucose breakdown also reduces the osmotic concentration, as the gaseous $CO_2$is diffused away and the H_2O decreases the intracellular osmolarity(Rutz 2004). In parallel, it has long been known that elevated concentrations of sucrose can affect the mitochondrial activity (Lehninger 1962). Further studies indicated that high osmolarity was to blame for this effect, by inhibiting the mitochondrial transport of adenine nucleotides (Chávez, et al. 1987) through morphological changes of the mitochondrial membrane structure (Packer, et al. 1971). Taken together, these results indicate that osmotic pressure can have a profound effect on cellular activity, which, in turn, affects the osmolarity control. Being so, while balanced ion trafficking will have no osmotic consequences, an improper compensation for this movement can cause alterations in osmotic pressure.

Indeed, most cells can have their survival and function highly disrupted by incorrect ionic homeostasis (Burg, et al. 2007), and the nervous system is no exception. Since the main functions of the nervous system are based on ion movements (Hodgkin and Huxley, 1952, b), a proper compensation for these movements is crucial to neuronal (and axonal) homeostasis, both biologically and functionally. Biologically, basic functions such as maintenance of the neurites cylindrical shape depend on volume regulatory mechanisms (Pullarkat, et al. 2006). Functionally, variations in potassium concentration in

the periaxonal space have been shown to modify many membrane electrical parameters (Adelman, et al. 1973, Kapoor et al, 1993, Brazhe et al, 2011), which suggests that the ionic compositions of intercellular clefts need to be tightly controlled so that axonal activity is undisturbed. Since extracellular potassium has a profound influence on excitability (Kapoor, et al. 1993, Brazhe, et al. 2011), efficient potassium clearance is crucial if normal nerve functions are to be maintained (Kofuji and Newman 2004). In some conditions such as brain ischaemia or demyelination, disrupting the glial flow of K^+ leads to its accumulation in the periaxonal space, either leading to a membrane depolarization, to an activation of the axonal sodium pump that creates hyperpolarizing currents, or to K^+ pumping into the Schwann cell, causing its swelling and myelin structure alteration (Bostock, et al. 1991, Kiernan, et al. 1997, Baker 2000). Such an effect can occur in neuromyelitis optica, characterized by reduced conduction caused by K^+-induced osmotic swelling of myelin (Wingerchuk, et al. 2007). Similarly, there is some evidence that in neurodegenerative diseases disruption of ionic buffering in the axon plays an important role in pathology, mostly by causing myelin swelling due to osmotic pressure (Rash 2010).

In an analogous way, it may also be expected that the diffusion of Na^+ ions following repetitive propagation of the action potential, especially if operating under pathological conditions, could also have osmotic disrupting effects. Osmotic alterations have been indicated as the cause of morphological distortions observed in both the axon and the Schwann cell (Baker 2002) following treatment with Phoneutria spider venom (Love, et al. 1986), and have also been linked to demyelinating brain lesions (Sterns, et al. 1986) in

chronic hyponatremia (Wald, et al. 2010). Additionally, the activity of ionic channels has been recently described as being susceptible to modulation by osmotic stress (Kukita 2011).

1.7 Axonal morphology and signal conduction

Guillain-Barré syndrome (GBS) is an acute, inflammatory and demyelinating neuropathy afflicting between one and four people out of 100,000 worldwide, that is clinically pictured as a generalized polyradiculoneuropathy (Hughes, et al. 1999). Other neuroinflammatory diseases, such as multiple sclerosis (MS) in the central nervous system, share several common features with GBS, including the expression of reversible neurological deficits which can last for a day or, more typically, for a month or more. Relapses of a month or so are likely to involve demyelination (Smith, et al. 1997); however, brief relapses lasting only a day or so cannot be explained in this way and other factor(s) must be invoked.

Evidence has been accumulating over the last 15 years suggesting that temporary axonal conduction block can be at least partially due to inflammatory factors such as nitric oxide (NO) (Redford, et al. 1995). NO is known to inhibit mitochondrial metabolism *in vivo*, thus inhibiting the production of ATP (Duchen 2004), and *in vitro,* exogenous NO has been described to increase the opening of Na^+ channels, resulting in a persistent Na^+ influx (Hammarström and Gage, 1999), and to impair the maintenance of Na^+ homeostasis by inhibiting the activity of the sodium pump (Sato, et al. 1997). It is interesting to consider whether such increases in intracellular Na^+ at the sites of inflammation may have osmotic consequences. If such ionic imbalances are indeed confirmed, one of its most important effects could be the excessive intracellular accumulation of free Ca^{2+} ions (Stys and

Lopachin, 1998), since this may initiate a cascade of biochemical processes culminating in the activation of cell death mechanisms (Doyle, et al. 2008).

Disruptions of the node of Ranvier and the paranode, both structural, such as widening of the paranode or nodal swelling, and functional, such as delocalization and mis-expression of nodal proteins, have been correlated with axonal pathology and the degree of local inflammation in human demyelinating diseases (Howell, et al. 2006). In GBS patients, it has been frequently reported that the mildest observed histological alteration is the lengthening of the nodal gap, sometimes associated with distortion of the paranodal myelin and its attachment sites. This widening was found to vary from a few micra to about one-third of an internode (Cummings and Haas, 1966), and was observed in the ventral and lumbar dorsal roots and in peripheral nerves, in early and pathologically mild situations (Cummings and Haas, 1966, Carpenter 1972, Griffin, et al. 1996). Electron microscopy also showed that the dense cytoskeleton undercoating of the nodal axolemma was not altered, meaning that the Schwann cell processes and microvilli were displaced in a way that the node was often covered only by the Schwann cell basal lamina (Griffin, et al. 1996). In MS, some of its earliest clinical symptoms have also been suggested to be caused by a reduction in axonal conduction velocity caused by disruption of the myelin-axon complex at the node of Ranvier, in a stage prior to demyelination (Compston and Coles, 2002, Wolswijk and Balesar, 2003, Howell, et al. 2010).

Disruption of the node of Ranvier is thought to reduce axonal conduction velocity, even if the Na_v channels remain restricted to the unaltered region

with dense undercoating (Sherman and Brophy, 2005). In fact, the nodal lengthening itself is sufficient to lower the safety factor for impulse conduction past these sites, contributing to impulse conduction failure (Korobkin, et al. 1975). Notably, the paranode has been suggested to be capable of slow distension via membrane slippage of the paranodal myelin attachments (Cavanagh 1982), a complex but reversible process (Jones and Cavanagh, 1983).

In GBS, impulse conduction in nerve fibres may also fail as a result of some internodal morphological alterations. The most obvious change is the widening of the periaxonal space, occurring by separation of the Schwann cell membrane from the axon (Griffin, et al. 1996). Theoretically, the process of expansion of the periaxonal space would be expected to result in an increase in resistance to longitudinal current flow due to the partial constriction of the axoplasm. However, this increase in resistance may be negligible because the current can alternatively pass through the periaxonal fluid (the current has to cross the axonal membrane in either case).

The application of several drugs that open sodium channels, such as batrachotoxin (Moore, et al. 1986), ciguatoxin-1b (Bennett, et al. 1997), the venoms of the scorpions *Leirurus quinquestriatus* and *Centruroides sculpturatus*, and of the spider *Phoneutria nigriventer* (Baker, et al. 1985, Love and Cruz-Höfling, 1986) has been shown to result in a prominent widening of the periaxonal space. Treatment with ciguatoxin-1b and *Leirurus* and *Centruroides* venoms was also found to cause widening of the nodal gap or swelling of the node of Ranvier (Bennett, et al. 1997, Benoit et al. 1996,

Love and Cruz-Höfling, 1986), which in some cases was associated with loss of conduction capacity (Cruz-Höfling, et al. 1985).

All of these drugs alter the kinetics of the voltage-gated sodium channels in such a manner that the ionic influx mimics that of high frequency stimulation. Ciguatoxin-1b, for instance, causes a shift in the voltage-gated sodium channels activation gating (Bennett, et al. 1997), whereas the scorpion and spider venoms prolong the duration of channel opening (Baker, et al. 1985), both situations inducing high frequency discharges of action potentials. Batrachotoxin causes persistent channel activation leading to depolarization of the resting membrane potential and repetitive firing (Baker, et al. 1985, Ulbricht 1998,Wang and Wang, 2003)**.** In the above-mentioned pharmacological experiments, treatment with a potent Na_v blocker such as tetrodoxin (TTX) significantly attenuated the expansion of the periaxonal space (Rosenbluth, et al. 2006, Cruz-Höfling, et al. 1985, Moore, et al. 1986). Moreover, the swelling of the node of Ranvier following treatment with ciguatoxin was reversed in the presence of hyperosmolar external solutions (Bennett, et al. 1997), which strengthens the belief that these modifications are indeed happening as an osmotic response to the excessive opening of voltage-gated sodium channels.

The observations described above have partly inspired the research presented in this thesis, as they indicate that ion channel opening may have morphological and pathological significance. However the former findings are unsatisfying in that while they describe morphological phenomena, they do

not provide mechanisms and they do not extend the observations into fundamental physiological principles, or provide outcomes of the pathology.

1.8 Hypothesis

Sodium ions presumably transported to the periaxonal space following signal conduction could possibly return to the extracellular space following one or more of three pathways: directly through the myelin sheath (unlikely), through the Schmidt-Lantermann incisures, or by travelling to the paranodes and there crossing to the nodal gap. Current data seem to suggest that this last pathway could happen through three different ways: through the junctional cleft across the transverse bands, along the spaces between the transverse bands, or between the paranodal loops (Mierzwa, et al. 2010).

We hypothesize that by exploring some of the fundamental aspects of axonal biophysics, taking advantage of a new observation regarding changes in axonal morphology with sustained impulse activity, we will be able to understand more clearly how homeostasis is restored in the axon following signal conduction. This approach has been adopted because the ionic changes that accompany an individual action potential are largely reproduced for each action potential of a sustained train, and so a strategy of imposing sustained stimulation can exaggerate ion changes, making their consequences easier to study.

This knowledge should not only reveal aspects of the normal physiology of impulse conduction that may hitherto have remained undescribed, but also help to unravel the manner by which the axon is functionally affected while working under various pathological conditions, including inflammatory conditions.

2 *In vivo* evoked stimulation

2.1 Introduction

It is well established that the propagation of an action potential along myelinated axons involves an influx of sodium ions (Na^+) through nodal axolemmal sodium channels (Ritchie 1982) and a subsequent efflux of potassium (K^+) through voltage-gated potassium channels located within the internode and juxtaparanode (Baker 2000). However, surprisingly, several fundamental aspects of impulse conduction remain unknown, including the pathway(s) taken by the sodium and potassium ions.

Specifically regarding the sodium ions, the path they take after entering the axon via the nodal axolemma remains a mystery. An initial notion that they were pumped back out of the axon at the nodal membrane was confounded by the realisation that the sodium, potassium ATPase (sodium pump) is located in the internode, beneath the myelin (McGrail, et al. 1991, Mata, et al. 1991, Young, et al. 2008). If so, it seems that upon leaving the axons the Na^+ ions must accumulate in the periaxonal space, and then presumably travel from that space back to the extracellular space, either at the node of Ranvier, or through the myelin: the precise route taken is not known. The presence of the sodium pump along the internodal axolemma would permit extrusion of K^+ ions from the periaxonal space back into the axoplasm, which poses much less of a problem.

In parallel, since the morphology of the axon-Schwann cell interface has been suggested to have its function impaired in pathological

neuroinflammatory situations (Sato, et al. 1997, Hammarström and Gage, 1999, Duchen 2004) with possible direct impacts on axonal conduction capacity, we also aimed to obtain a model that allowed characterization of its activity via a visual morphological indicator.

We aimed to explore some of these fundamental aspects of axonal biophysics using sustained impulse activity. This approach has been adopted because the ionic changes that accompany an individual action potential are largely reproduced for each action potential of a sustained train, and so a strategy of imposing sustained stimulation can exaggerate ion changes, making their consequences easier to study. We opted to start our work using a mouse line (Thy1-YFP-16) in which the axoplasm of a small percentage of axons is labelled transgenically to express yellow fluorescent protein (YFP) under the control of neuron-specific elements from the thy1 gene. Thy1-YFP expression depends on a combination of elements in both the transgene and in flanking DNA, such as the presence of promoter sequences in the transgene or other elements at the integration site, or the conformation of chromatin near the integration site(Feng, et al. 2000). These transgenes allow axonal morphology to be monitored in real time using confocal imaging, *in vivo*.

To increase the physiological relevance of our experiments, we have aimed to develop an *in vivo* model to allow direct observation of axonal morphology, in real time, in nerves that have a maintained vascular supply and that are undisturbed, apart from simply being exposed: we decided to use the saphenous nerve. This nerve is the longest sensory branch of the femoral

nerve (Hunter, et al. 1979), lying lateral to the femoral artery in the proximal thigh, and continuing distally through the lower leg's anteromedial aspect. It offers potential advantages in terms of physiological experimentation to tackle this specific task, requiring minimal invasive surgery (simple skin and connective tissue incisions) to obtain a preparation with undisturbed, intact nerve. Another advantage of using the saphenous nerve is that, being exclusively a sensory nerve with no motor fibres affected, no motor stimulation occurs, greatly increasing image stability during *in vivo* observation.

The stimulation frequencies utilized in these experiments were 20-100 Hz, namely frequencies that are within the physiological range of many axons (Prochazka and Gorassini, 1998). It is acknowledged that axons of different modalities will fire at different frequencies, which means that no single physiological frequency will describe all groups of axons. However, some axons are known normally to be active for protracted periods of time, and recordings from hamstring afferents in freely moving preparations have revealed maximum average firing rates of 100 Hz or more during normal stepping (Prochazka and Gorassini, 1998). It should also be noted that it has been previously demonstrated in our laboratory that axons in rat dorsal roots can faithfully conduct impulses continuously at 50 Hz or 100 Hz for periods up to 5 or 6 hours (Smith, et al. 2001). The main goal of the proposed experiments is to make the axons function towards the limits of normal activity to eventually reveal any morphological alterations that might normally be expressed only faintly, and to unravel a possible association between this correlation and the cause of axonal conduction block in neuroinflammatory

pathologies. The morphological studies coupled with the electrical observations should reveal the consequences of electrical activity, under normal and pathological conditions.

2.2 Material and methods

In order to have a visual measure of morphological alterations, we decided to use transgenic mice (Thy1-YFP-16, supplied by Dr. Michael Coleman, Cambridge) (Feng, et al. 2000)in which 1-2% of the sensory and motor axons are labelled with yellow fluorescent protein (YFP), with labelling in no other cells. These animals were allowed free access to food and water throughout the study and artificial light was supplied on a 12-h light/dark cycle. The animals were anaesthetized with 3.5% isoflurane, with the quantity of anaesthetic monitored, in part by checking for pinch withdrawal, and in part by observing the breathing frequency. All surgical procedures were performed under sterile conditions.

This study was conducted mainly on the saphenous nerve. The saphenous nerve was exposed in the mid-thigh, using sterile conditions. After a small incision to the skin to expose the saphenous nerve, the stimulating electrodes were attached to an isolated simulator (Model DS2, Digitiser Ltd.) and placed directly in contact with the saphenous nerve, distally to the imaging site. The nerves were immersed in mineral oil and covered with Teflon tape in order to insulate the preparation electrically and to prevent evaporation; the recording electrode (20% iridium, 80% platinum, Teflon-coated except at the tip) was placed directly in contact with the saphenous nerve (exposed through the skin via a small incision) proximal to the imaging site, i.e., employing antidromic conduction, and covered with mineral oil. This electrode, together with the reference electrode (a 25 G needle inserted percutaneously in the contralateral paw), was connected to the inputs of a

differential AC preamplifier and thereby to an AC-DC amplifier (Neurolog system, Digitimer). The ground electrode was inserted under the skin of the thigh between the stimulating and recording electrodes. Threshold and supramaximal stimulus intensities were determined and the stimulation voltage set to twice the supramaximal. In order to compare the evoked compound action potentials (CAPs) before and after high frequency stimulation, stimuli were applied at 1 Hz frequency. The recordings were viewed on an oscilloscope (Sigma 60 200 MS/s Digital Oscilloscope Station, Sigma) and stored as averaged records of at least ten CAPs. Sustained high frequency stimulation was performed by stimulation at 20 or 100 Hz (Smith, et al. 2001) for a period of 2 hours (preliminary studies showed that the peak of the CAP decreases when sustained stimulation is applied, but it stabilised after 30 to 50 minutes, and we selected a period approximately twice as long).

After stimulation, the remaining portion of the saphenous nerve that still was covered with skin was exposed, a cover slip was applied and it was imaged, *in vivo*, using a confocal laser-scanning microscope (LSM 5 Pascal, Carl Zeiss, Jena, Germany). At least 9 different nodes of Ranvier in different axons were imaged in an individual preparation, and either a single image was recorded every 10 minutes, or a z-stack was recorded every 20 minutes, for a period varying between 5 and 10 hours after stimulation. When the nerves were imaged at later time periods (one or seven days after stimulation), the surgical incisures were stitched after stimulation/imaging and the animal was allowed to recover and returned to the animal house before being imaged.

In some experiments the blood supply to the saphenous nerve was deliberately impaired by pushing down on the coverslip holder so that the nerve was blanched due to occluding the blood circulation during the whole imaging period.

After *in vivo* imaging, the nerves were fixed in glutaraldehyde for at least 24 hours and the central 5 mm length of each fixed nerve was excised. The nerves were then subjected to three consecutive 10-minute washes in 0.1 M PO_4 buffer (pH 7.4) and subsequently post-fixed in 1.5% osmium tetroxide for 1 hour, before undergoing a further 3 x 10-minute washes in 0.1 M PO_4 buffer (pH 7.4). The nerves were then dehydrated in an ascending series of alcohols: 15 minute washes in 30%, 50%, 70% and 90% ethanol ending with three 20-minute washes in 100% anhydrous ethanol. In order to prepare for Epon resin infiltration, two 30-minute washes in 100% propylene oxide were followed by 2 hours in 75% propylene oxide/ 25% resin, 2 hours in 50% propylene oxide/ 50% resin, 2 hours in 25% propylene oxide/ 75% resin and finally left overnight at 4ºC in fresh 100% resin. The tissue was embedded in resin, using Beem capsules for longitudinal sections or coffin moulds for transverse sections, and heated at 60ºC for 48 hours. 0.7 µm thick sections were cut and collected onto slides and stained with thionin acetate and acridine orange. These sections were then screened in a light microscope with an attached photographic camera. Ultrathin (70 nm thick, silver color) sections from selected blocks were subsequently examined further in an electron microscope (JEM-1010 Electron Microscope, JEOL).

Processing of the obtained images was performed with ImageJ software (National Institutes of Health). The 'z-stacks' were used to measure volumes; in order to do so, the region of interest was defined and the whole series of images were converted to a binary picture, in a dark background, with the threshold being defined manually. The histogram function was used to determine the number of black pixels in the region of interest in the whole series of images. These were normalized to the volume of a cylinder with the same dimensions as each quantified axon. In order to measure the length and width of the axon, the straight lines selection tool was used. The recorded compound action potentials were processed using the OriginPro 7.5 software (Origin Lab Corporation). The region of interest was defined to include the CAP and the area under the curve was obtained with the Integrate function, and comparing the timing of the peak of the different CAPs assessed existence of delay in the CAP.

In the thionin acetate and acridine orange stained bright field imaged sections, the area of the nodes of Ranvier was determined by delineating the region of interest followed by using the histogram function. The area of the node of Ranvier and the distance between the paranodes were measured with the straight lines selection tool.

All the graphics here presented were obtained with GraphPad Prism (GraphPad Software, Inc.), after initial data processing with Microsoft Excel (Microsoft Corporation), unless stated otherwise. The statistics test used was 1 way ANOVA with Tukey's multiple comparison test post-hoc, unless stated otherwise.

2.3 Results

Appearance of normal YFP positive axons *in vivo*

Imaging of normal YFP axons *in vivo* (figure 4) shows that, in contrast to what is typically illustrated in textbooks, the axon is not a perfectly shaped cylinder. Small irregularities can be observed along the axoplasm, with more obvious features in the area of the paranode and juxtaparanode. These are due to the presence of 'fluting' of the axon and myelin in this location (figure 5) (Brown and Abbott, 1993, Rosenbluth 2009).
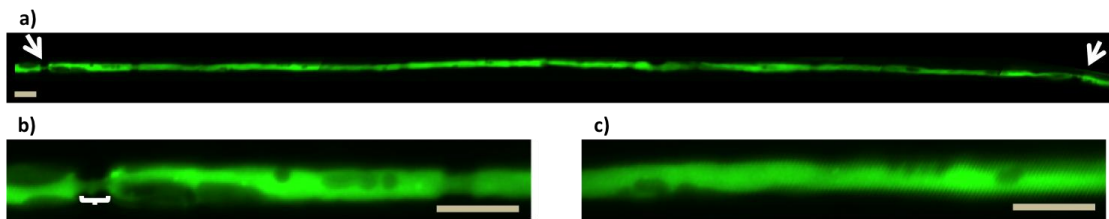
Figure 4a-c – Appearance of a normal YFP positive axon imaged *in vivo*.

In vivo confocal imaging of a YFP positive axon in an undisturbed saphenous nerve of a transgenically labelled mouse, with tiling of a series of images to show the full extent of the axon between two nodes of Ranvier (**a**, **arrows**), and a magnified view of the node of Ranvier and paranodes (**b**, **bracket**) and the internode (**c**). Scale bars are 10 µm.
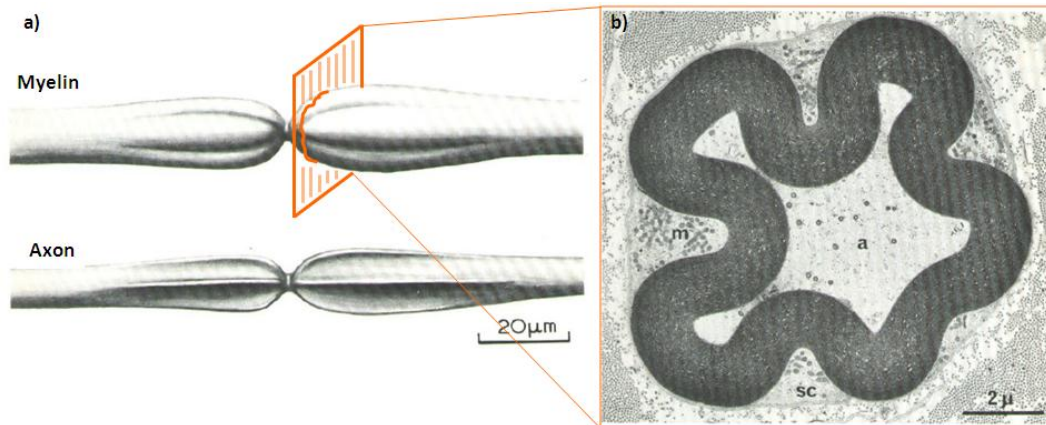
Figure 5a-b – '**Fluting' of the axon in the paranode.**

Illustration of the surface contour of the paranodal bulbs and the surface contour of the enclosed axon after removal of the myelin sheath showing its fluted conformation (**a**). The myelin sheath is convoluted and the longitudinal grooves on its external surface are filled with Schwann cell cytoplasm (**SC**) rich in mitochondria (**m**), as seen in an electron micrograph of a transverse section of the paranode of a myelinated fiber (**b**). The internal contour of the myelin sheath conforms to that of the axoplasm (**a**). This phenomenon is illustrated by a diagrammatic view of the structure of the node of Ranvier of a large mammalian peripheral myelinated nerve fiber (**a**). Adapted (Culp and Ochoa, 1982).

Sham surgery and *in vivo* confocal imaging caused no morphological alterations to YFP-positive axons

Confocal microscopy time lapse imaging of the sham-operated nerves showed no visible alterations to the morphology of the axon (imaging period extended up to 10 hours) (figure 6).
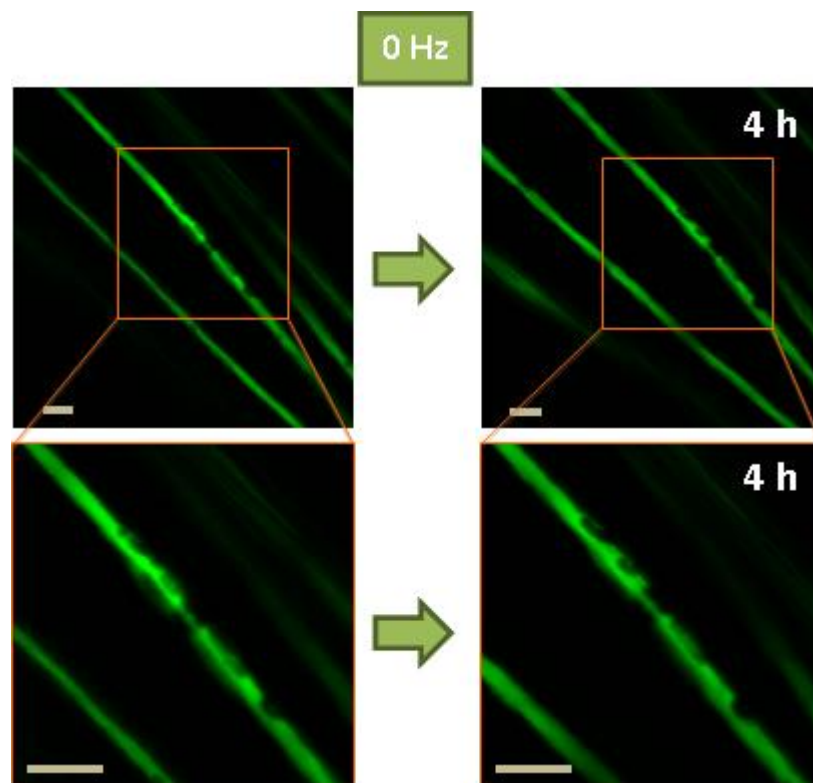
Figure 6 – Sham surgery and confocal imaging cause no alterations to the axon.

In vivo confocal imaging of YFP positive axons in the mouse saphenous nerve before (left panels) and 4 hours after (right panels) sham surgery. The axoplasm of YFP positive axons was not altered during an observation period of 4 hours. Scale bars are 10 µm.

Electrical stimulation induces swelling of the paranodes and expansion of the periaxonal space

After 2 hours of stimulation at 20 Hz with twice supramaximal stimulus voltage, the amplitude of the compound action potential (CAP) decreased to approximately 60% of the pre-stimulus value. After 2 hours of stimulation at 100 Hz with twice the supramaximal voltage the CAP decreased to approximately 20% of the pre-stimulation value, and with a delay of approximately 60% of the pre-stimulation control (figures 7 and 8).
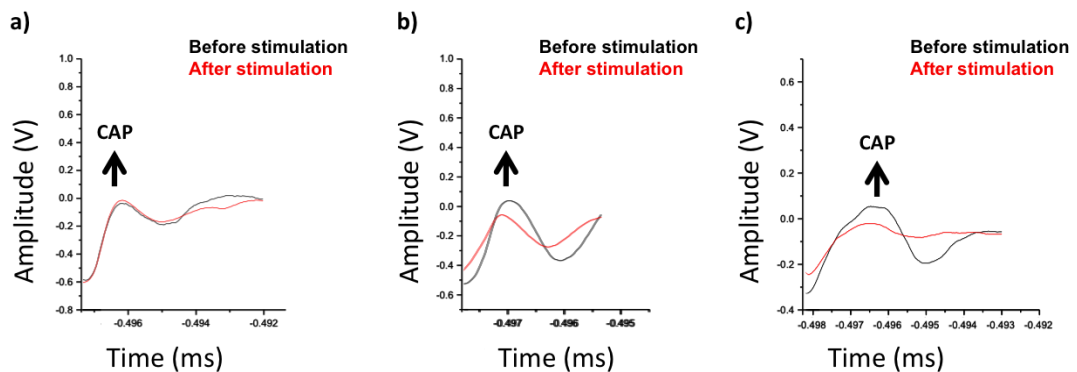
Figure 7a-c – Effects of electrical stimulation on the form of the compound action potential.

CAPs obtained from proximal saphenous nerve in response to supramaximal, distal electrical stimulation, before (**black lines**) and after (**red lines**) 2 hours of sustained stimulation. Nerves had either sham surgery (**a**) or stimulation at 20 Hz (**b**), or 100 Hz (**c**). Graphics obtained using OriginPro 7.5.
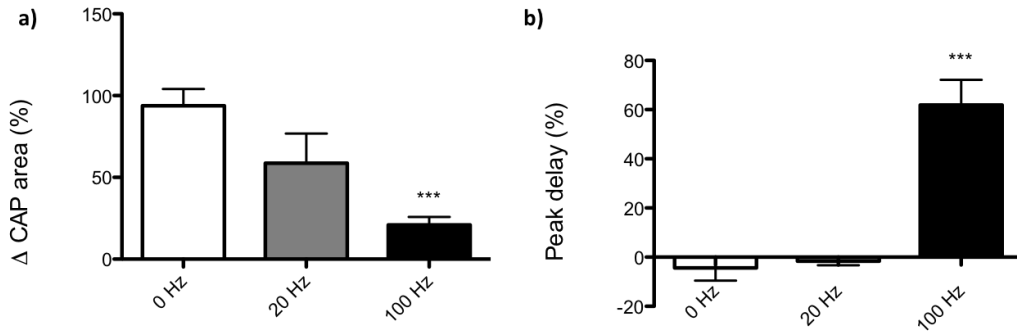
Figure 8a-b –Variation of the area of the CAP (a) and the delay of its peak (b) with the frequency of stimulation.

Nerves were stimulated for 2 hours at 20 Hz, 100 Hz or just sham operated without stimulation (0 Hz), and the area (**a**) and the peak latency (**b**) of the CAP after stimulation were compared with pre-stimulation values. Values normalized to the sham-operated situation. $P<0.05$ *, $P<0.001$***.

In vivo confocal time lapse imaging (figure 9) of the nerves stimulated at 20 Hz for 2 hours did not show any visible alterations to the morphology of the axon (figure 9b). However, nerve stimulation at 100 Hz for 2 hours caused virtually all of the imaged nodes to develop a reversible, bi-lobed mushroom-like dilation during the following 7 - 10 hours of imaging. In most cases the change would start between one and two hours after stimulation, peaking around 4 hours after stimulation. Thereafter the changes diminished, reverting to a more normal appearance by approximately 8 hours after stimulation, on average. In some of the imaged nodes, the swelling process was already occurring immediately after stopping the electrical stimulation, when the imaging in the confocal microscope was initiated, and it continued to develop for up to 6 hours before starting to recede (figure 10). In other

cases, the swelling process was only initiated six or seven hours after stimulation had ceased.
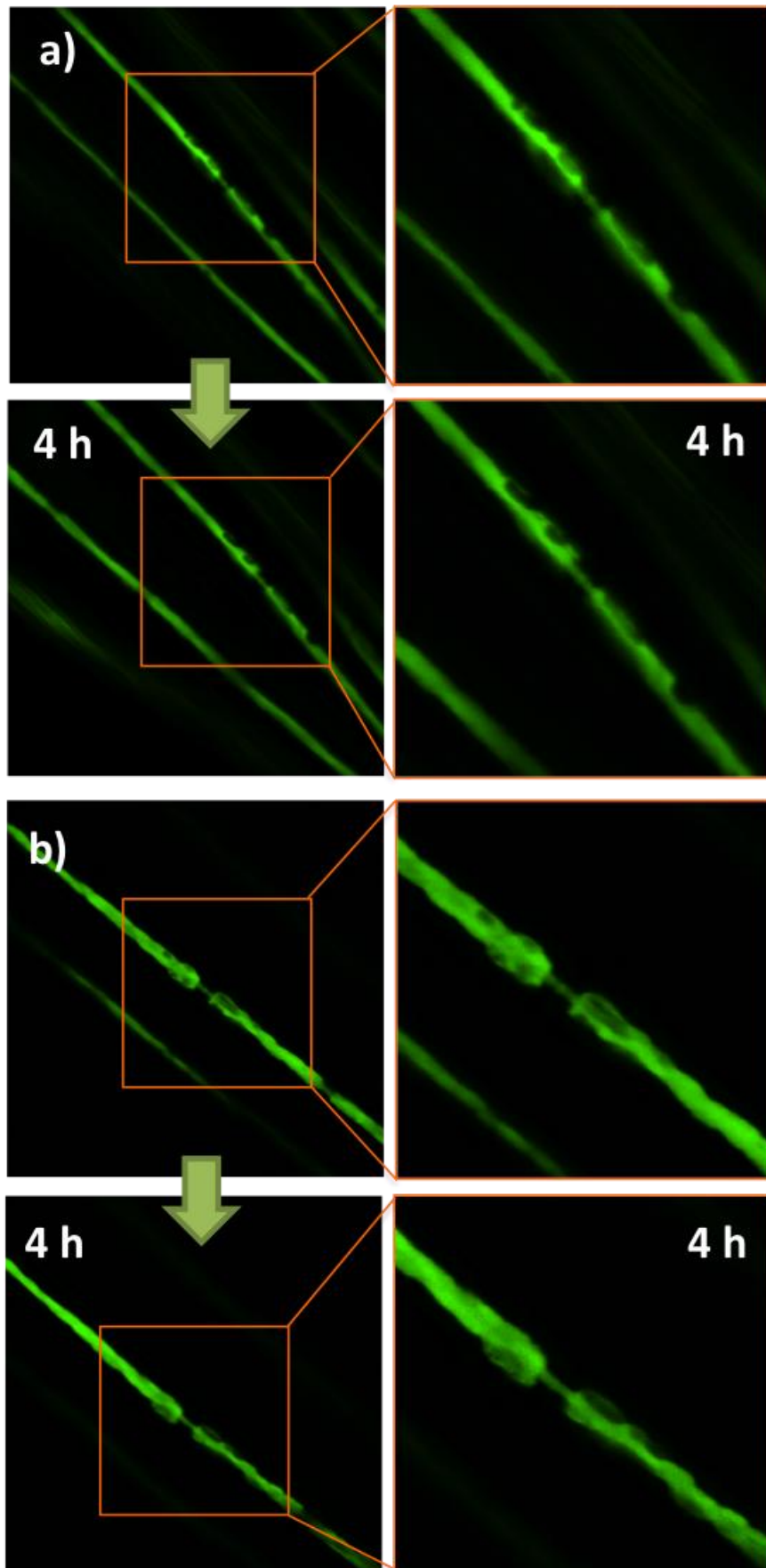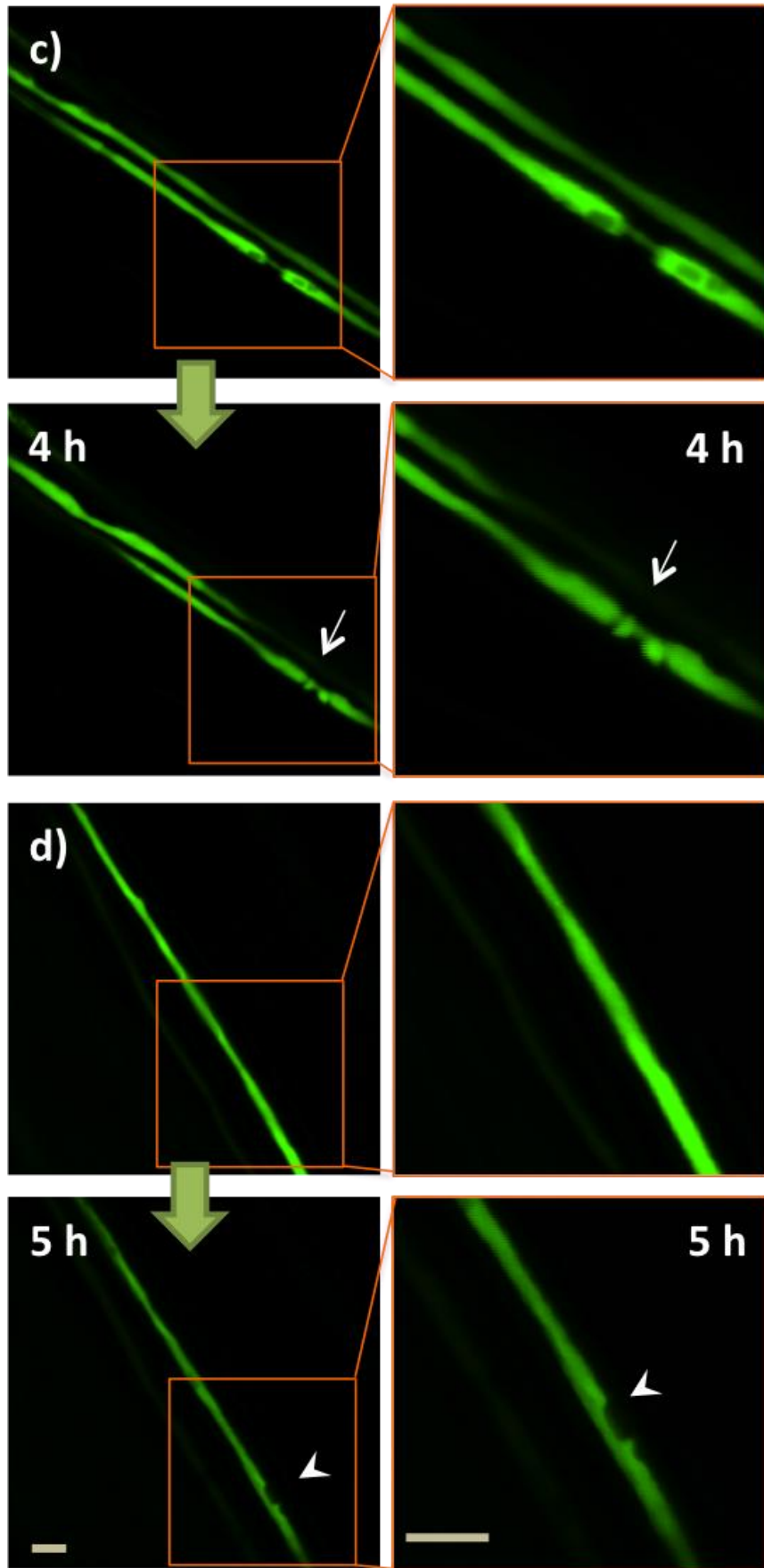
Figure 9a-d – Swelling of the paranodes in axons stimulated at high frequency.

In vivo confocal imaging of YFP positive axons in the mouse saphenous nerve before and 4 hours after stimulation. In control nerves (**a**), the nodes of Ranvier and the internodes of sham operated YFP positive axons did not change during the observation period. In other preparations a similar observation was made for nerves stimulated for 2 hours at 20 Hz (**b**), but in nerves stimulated for 2 hours at 100 Hz we observed the gradual appearance of a mushroom shaped expansion of the paranodes (**c**, **arrow**), followed by constrictions of the axoplasm (**arrowhead**) in the internode (**d)**. Scale bar is 10 μm.
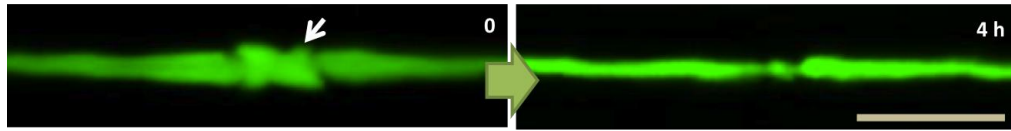
Figure 10 – Reversion of the paranodal swelling in axons stimulated at high frequency.

In vivo confocal imaging of YFP positive axons in the mouse saphenous immediately after and 4 hours after stimulation. In some nerves stimulated for 2 hours at 100 Hz, the mushroom shaped expansion of the paranodes was present immediately after stimulation (**arrow**), and it decreased in size 4 hours after stimulation. Scale bar is 10 μm.

It was also observed that there was a constriction of the internodal axoplasm (figure 9d), starting approximately three to four hours after stimulation, and continuing to expand for the duration of the imaging period (up to ten hours after stimulation). These constrictions were consistent with an interpretation of an expansion of the periaxonal space, such that the axoplasm was compressed away from the myelin. Further observation revealed that these constrictions could become 'droplet-like', and motile, eventually travelling to the node/paranode. The constrictions frequently appeared before the expansion of the paranode occurred (figure 11).
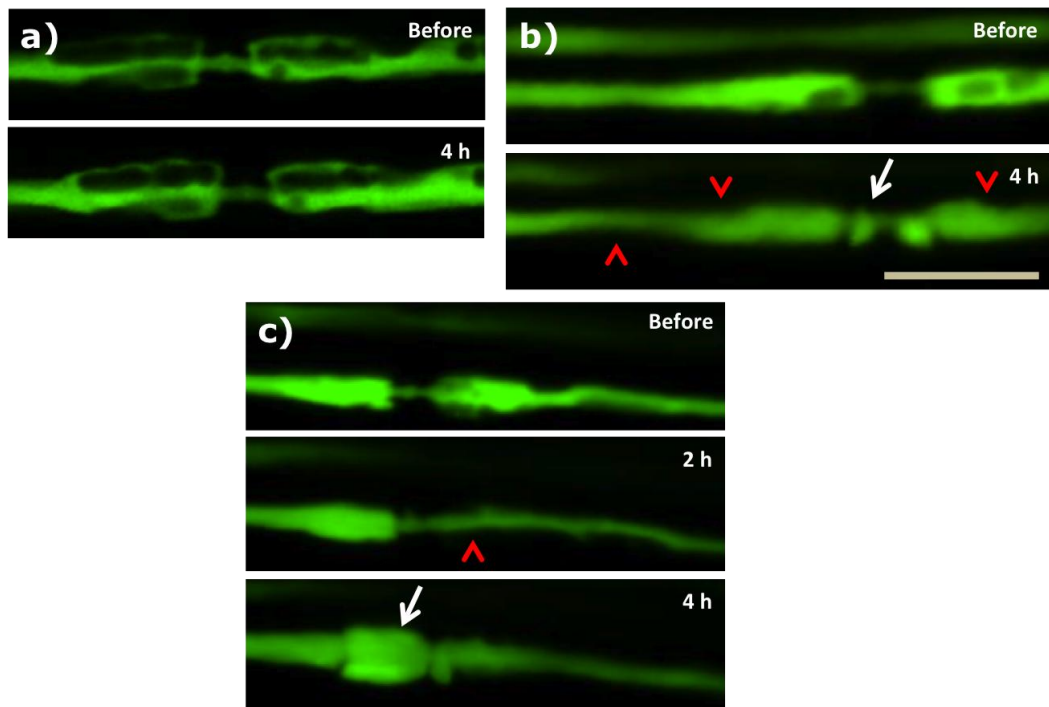
Figure 11a-d – Expansion of the periaxonal space and the swelling of the paranode.

In vivo confocal imaging of YFP positive axons in the mouse saphenous nerve before and after stimulation. In control nerves (**a**), the nodes of Ranvier and the internodes of sham operated YFP positive axons did not change during the observation period. In nerves stimulated for 2 hours at 100 Hz we observed the expansion of the periaxonal space at the paranodes (**red arrowhead**) preceding (**b**) or coinciding (**c**) with the swelling of the paranodes (**arrow**). Scale bar is 10 μm.

When these same nerves were later imaged by conventional bright field microscopy in semi-thin plastic longitudinal sections (after fixation and staining with thionin acetate and acridine orange) (figure 12) the interpretation of an expansion of the periaxonal space was reinforced. Even though the axonal morphology was not obviously altered upon direct observation on the confocal microscope following stimulation at 20 Hz, more detailed examination at bright field showed that the area of the nodes of

Ranvier and the distance between the paranodes (i.e. the nodal gap) tended to be increased in comparison with controls, even though the change was not statistically significant (figure 13).

These alterations were frequency-dependent, since axons stimulated at 100 Hz had a greater increase in both the area of the nodes of Ranvier and the length of the nodal gap than axons stimulated at 20 Hz. The imaging of these resin sections also showed that axons stimulated at 100 Hz exhibited a narrowing of the axoplasm in the internode, perhaps due to compression by an expansion of the periaxonal space. Indeed, the myelin was intact, but the axoplasm was constricted due to the appearance of a large, seemingly empty, space running longitudinally along the internode. It is easy to imagine that the images obtained by confocal microscopy *in vivo*, and by conventional microscopy after fixation, provide different views of the same phenomenon.
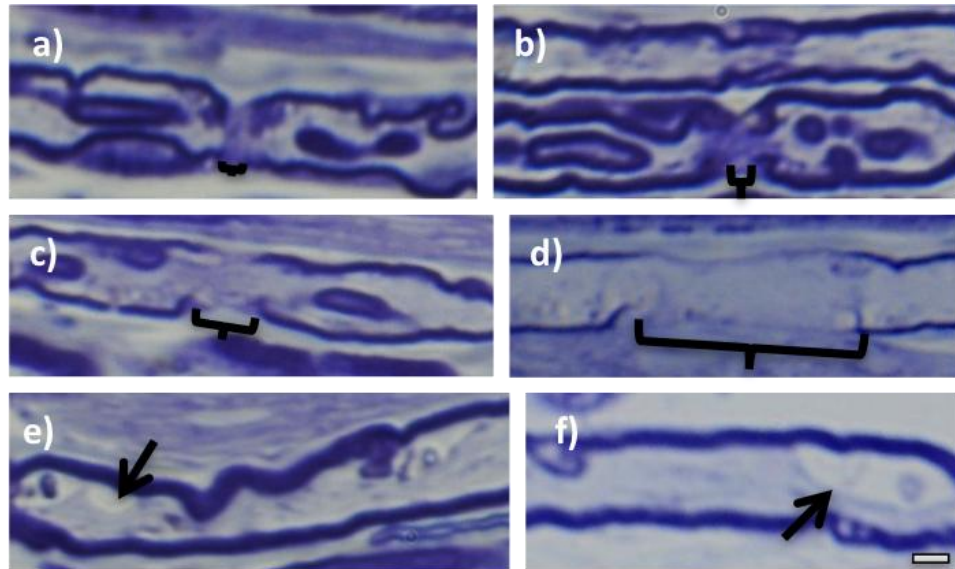
Figure 12a-f – Swelling of the nodes of Ranvier and expansion of the periaxonal space in electrically stimulated axons.

Longitudinal sections of saphenous nerves of mice fixed 6 hours after being sham operated (**a**), or stimulated for 2 hours with either 20 Hz (**b**) or 100 Hz (**c**, **d**, **e**, **f** and **g**), embedded in resin and stained with thionin acetate and acridine orange. Axons stimulated at 20 Hz for 2 hours exhibited a slight increase in the distance between the paranodes and a minimal swelling of the nodes of Ranvier (**b**, **brackets**). Axons stimulated at 100 Hz for 2 hours exhibited a longer nodal gap and a greater swelling of the nodes of Ranvier (**c**, **d** and **e**, **brackets**), as well as an expansion of the periaxonal space (**f**, **g**, **arrows**). Scale bar is 1 μm.
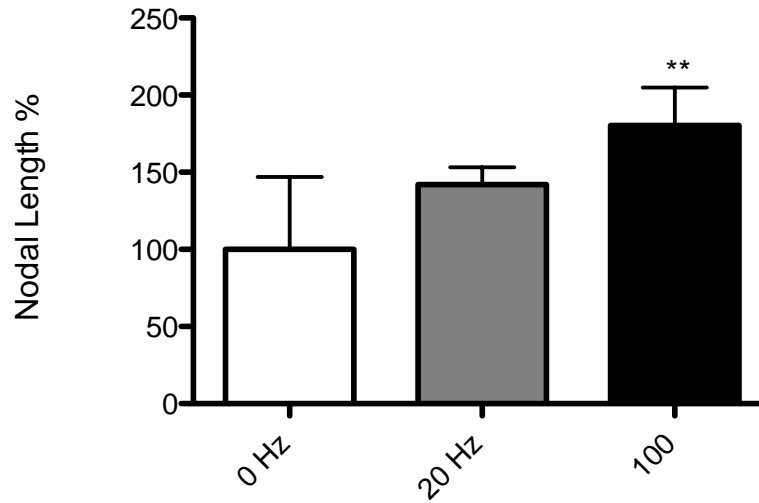
Figure 13 – Measurement of the nodal length of axons after high frequency stimulation.

Nerves stimulated at 20 Hz for 2 Hours showed in nodal length; these increases were greater in nerves stimulated at 100 Hz for 2 hours. The values were obtained by quantification of the bright field images and normalized to the values for the vehicle-treated axons (%). $p < 0.01$ **. N=>10 nodes from each of 4 animals.

Bright field imaging of resin-embedded, transverse sections, fixed after *in vivo* imaging (figure 14) also showed an expansion of the periaxonal space, separating the axoplasm from the myelin sheath. These sections also revealed the absence of oedema in electrically stimulated nerves (figure 14-c), assessed by determining the density of axons per nerve area.

Figure 14a-d– Expansion of the periaxonal space in electrically stimulated axons.

Transverse sections of saphenous nerves of mice fixed 6 hours after being sham operated (**a**), or stimulated for 2 hours with 100 Hz (**b**), embedded in resin and stained with thionin acetate and acridine orange. Stimulated axons exhibited an expansion of the periaxonal space (**arrow,** quantified in **d**), even though the number of axons per µm^2 remains unaltered (**c**). Scale bar is 10 µm.

Further electron microscopy imaging of the same and similar preparations (figure 15) confirmed the swelling of the nodes of Ranvier in axons stimulated at 100 Hz, with an increase in the volume of axoplasm, associated with shape reminiscent of the bi-lobed mushroom shape observed under the confocal microscope. Electron microscopy also showed that the dense undercoating of the nodal axolemma was not altered.
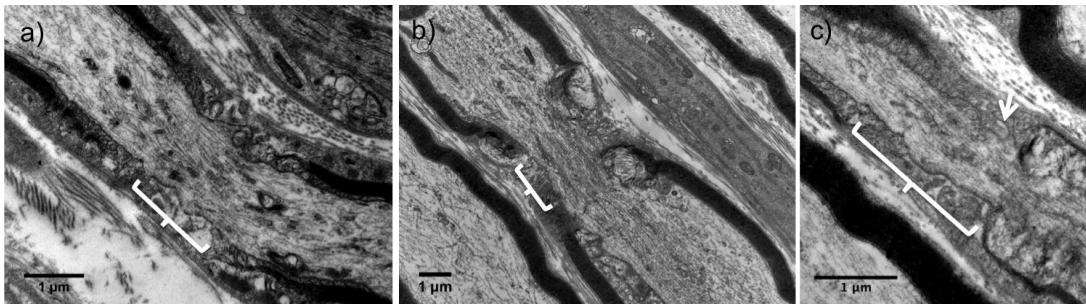
Figure 15a-c– Expansion of the nodal gap in electrically stimulated axons.

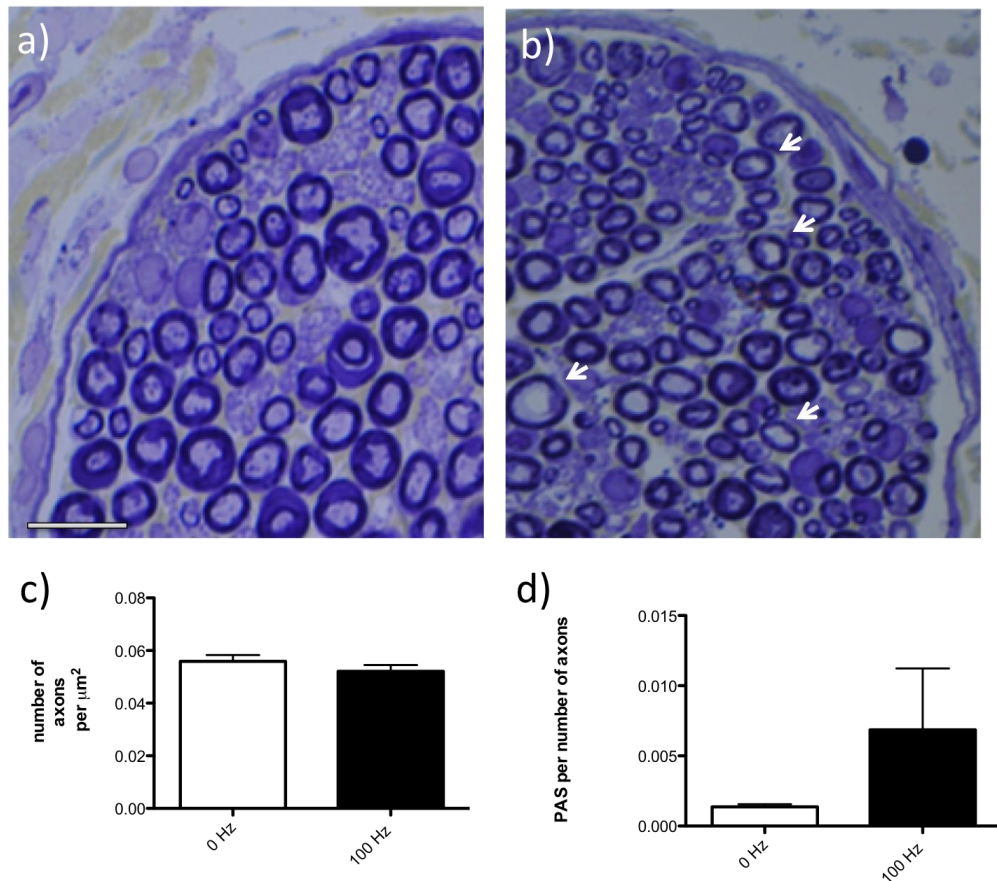Electron micrographs showing longitudinal sections of saphenous nerves of mice fixed 6 hours after being sham operated (**a**), or stimulated for 2 hours with 20 (**b**) and 100 Hz (**c**), embedded in resin stained for electron microscopy. Axons stimulated at 100 Hz for 2 hours exhibited a longer nodal gap and a swelling of the paranodes (**b**, **arrow**).

Similarly, electron microscopy imaging of the internodal area also revealed an expansion of the periaxonal space in electrically stimulated axons (figure 16). The axolemma separates from the Schwann cell membrane (figure 16-c) and the periaxonal space seems to assume the form of vacuole with some tissue on it (figure 16-d). The separation does not appear too disruptive to the myelin, as it showed no obvious morphological alterations.
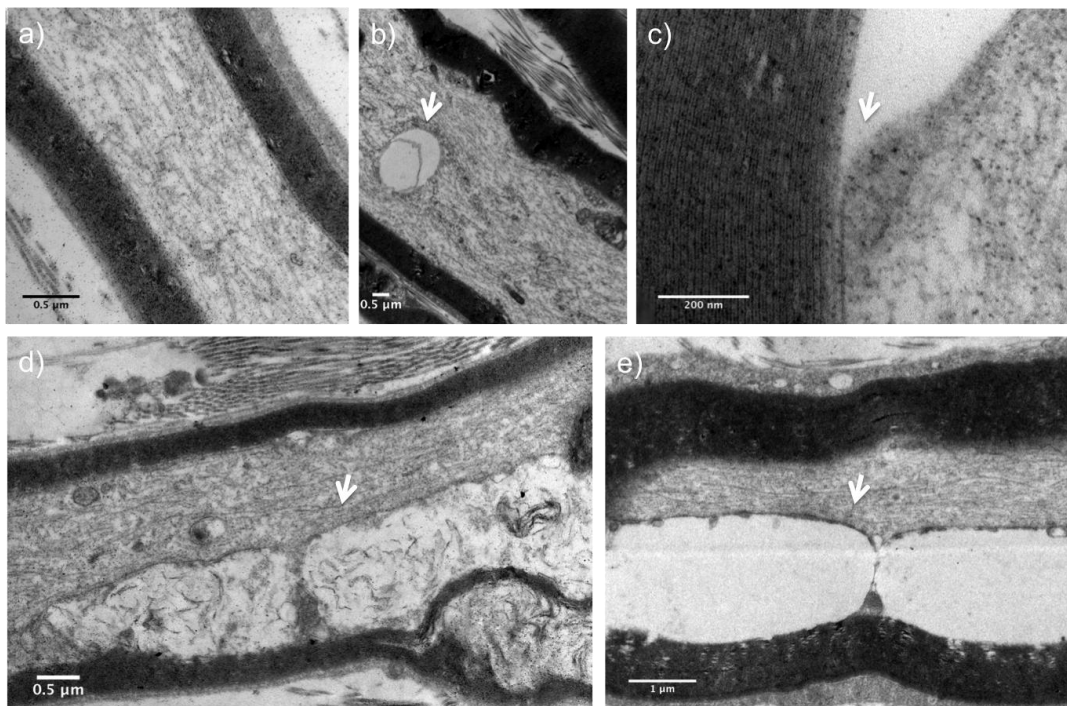
Figure 16a-d – Expansion of the periaxonal space in electrically stimulated axons.

Electron micrographs of longitudinal sections of saphenous nerves of mice fixed 6 hours after sham operation (**a**), or following electrical stimulation for 2 hours at 20 (**b**) and 100 Hz (**c**, **d** and **e**). Stimulated axons show the presence of vacuoles along the axoplasm, seemingly resulting from the separation of the axolemma from the Schwann cell membrane and consequently expansion of the periaxonal space (**arrows**).

Axonal morphological alterations do not noticeably impair the success of axonal conduction

In a parallel experiment, after *in vivo* stimulation of the saphenous nerve at 100 Hz for 2 hours, the CAPs were recorded every hour after stimulation, in a time-window similar to that of the *in vivo* imaging (figure 17).
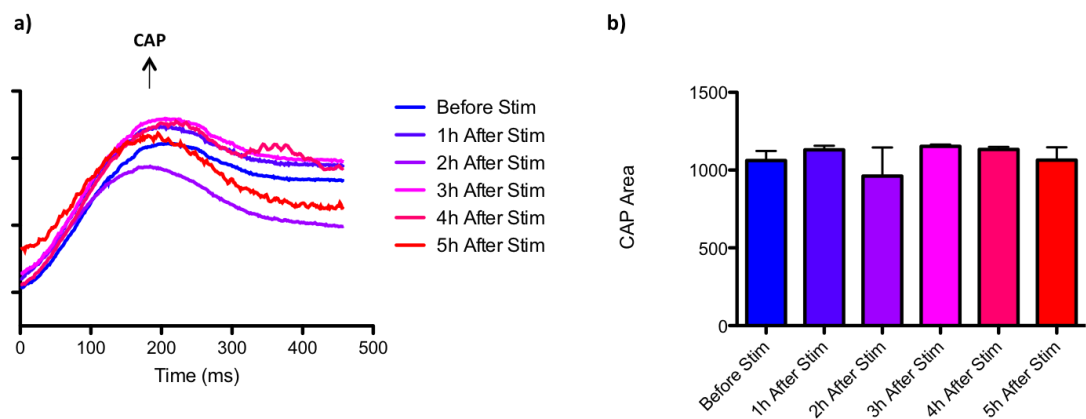
Figure 17a-b - Evolution of the compound action potential following sustained electrical stimulation.

CAPs obtained from proximal saphenous nerve in response to supramaximal, distal electrical stimulation, following 2 hours of stimulation at 100 Hz. The shape (**a**) and area under the curve (**b**) of the CAP is relatively constant during the first 5 hours after sustained stimulation, and similar to that obtained before the onset of sustained stimulation. N=3 animals.

These results show that the CAP returns to its original shape by 1 hour after stimulation, and during the time-window in which the morphological changes are prominent the axonal conduction persists and the CAP largely maintains its shape.

Unmyelinated fibres appear to be morphologically unaltered following sustained high frequency stimulation

Electron microscopic imaging of electrically stimulated nerves does not reveal any obvious morphological alterations in unmyelinated fibres, such as oedema or swelling (figure 18).
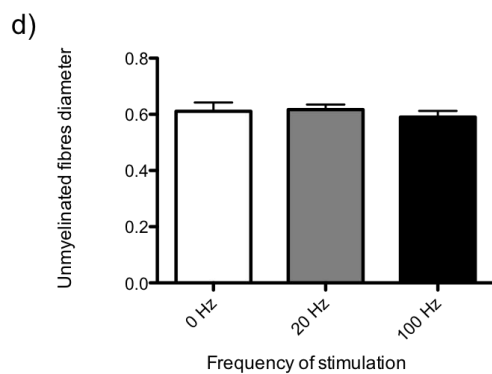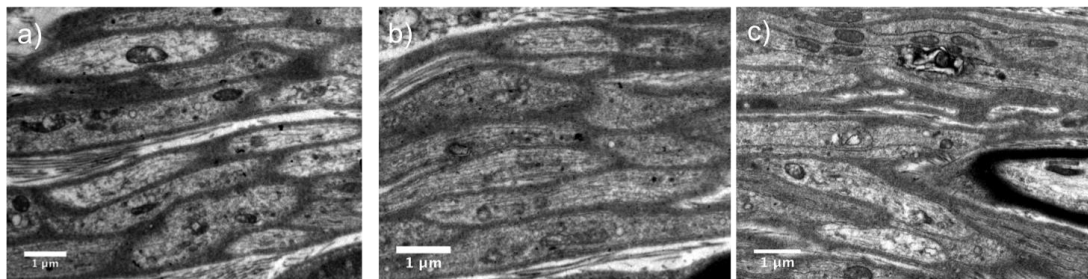
Figure 18a-d – Stimulated unmyelinated fibres do not show obvious morphological alterations

Electron micrographs of longitudinal sections of saphenous nerves of mice fixed 6 hours after sham operation (**a**) or following electrical stimulation for 2 hours at 20 (**b**) and 100 Hz (**c**), show no obvious morphological alterations. There was no variation in unmyelinated fibre diameter with stimulation (**d**). N=>20 axons from each of 3 animals.

Reversibility of the axonal morphological alterations in response to electrical stimulation

Imaging of saphenous nerves 24 hours after stimulation showed no alterations in the paranodes and nodes of Ranvier, compared with control, but imaging of the internode showed the presence of deformations of the axoplasm, which suggests that the periaxonal space is still expanded. This expansion of the PAS seemed to be reversible, since it diminished over the next days, being nearly resolved one week after stimulation (figure 19).
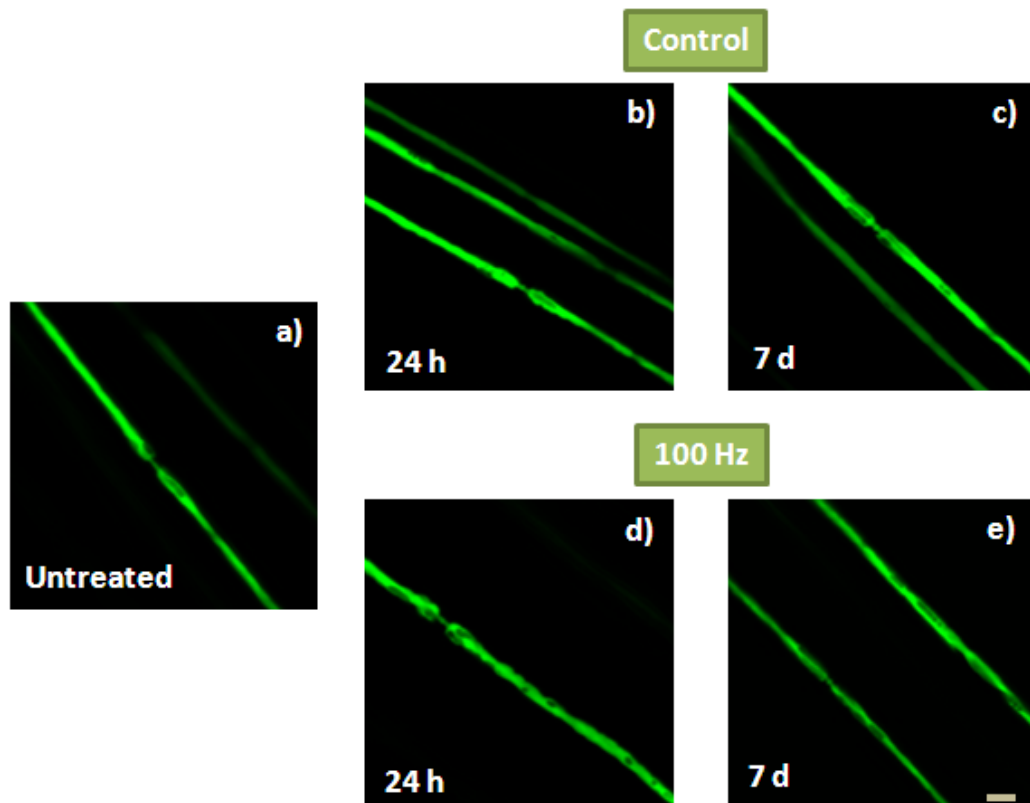
Figure 19a-e - Evolution of the expansion of the periaxonal space through time.

In different preparations control nerves (submitted to sham surgery but no stimulation) exhibit normal looking axons, similar to untreated ones (**a**), both 24 hours (**b**) and 7 days (**c**) after surgery. In other preparations, 24 hours after electrical stimulation at 100Hz (**d**), the axons present a high number of 'holes' and constrictions in the

internodal axoplasm, while 7 days after electrical stimulation at 100 Hz (**f**), in a different preparation, the appearance of the axon looks more similar to controls. Scale bar is 10 µm.

The recovery from expansion of the PAS was confirmed by measuring the volume of 'z-stacks' (i.e. serial scans of the node at different focal planes with a separation of 0.3 µm, as to allow a full three dimensional reconstruction of the imaged object) of all the imaged YFP-positive axons at different time points after electrical stimulation at 100 Hz. That is, the gaps and 'holes' that appeared in the internode immediately after stimulation caused a decrease in the volume of the axon when compared with the control nerves (figure 20). The PAS thereafter started to recover its original dimensions. It is notable that no degeneration or demyelination were observed either by confocal or bright field microscopy at any time points, especially in transverse sections, seven days after stimulation (figure 21).
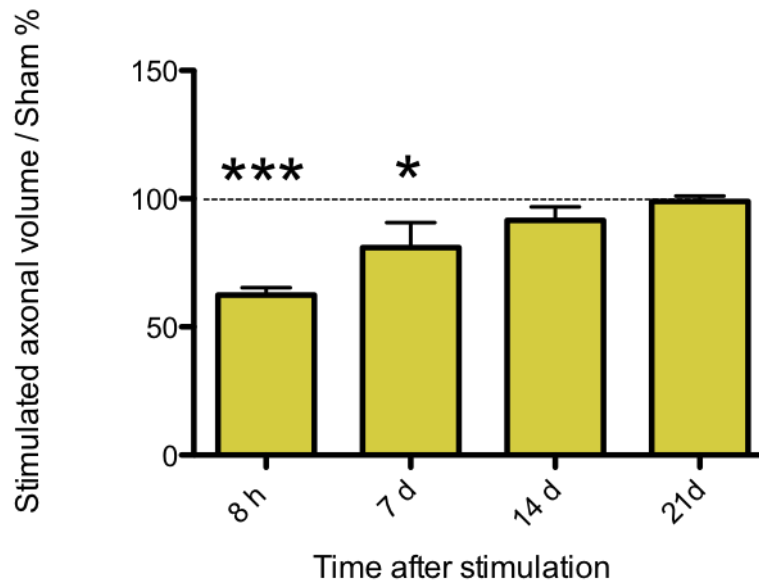
Figure 20–Variation over time of the volume of the whole axon in nerves stimulated at 100 Hz for 2 hours.

The volume of axons stimulated for 2 hours at 100 Hz is reduced in comparison with controls at 8 hours following stimulation. The normal volume was partially restored by 7 days, and fully restored by 2 and 3 weeks. The images analysed were z-stacks (0.3 µm slice thickness) obtained with confocal microscopy and quantification was performed for the whole portion of the axon imaged. *=p<0.05, ***=p<0.001. N = >9 axons from each of 4 animals/condition.
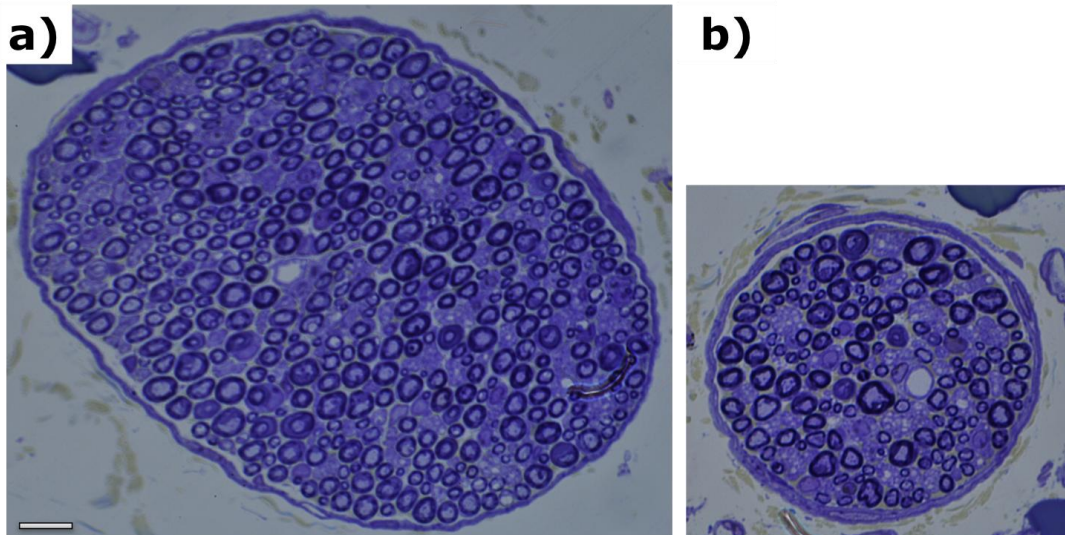
Figure 21a-b - Absence of degeneration or de/remyelination in electrically stimulated axons.

Light microscope imaging of transverse sections of the saphenous nerve seven days after electrical stimulation at 100 Hz for 2 hours. The stimulated nerves (**a**) are similar to control (**b**), with no evidence of axonal degeneration, demyelination or remyelination. Scale bar is 10 μm.

Impairment of blood supply provokes an expansion of the node of Ranvier at lower frequencies of stimulation

Studies of axonal function in situations of impaired blood supply have revealed an interesting finding: in animals in which the circulation of blood was impaired by compression of the nerve and its surrounding blood vessels, stimulation at only 20 Hz at supra-maximal voltage for 2 hours showed both axoplasmic herniation at the node and expansion of the periaxonal space (figure 22). Even though the extent of these phenomena was not as dramatic as that in control animals stimulated at 100 Hz for 2 hours, it was still much more intense than what was observed in control animals stimulated with the same conditions but with normal blood circulation (figure 23).
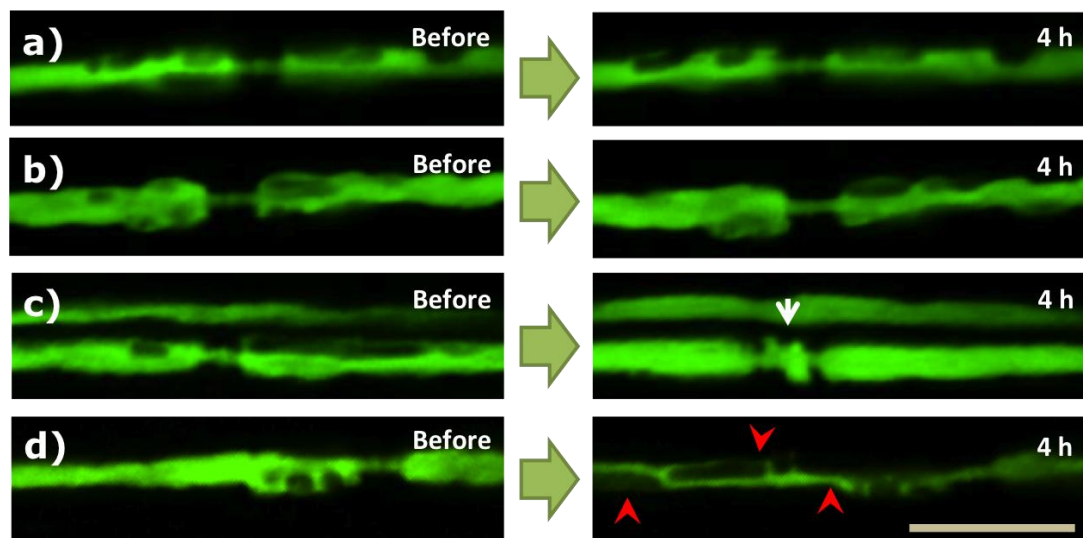
Figure 22a-d – Axonal morphological alterations after electrical stimulation in axons with impaired blood flow.

In vivo confocal imaging of YFP+ positive axons in the mouse saphenous nerve before, and 4 hours after, either sham stimulation (**a**), stimulation at 20 Hz for two hours (**b**), or stimulation at 20 Hz for two hours during impaired blood circulation (**c** and

d). The two control conditions did not result in any morphological changes, but stimulation of partially ischaemic nerves caused an expansion of the nodes of Ranvier (**c**, **arrow**), as well as the appearance of discontinuities of the axoplasm along the internode (**d**, **red arrowhead**). Scale bar is 10 µm.
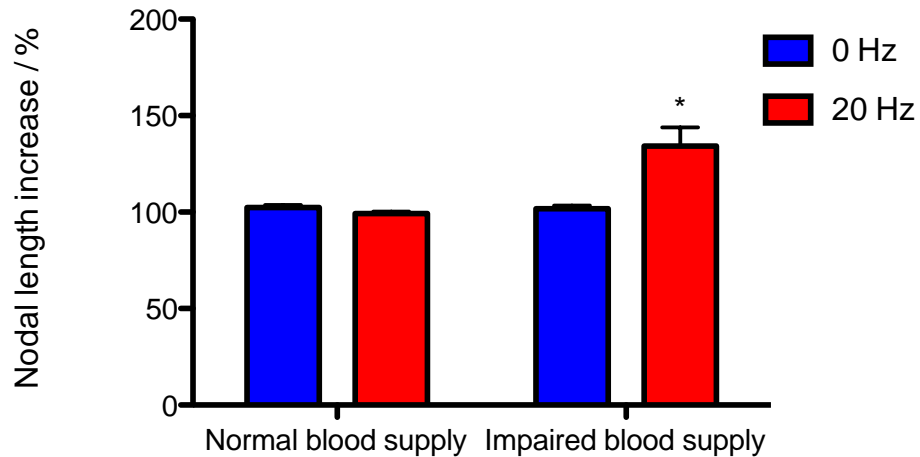
Figure 23 – Increase in nodal length in axons with impaired blood supply, following stimulation at 20 Hz.

Quantification of increase in nodal length 4 hours after stimulation and comparing with before stimulation, in axons with normal and impaired blood supply following stimulation for two hours at 20 Hz. The normal blood supply conditions did not result in any morphological changes, but stimulation of partially ischaemic nerves caused an increase in nodal length in stimulated nerves. The images analyzed were obtained *in vivo* with confocal microscopy. Statistical test used was Student's t-test with two-tailed distribution, two-sample equal variance. *=$p<0.05$, N=9 nodes from each of 4 animals.

2.4 Discussion

We have studied the morphological consequences of sustained impulse activity in nerve fibres. The findings show that the axons in the peripheral nervous system undergo reversible drastic morphological changes. However, the facts that these morphological changes are triggered by a physiological phenomenon (i.e. impulse activity) and the reversibility of these alterations show that they can be part of the normal repertoire of axonal function.

First, the internodal periaxonal space is focally expanded, such that the axoplasm becomes displaced to one side. Some material is adherent to the outer aspect of axolemma, bordering the widened periaxonal space. This is consistent with a shearing between membranes at the Schwann cell-axon interface, and would also explain the presence of lamellar material. However, there is no evidence of breaching of the paranodal axolemma. Interestingly, these expansions are mobile and travel down the internode until they reach the paranode. Second, a transient, localised herniation of the axoplasm is confined to the paranodal regions, on either side of the node of Ranvier, that becomes directed back over the outside of the axon in a 'capping' manner, seemingly channelled by the basal lamina, associated with an increase in the nodal gap and volume.

Surprisingly, both changes are fully reversible over time: the nodal changes resolve over hours/days, whereas the periaxonal space returns to normal over a period of days/weeks. The Schmidt-Lanterman incisures and internodal myelin appear unaffected, as does the perineurium. Indeed, there

is no evidence of widened endoneurial space or disturbance of the orientation of endoneurial collagen, and no obvious abnormalities were found in the endoneurial blood vessels. The mitochondria in both the paranodal Schwann cytoplasm and throughout the axoplasm of myelinated axons look morphologically normal. Schwann cell basal laminae are intact, with no evidence of redundant loops of basal lamina. Our data show that axons can continue conducting while the changes are present, and that no degeneration is associated with these alterations, which is not particularly surprising considering that the nodal membrane is unaltered even during the most extreme morphological alterations, therefore maintaining the impulse conduction (Korobkin, et al. 1975).

The fact that one of the morphological changes (expansion of the periaxonal space) normally precedes the other (swelling of the paranodes) raises the hypothesis of a direct physical correlation between the two (i.e. negative axonal pressure due to a nodal expansion being resolved by an expansion of the PAS, or positive axonal pressure caused by the PAS expansion leading to the paranodal swelling). Osmotic pressure effects could potentially explain the observed axon bites due to expansion of the periaxonal space: the efflux of ions to the PAS due to the sodium pump would cause the swelling. The paranodal swelling could be seen as resulting from osmotic pressure caused by the influx of Na^+ ions during stimulation that reversibly distorts the axon morphology, since this situation resolves after a couple of hours. However, the observed time delay (in some cases up to 4 hours after electrical stimulation has ceased) does not sit easily with this explanation. Another explanation would be an increased pressure in the axoplasm due to the

expansion of the periaxonal space, which would cause the axoplasm to herniate in the region where it is less tightly bound, rather like squeezing toothpaste from a tube by pressing the barrel. However, even though the case could be made that osmotic factors are consequential to ionic displacement following sustained stimulation, not enough data has been presented to propose a definitive mechanism behind it.

The facts that these morphological changes are triggered by a physiological phenomenon (impulse activity) and that the alterations are reversible, show that they could be part of the normal repertoire of axonal function. It is interesting to consider whether this 'normal' property of axons might also contribute to axonal pathology in neuroinflammatory disease.

Additionally, the reversibility of these morphological alterations suggests that the recovery mechanism must be a local one, which suggests that Schwann cells might not be passive spectators, but actively participate in the maintenance of axonal integrity. Schwann cells have been previously indicated to actively participate in axonal organelle scavenging in both normal and pathological fibres (Spencer and Thomas 1974). Indeed, analysis of the electro-micrographs suggests that some of the paranodal vesicles could also result from the disruption of the axon-Schwann cell network. This network usually contains membranous debris and residual bodies, reflecting its ability to sequester and degrade worn-out constituents (Spencer and Thomas 1974, Snyder 1989, Gatzinsky and Berthold, 1990). The axon-Schwann cell network could then be one of the components dealing with the paranodal alterations, expansion of the periaxonal space, and the associated

cell membrane disruption and resulting debris created following sustained electrical stimulation.

The observation of the swelling of the paranodes following sustained stimulation is similar to that obtained following treatment with venoms that slow the inactivation of sodium channels (Love and Cruz-Höfling, 1986). They observed a swelling at the node of Ranvier, with the greatest axonal distension also happening in the myelin attachment zone, and discuss that it might be caused by a rise in intra-axonal pressure. This was suggested to be due to the reinforcement of the nodal axolemma by its electron-dense undercoat, composed by network of fine filaments circumferentially oriented (Ellisman and Porter, 1980). Evolutionarily, it would make sense for the node of Ranvier to be reinforced, due to its critical role in saltatory conduction (Korobkin, et al. 1975), with the paranodes providing the region with enough plasticity to cope with eventual volume adaptations.

Indeed, the paranodal constriction has been described as capable of slow distension (Jones and Cavanagh, 1983), and myelin membranes are mobile during PNS myelination and pathologic conditions, due to a dynamic interaction between actin microfilaments and transmembrane proteins (Trapp 1990). The slippage of membranes has been discussed in the process of myelin sheath expansion in swollen nerve fibres (Friede and Martinez, 1970, Friede and Miyagishi, 1972), and in some pathological conditions the axon can actually be separated from its Schwann cell by an invading monocyte or lymphocyte (Scholz and Woolf, 2007).

Whatever the mechanism behind these alterations is, the results show that axons can undergo profound, yet reversible, morphological changes in response to sustained electrical activity, suggesting an extraordinary degree of plasticity. The fact that these changes are worsened by impairment of blood supply suggests that similar, reversible morphological changes may occur during normal life, and especially under pathological conditions. When present, the changes may confer a susceptibility to permanent structural damage, including degeneration and loss of signal conduction.

In our laboratory, it was previously observed that in *ex vivo* preparations of normal axons, pharmacological opening of Na_v channels with veratridine (a lipid soluble sodium channel modifier that causes persistent activation of the channel) results in a reversible, prominent widening of the PAS. The widening takes the form of 'balloons' that compress the axon, giving the impression that the PAS might be acting as a membrane bound 'extracellular cell', swelling by osmotic force (KJ Smith, unpublished observations), with the cell membrane on one side being formed by the axolemma and on the other by the Schwann cell membrane. If osmotic pressure is indeed the force behind this morphological alteration, the identity of the ions(s) responsible for the imbalance is unclear. However, an educated guess would indicate the accumulation of Na^+ ions that have been held up on their way back to the extracellular space as a plausible candidate. This will be pursued in further chapters of this thesis.

3 Modulation of nerve stimulation: a chemical approach

3.1 Introduction

Our earlier results have shown that axons undergo profound, reversible, morphological changes in response to sustained electrical activity. These include an expansion of the internodal periaxonal space, which compresses the internodal axoplasm. Later, the axoplasm can herniate on either side of the nodal membrane, displacing the paranodal loops and resulting in a greatly widened nodal gap. The herniating axoplasm appears to be constrained by the basal lamina so that it becomes directed back over the outside of the axon in a 'capping' manner. Surprisingly, these morphological alterations are entirely reversible over days, and the normal axonal morphology is restored, and impulse conduction continues throughout.

Time-lapse study suggests that the herniation is due to a rise in intraxonal pressure arising from the expanding periaxonal space. To further study these alterations, our strategy has been to increase sodium channel opening by chemical methods. To do so, we have used veratridine, which is an agonist of voltage gated sodium channels, increasing their open time and thereby facilitating depolarization of the resting membrane potential and repetitive firing.

To characterize the mechanism behind these morphological alterations, we wanted to be able to modulate the environment of the axon while dealing

with sustained stimulation. The simplest way to attain this was by modifying the environment of excised spinal roots. Ventral (motor) and dorsal (sensory) spinal nerve roots emerge from the lateral surfaces of the spinal cord. These are very useful tools to be used in *ex vivo* experiments, since the high number of roots per animal enables alteration of the experimental parameters in different roots originating from the same animal, whilst simultaneously using some roots as internal controls for each experiment.

The specific effect of the initial influx of sodium ions into the axon was studied with the drug veratridine, which facilitates the opening of sodium channels, and the drug lidocaine, which blocks sodium channels. To understand the consequences of the movement of different ions and the part played by the different ionic channels and transporters in the morphological alterations, we have employed other chemical tools. The movement of potassium ions was studied with the drug 4-aminopyridine, which blocks K_v channels. We finally used ouabain, which blocks the sodium pump, to understand the role of this complex in the restoration of homeostasis and its correlation with the previously observed morphological alterations.

Uncontrolled ionic movement can alter the osmotic homeostasis, which could be the explanation for at least some of the observed morphological alterations following sustained stimulation. To assess the role of osmotic pressure, we decided to modulate the saline content of the medium bathing the nerve, and hence its osmolarity, to generate different hyper- and hypotonic conditions. That way, whilst maintaining the original ionic content of the excised spinal roots, we would be able to observe their morphological

responses to the effects of water movement to and from the axon in response to osmotic pressure, and how that correlates with our previous observations.

The first goal of the proposed experiments was to determine whether the results obtained with electrical stimulation could be replicated with chemical stimulation. Secondly, by modulating the axonal environment, we hoped to shed light on the cause of these morphological alterations, revealing the mechanism behind the consequences of electrical activity, and hopefully providing us with new information concerning the homeostasis of the axonal conduction in normal situations, which could be further applied to pathological conditions.

3.2 Material and methods

In order to have a real time visual measure of morphological alterations, we decided to continue using the same transgenic mice(Feng, et al. 2000),Thy1-YFP-16,in which 1-2% of the sensory and motor axons are labelled with yellow fluorescent protein (YFP). All surgical procedures were performed under sterile conditions.

This study was conducted mainly on the saphenous nerve. For the *in vivo* chemical stimulation studies the animals were anaesthetized with 3.5% isoflurane, with the quantity of anaesthetic monitored. The saphenous nerve was exposed in the mid-thigh and following an initial imaging period, veratridine (100 µM) or vehicle (0.67% DMSO in saline solution, the same concentration of the veratridine treatment) was applied topically with cotton balls immersed in the solution. After drug treatment, a coverslip was placed on the saphenous nerve and it was imaged, *in vivo*, using a confocal laser-scanning microscope (LSM 5 Pascal, Carl Zeiss, Jena, Germany). At least 9 different nodes of Ranvier in different axons were imaged in an individual preparation, and either a single image was recorded every 10 minutes, or a z-stack was recorded every 20 minutes, for a period varying between 5 and 10 hours after stimulation.

After *in vivo* imaging, the nerves were fixed in glutaraldehyde for at least 24 hours and the central 5 mm length of each fixed nerve was excised. The nerves were then embedded in resin as previously described, using Beem capsules for longitudinal sections or coffin moulds for transverse sections.

0.7 μm thick sections were cut and collected onto slides and stained with thionin acetate and acridine orange. These sections were then screened in a light microscope with an attached photographic camera. Ultrathin (70 nm thick, silver color) sections from selected blocks were subsequently examined further in an electron microscope (JEM-1010 Electron Microscope, JEOL).

Ex vivo drug experiments were performed in both excised saphenous nerves and spinal roots. Saphenous nerves, approximately 2 cm in length, or dorsal and ventral spinal roots, approximately 1 cm in length, were removed from terminally anesthetized Thy1-YFP-16 mice and placed on a petri dish, held in place by Vaseline. Vaseline was also used to delimit an individual chamber for each nerve or root. The excised tissue was incubated at 37º C in oxygenated artificial cerebrospinal fluid, renewed every 45 minutes. The aCSF composition was NaCl 125 mM, KCl 2.5 mM, $MgCl_2.6H_2O$ 1 mM, $CaCl_2.2H_2O$ 2 mM, $NaH_2PO_4.H_2O$ 1.25 mM, and $NaHCO_3$ 25 mM, in $_dH_2O$. Different dilutions of hypo-osmotic aCSF were used in the osmotic studies. For that, dH_2O was used to obtain aCSF with a 10%, 25% and 50% dilution. Hyper-osmotic aCSF was obtained by adding an excess of 200 mM NaCl (Iitake, et al. 1989).

When the experiment involved *ex vivo* drug treatments, unless stated otherwise, the spinal roots were incubated immediately after excision in aCSF (control) or in aCSF containing ouabain (1 mM, dissolved in aCSF; blocks the sodium pump), 4-aminopyridine (100 μM dissolved in aCSF; potassium channel blocking agent) or lidocaine (500 μM, dissolved in aCSF;

blocks sodium channels). Following an initial imaging observation, these roots were incubated with veratridine (100 µM; opens sodium channels) or vehicle (0.67% DMSO in aCSF) for 10 minutes and then re-incubated with the original solution, and imaged every 45 minutes with a water-dipping objective in a confocal microscope. Imaging consisted of 5 nodes imaged per condition per time point, with collection of z-stacks with 0.5 µm thick slices.

When electrical stimulation was applied to the saphenous nerve, *in vivo*, it was done using the same protocol as previously described. Briefly, after a small skin incision to expose the saphenous nerve, a pair of stimulating electrodes was placed directly in contact with the saphenous nerve, distally to the imaging site: the recording electrode was placed directly in contact with the saphenous nerve proximal to the imaging site. The ground electrode was inserted under the skin of the thigh between the stimulating and recording electrodes. Sustained high frequency stimulation was performed by stimulation at 100 Hz for a period of 2 hours. Following stimulation, ouabain (1 mM, dissolved in aCSF) or vehicle (aCSF) was applied topically with cotton balls immersed in the solution. Imaging was performed as previously described.

All the graphics here presented were obtained with GraphPad Prism (GraphPad Software, Inc.), after initial data processing with Microsoft Excel (Microsoft Corporation), unless stated otherwise. The statistics test used was 1 way ANOVA with Tukey's multiple comparison test post-hoc, unless stated otherwise.

3.3 Results

Chemical "stimulation"

Having established that electrical stimulation at physiological frequencies can result in morphological changes in myelinated axons, we now wished to develop a method that would allow the molecular modulation of the behaviour of ionic channels during the period of electrical activity. We therefore firstly employed a drug, veratridine, which causes a persistent opening of sodium channels, hoping to replicate the morphological effects of sustained electrical stimulation.

Axon treatment with vehicle did not cause morphological alterations

Topical application of the vehicle used to deliver veratridine (0.67% DMSO in saline, applied for 10 minutes) to the saphenous nerve of Thy1-YFP-16 transgenic mice showed no morphological disturbances when the preparation was imaged *in vivo*, via confocal microscopy, for the whole imaging period (up to 7 hours) (figure 24).
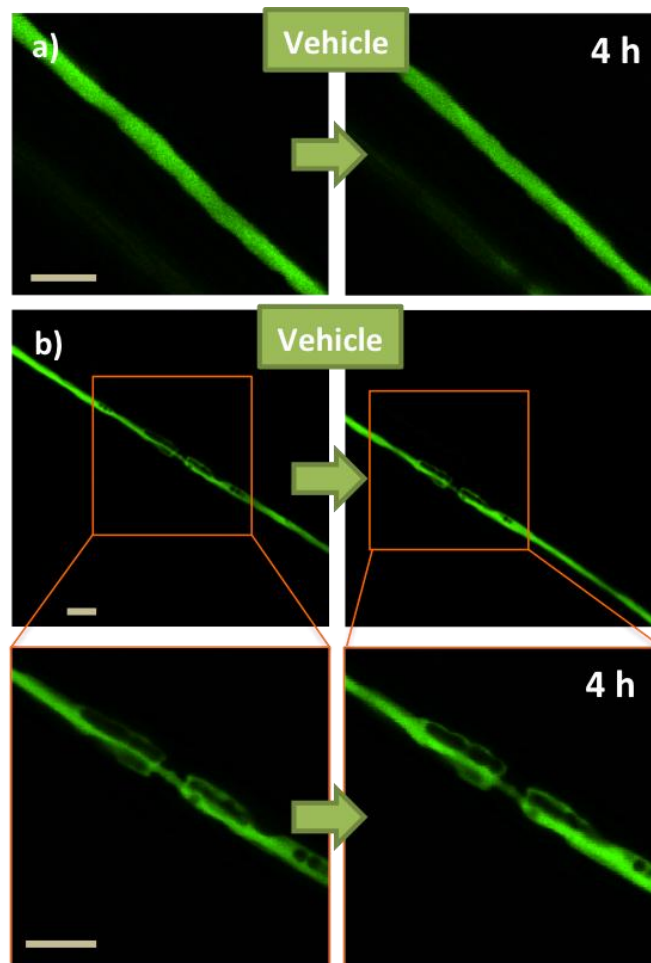
Figure 24a-b – **Absence of morphological alterations of the axoplasm of axons treated with vehicle.**

In vivo confocal imaging of YFP positive axons in the mouse saphenous nerve before (left panels) and 4 hours after (right panels)exposure to vehicle. The axoplasm of the internode (**a**) and the node of Ranvier (**b**) in YFP positive axons treated for 10 minutes with vehicle (saline + DMSO) did not change during an observation period of 4 hours. Scale bars are 10 µm.

Veratridine replicates the effects of electrical stimulation in the morphology of the axon

Topical application of veratridine (100 µM, applied for 10 minutes) to the saphenous nerve of Thy1-YFP-16 transgenic mice revealed a series of events consistent with the herniation of the paranodal axoplasm, forming the same bi-lobed mushroom shape that was observed after electrical stimulation (figure 25). This phenomenon was examined in more detail using serial confocal 'z-stacks', taken at different times (images obtained every 20 minutes) to reveal the temporal changes in the structure of the node.

The paranodal herniation was initiated within as early as one hour following veratridine application (figures 25 and 26), and just before it was initiated, the 'fluted' shape of the axon was lost and the paranodes appeared to retract, widening the nodal gap. This expansion continued for a period of 2-4 hours, when a 'mushrooming' of axoplasm occurred, happening semi-symmetrically on either side. The expansion reached a plateau and then started to revert towards normal, although the normal configuration was not achieved by the end of the observation period of up to 10 hours.
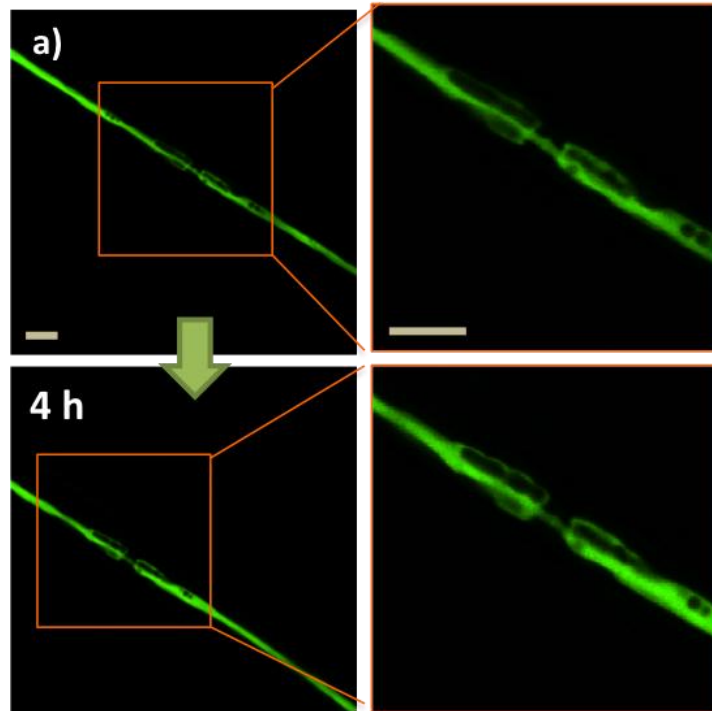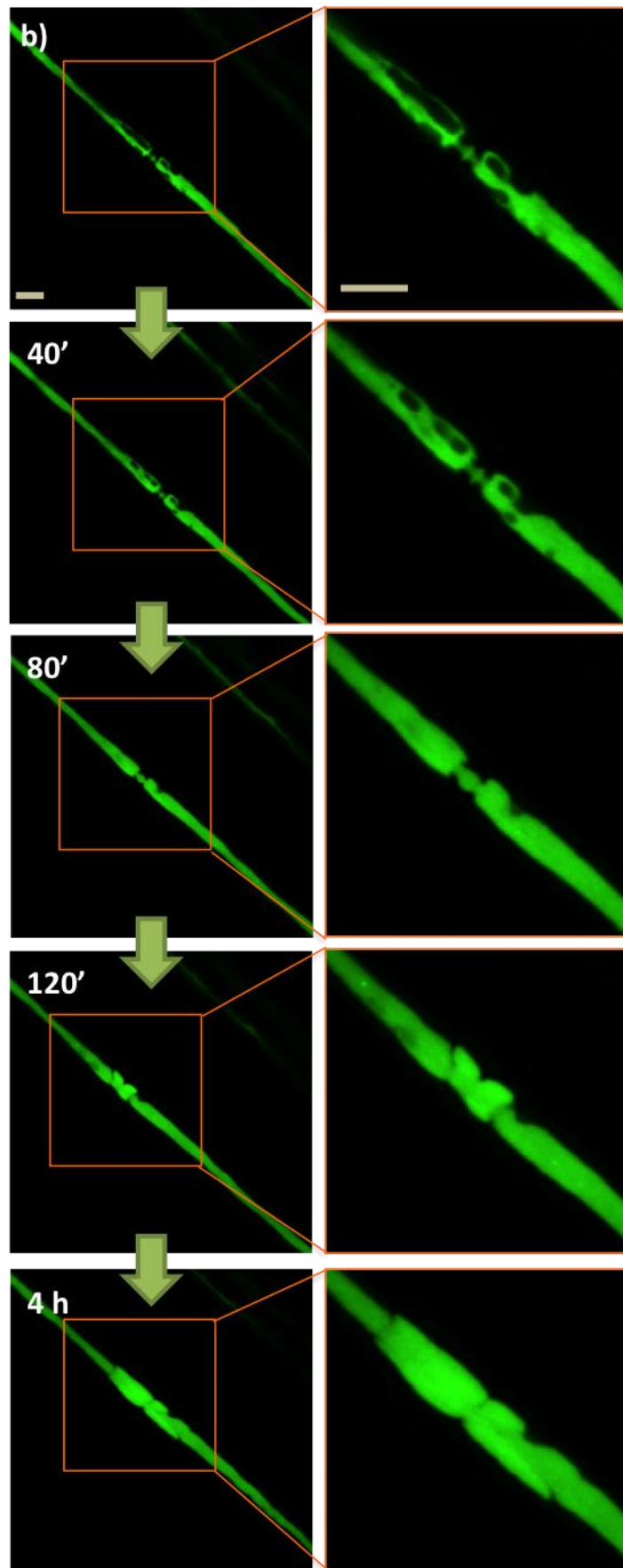
Figure 25a-b − Axoplasmic herniation at the paranodes in axons treated with veratridine.

In vivo confocal imaging of mouse YFP positive axons in the saphenous nerves before (left panels) and up to 4 hours after exposure to drug (right panels).In the control nerves (**a**), the axoplasm of the node of Ranvier of YFP positive axons did not change during an observation period of 4 hours before and after treatment, but in other preparations (**b**), treatment with veratridine for 10 minutes resulted in a retraction of the paranodes around one hour after treatment, at which point a mushroom like structure starts to expand from the paranodes, reaching a maximum bi-lobed volume 4 hours after treatment. Scale bar is 10 μm.

Similarly, measurement of the variation of the volume included in the nodal gap with time (figure 26) showed that it peaked four hours after treatment, after which it started to decrease, stabilizing to reach a plateau 10% above the control condition.
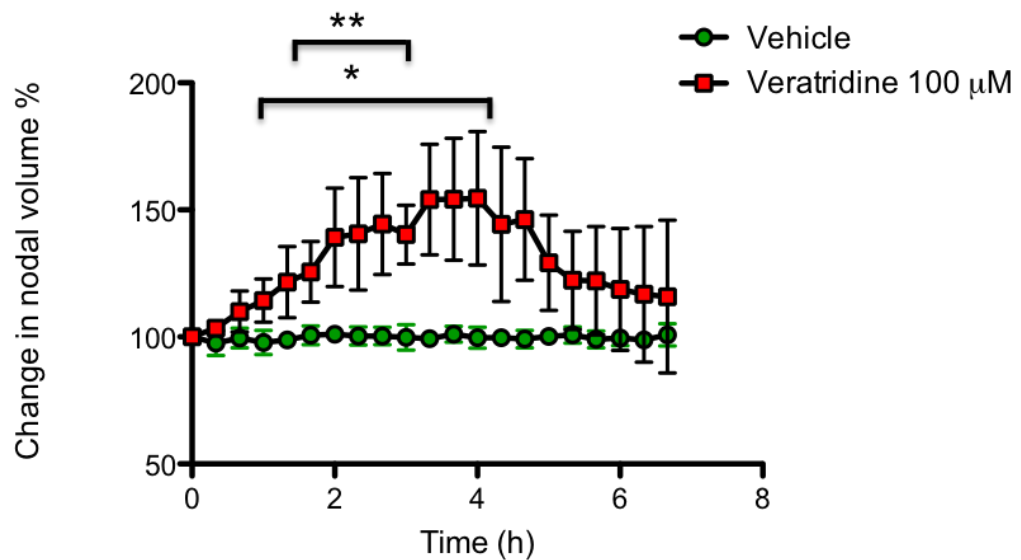
Figure 26 – Increase of the volume in the node/paranode in veratridine-treated axons.

Evolution of the volume of the axon in the region surrounding the node of Ranvier (50 µm to each side of the node of Ranvier), over time, after treatment either with vehicle (saline + DMSO) or with veratridine at a concentration of 100 µM, for 10 minutes. The images analyzed were z-stacks (slice thickness= 0.3 µm) obtained with confocal microscopy and normalized with the volume of a perfect cylinder that contains the quantified area of the axon. Statistical test used was Student's t-test with two-tailed distribution, two-sample equal variance. *=p<0.05, **=p<0.01,N=9 nodes from each of 3/4 animals.

Topical application of veratridine did also cause the appearance of constrictions along the internodes (figure 27). The constrictions continued to expand for the duration of the observation period (up to 7 hours after treatment). This finding was consistent with the observations regarding the expansion of the periaxonal space in response to electrical stimulation.
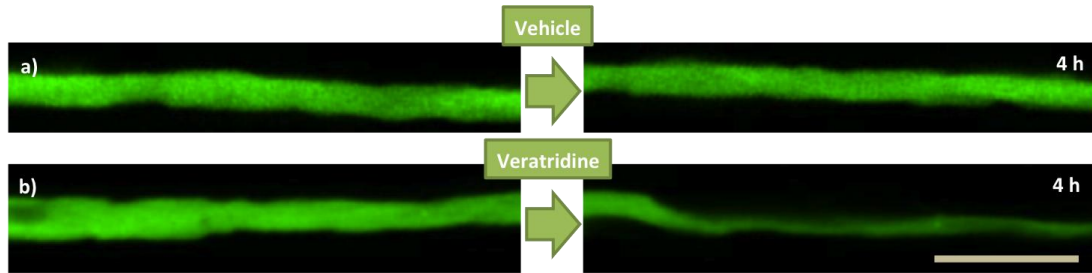
Figure 27a-b − **Appearance of constrictions of the axoplasm of axons treated with veratridine.**

In vivo confocal imaging of YFP positive axons in the mouse saphenous nerve before (left panel) and 4 hours after exposure to drug (right panel).In control nerves (**a**), the internodal axoplasm of YFP positive axons treated for 10 minutes with vehicle (saline + DMSO) did not change during an observation period of 4 hours, but in other preparations (**b**) treatment with veratridine for 10 minutes resulted in constriction of the axoplasm that in some cases reduced it to a thin sheetwithin4 hours of treatment. Scale bar is 10 µm.

Similarly to what was observed following electrical stimulation, these axoplasmic constrictions appear to collect into droplets that move until reaching the paranode (figure 28). This movement was normally coincident with, or preceded, the paranodal axoplasmic herniation, and the apparent droplet release at the paranode seemed to facilitate the initiation of recovery of normal paranodal volume.
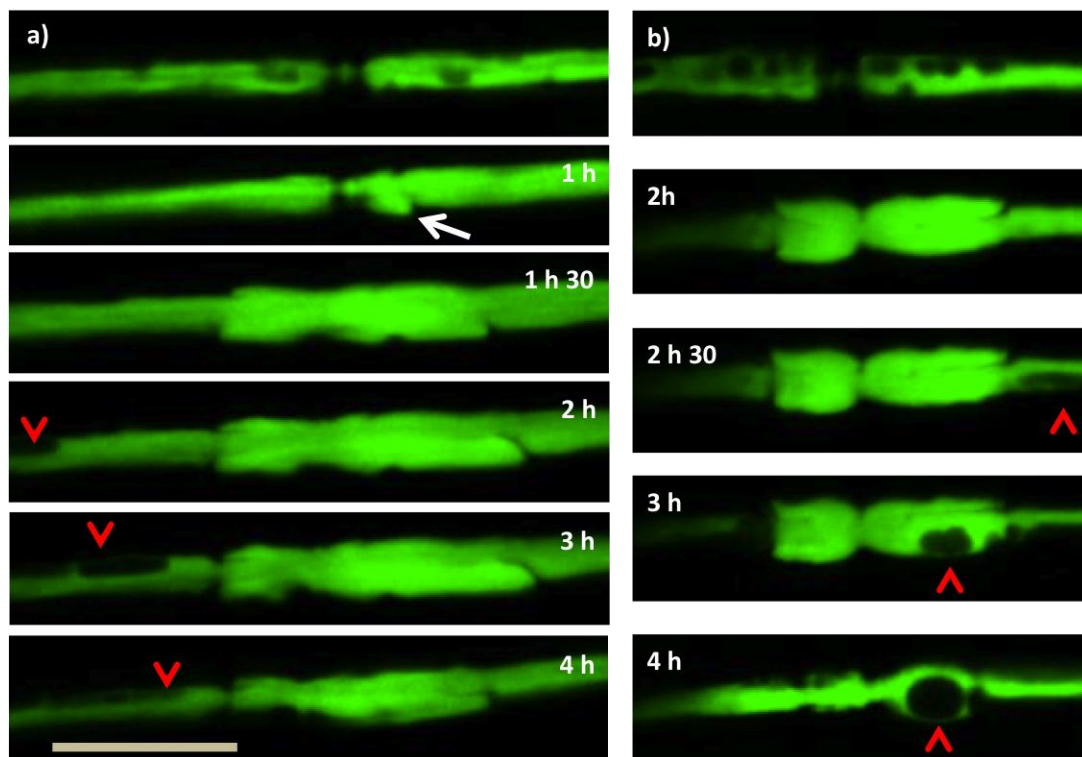
Figure 28a-b – Expansion of the periaxonal space and the swelling of the paranode.

In vivo confocal imaging of YFP positive axons in the mouse saphenous nerve before and after treatment with veratridine. Similar to what was observed following high frequency stimulation, we noted the movement of apparent droplets that reach the paranodes (**red arrowhead**), coinciding with the swelling of the paranodes (**arrow**). The expanded node/paranode seemed to start recovering after the droplets reached the paranodal region. Scale bar is 10 µm.

After imaging the nerves were fixed in glutaraldehyde(4% in 0.1M phosphate buffer), embedded in resin, and viewed in semi-thin (1 μm) longitudinal sections (figures 29). Bright field imaging confirmed the swelling of the paranodes, with a 10-fold increase in the nodal gap in the nerves treated with veratridine compared with control nerves treated only with vehicle (figure 29c).
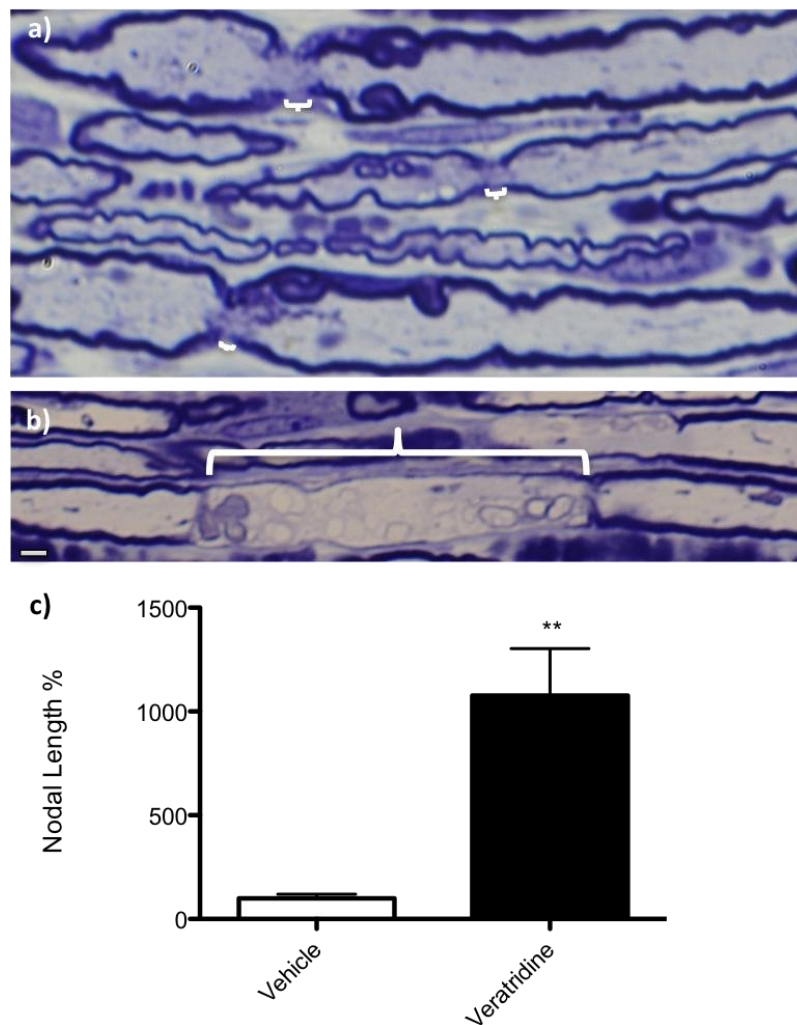
Figure 29a-c – Paranodal swelling in axons treated with veratridine.

Longitudinal sections of saphenous nerves of mice fixed 6 hours after treatment with either vehicle (saline + DMSO) (**a**) or veratridine (**b**), embedded in resin and stained with thionin acetate and acridine orange. Axons treated with veratridine show an

increase in the nodal gap and swelling of the nodes of Ranvier (**brackets**). Nerves treated with veratridine 100 µM concentration show a significant increase in both the area of the node of Ranvier and the nodal gap, relatively to the control preparations (**c**). The values were obtained by quantification of the bright field images and normalized to the values for the vehicle treated axons (%). $P<0.01$ **.N=>10 axons from each of 4 animals/condition. Scale bar is 1 µm.

Electron microscopy imaging of the same and similar preparations (figure 30) also confirmed the swelling of the paranodes in axons treated with veratridine. The paranodal loops appear to be reversed, with the axoplasm doubling back around the loops, giving it what could be expected to appear like the mushroom-like structure observed under confocal microscope. Electron microscopy showed that the dense undercoating of the nodal axolemma was not altered and the Schwann cell processes were, in some situations, reversed in such a way that the axolemma was doubling back around the processes and the node was found covered only by the Schwann cell basal lamina.

Figure 30a-e – Paranodal herniation in axons treated with veratridine.

Electron micrographs showing longitudinal sections through nodes of Ranvier fixed 6 hours after treatment with either vehicle (**a**) or veratridine (**b**, **c**, **d** and **e**). Axons treated with veratridine show an increased separation of the paranodes, with a swelling of the nodal axoplasm forming a mushroom shape (**yellow arrow**). Vesicle-like structures are also present in the paranodal region, seemingly resulting from the expansion of the periaxonal space loops (**red arrowhead**). Scale bar is 2 µm.

At the time of fixation, imaging of similar sections by conventional bright field microscopy confirmed the interpretation of an expansion of the periaxonal space following veratridine treatment (figure 31). Indeed, the myelin was intact, but the axoplasm was constricted due to the appearance of a large, seemingly empty, space running longitudinally along the internode.
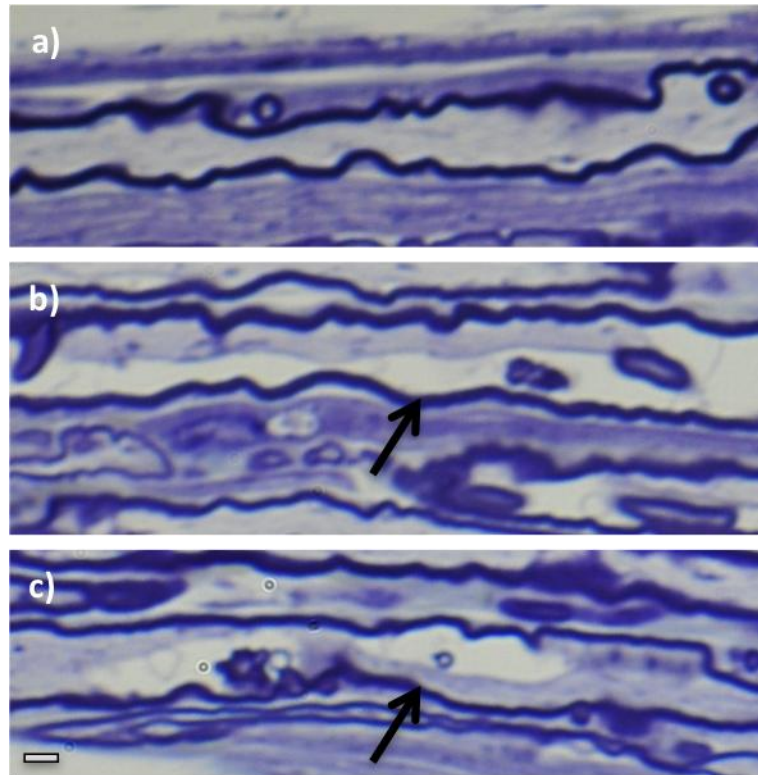
Figure 31a-c – Expansion of the periaxonal space in axons treated with veratridine.

Longitudinal sections of saphenous nerves of mice fixed 6 hours after treatment with vehicle (saline + DMSO) (**a**) or veratridine (**b** and **c**), embedded in resin and stained with thionin acetate and acridine orange. Axons treated with veratridine showed an apparent expansion of the periaxonal space (**arrow**) and compression of the axoplasm. Scale bar is 1 μm.

Similarly, electron microscopy imaging showed that the compression of the axoplasm is indeed due to an expansion of the periaxonal space(figure 32), since the axolemma separates from the myelin sheath in the area of expansion of the PAS, which assumed the shape of a vacuole apparently filled with liquid. In comparison, it can be observed that in the control situation the PAS is not visible, since the axoplasm appears to be immediately adjacent to the myelin sheath.
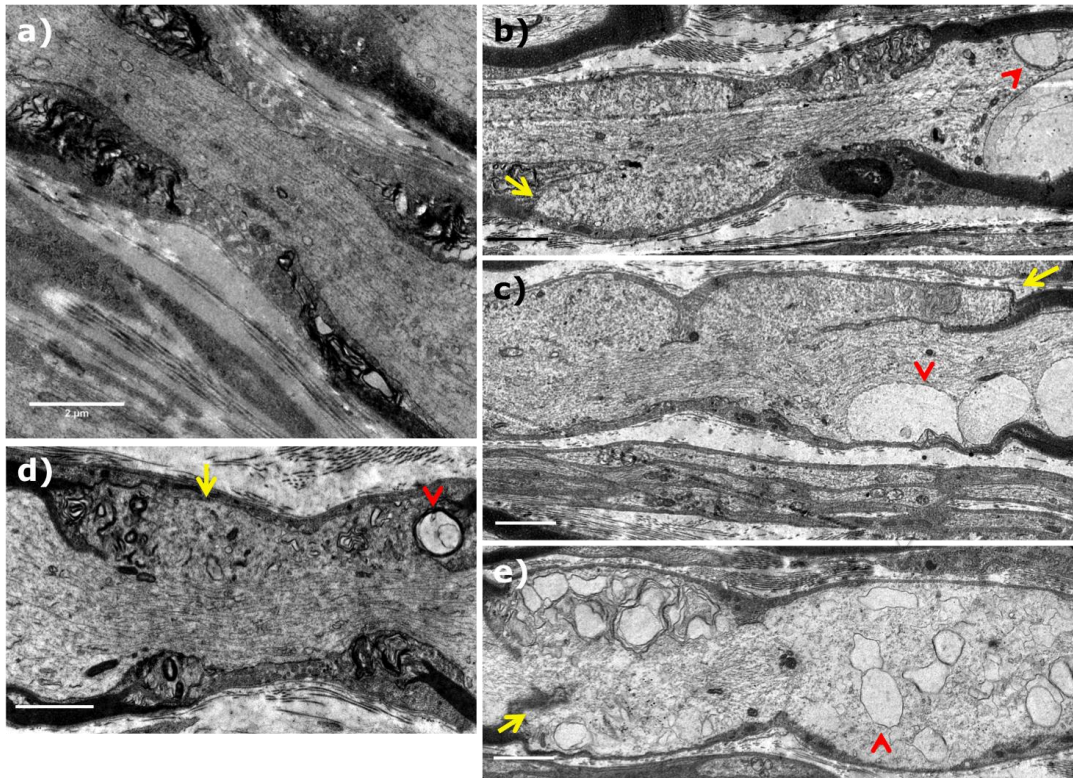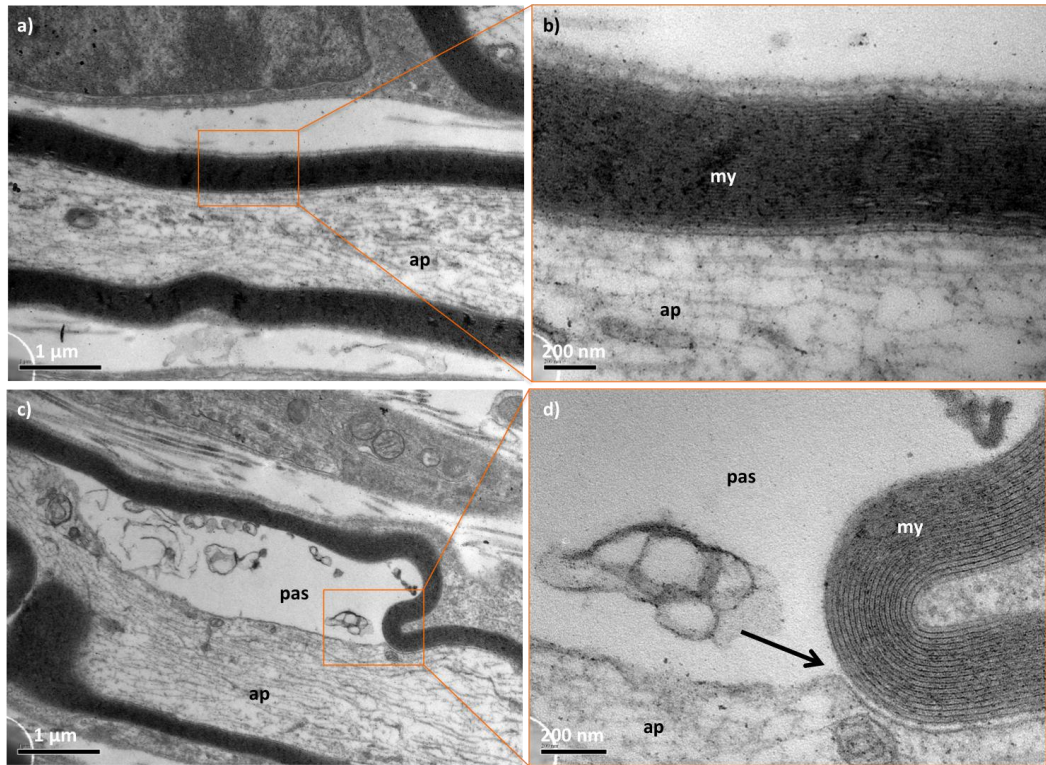
Figure 32a-d – Expansion of the periaxonal space in axons treated with veratridine.

Longitudinal sections of saphenous nerves of mice fixed 6 hours after treatment with either vehicle (saline + DMSO) (**a** and **b**) or veratridine (**c** and **d**), imaged under an electron microscope. Axons treated with veratridine show an expansion of the periaxonal space (PAS) that compresses the axoplasm (**ape**). It can be seen that the cell membrane separates from the myelin (**my**) where the PAS starts to expand (**arrow**). Scale bar is 1 µm in images **a** and **c** and 200 nm in images **b** and **d**.

Unmyelinated fibres appear to be morphologically unaltered following treatment with veratridine

Similarly to what was observed with electrically stimulated nerves, electron microscopy imaging of saphenous nerves treated with veratridine did not reveal any obvious morphological alterations of unmyelinated fibres, such as oedema or swelling (figure 33). All of the observed morphological alterations appear to be restricted to the myelinated axons.
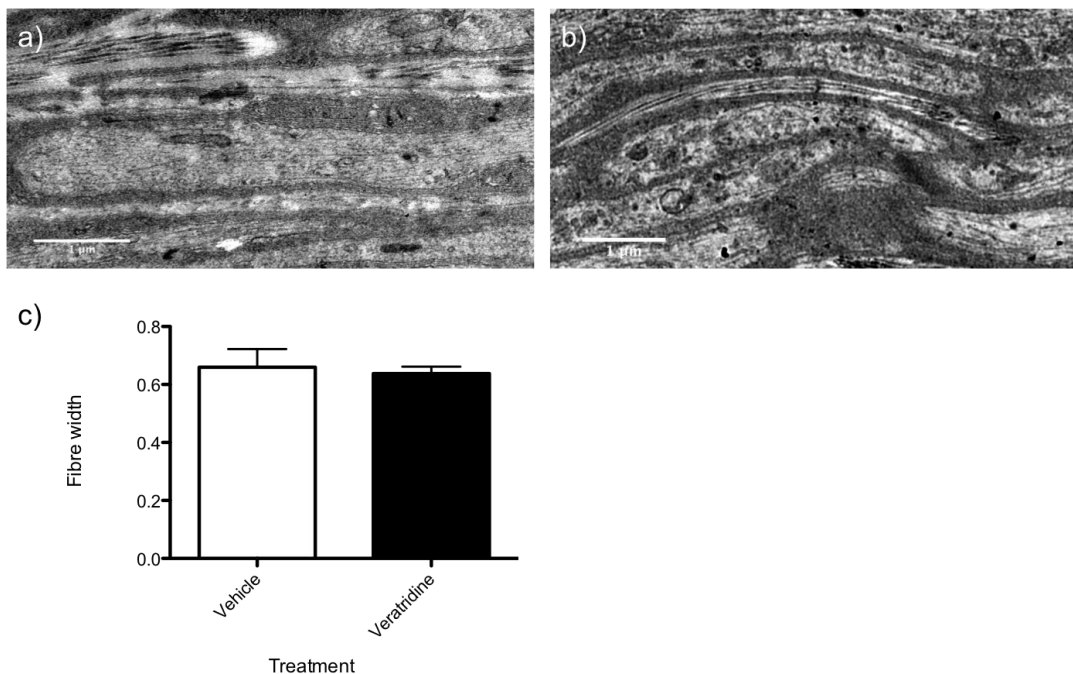
Figure 33a-c – Veratridine-treated unmyelinated fibres do not show any morphological alterations.

Electron micrographs of longitudinal sections of saphenous nerves of mice fixed 6 hours after treatment with either vehicle (saline + DMSO) (**a**) or veratridine (**b**) show no morphological alterations, and there is no variation in unmyelinated fibre width with stimulation (**c**). Scale bar is 1 µm. N=>20 axons from each of 3 animals.

The effect of veratridine on the axonal morphology appears to be reversible

Confocal imaging of the saphenous nerve of Thy1-YFP-16 transgenic mice a week after topical application of veratridine (100 µM, applied for 10 minutes) revealed that both the paranodal swelling and the expansion of the periaxonal space had reversed back to control-like situations, with the axoplasm presenting no morphological alterations, compared with control (figure 34).
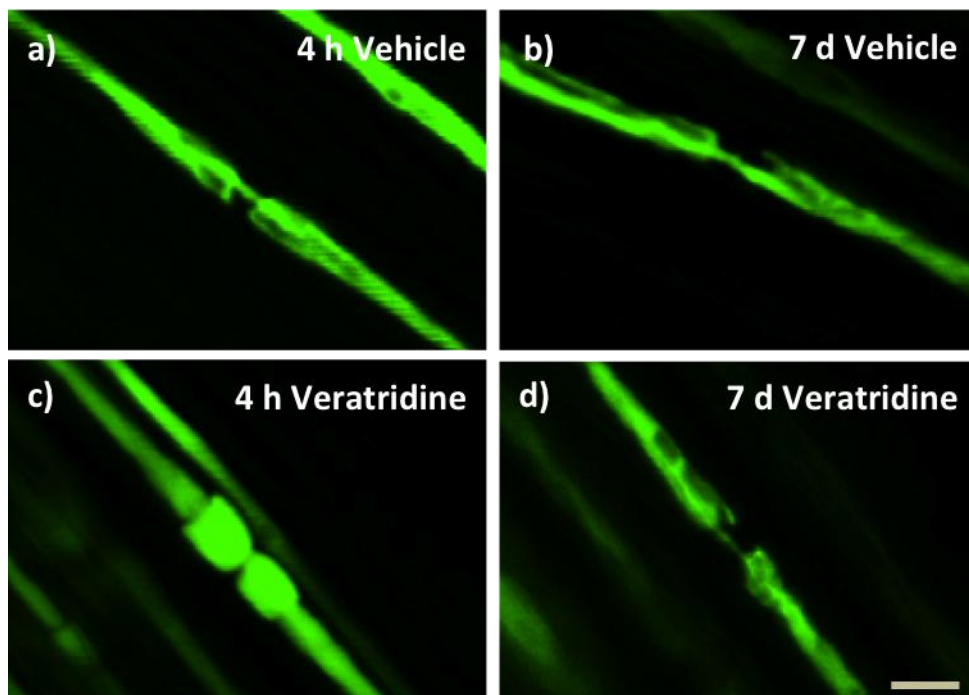
Figure 34a-d – Reversibility of paranodal swelling in chemically stimulated axons.

In vivo confocal imaging of YFP[+] axons in the mouse saphenous nerve. Control axons (**a**, **b**) remain unaffected, but axons swollen by veratridine treatment (**c**)regain control appearance within 7 days (**d**). Different axons were imaged in each time period, as the

scarring and incision healing process made the re-identification of the imaged axons impossible. Scale bar is 10 µm.

Similarly to what happened with electrically stimulated nerves, the morphological alterations appear not to have any long lasting effects on the normal nerve physiology, with no evidence indicating the presence of degeneration, demyelination, remyelination, or any other kind of pathology.

Dilation of the paranode happens in a bi-lobed manner that seems to be mostly independent of proximal/distal orientation

The expansion of the paranode in chemical and electrically stimulated axons did not always happen in a perfectly bi-lobed way (figures 35 and 36). Sometimes, in response to either chemical or electrical stimulation, a protrusion could start at either the proximal or the distal paranode following treatment. This change was typically followed by a similar event on the other side of the node, within 20-40 minutes. It was also observed that in some cases the symmetry of the bi-lobed structure was not as evident, since one of the lobes would be clearly bigger than the other.

Quantification of the number of events that started with a protrusion on the proximal or distal paranode (figure 37) showed that the bi-lobed initiation of the herniation process was the most common, while the proximal initiation was significantly decreased, if equal probabilities are assumed to either outcome (bi-lobed, proximal preference or distal preference). This could be either due to the Schwann cell being polarized in the proximal-distal orientation, or perhaps result from the direction of axonal transport. As most of the axoplasmic transport is anterograde, one could argue that any fluids accumulated in the periaxonal space would more rapidly move in the opposing direction, in a volume exchange manner. That way, the periaxonal 'droplets' would be travelling faster in the proximal direction, resulting in disruption of the proximal end of the affected internode. It is however observed that there is no preference for the magnitude of the swelling, which suggests that even though the initiation of the process is dependent on the

proximal/distal orientation of the axon, it is eventually irrelevant for the final outcome.
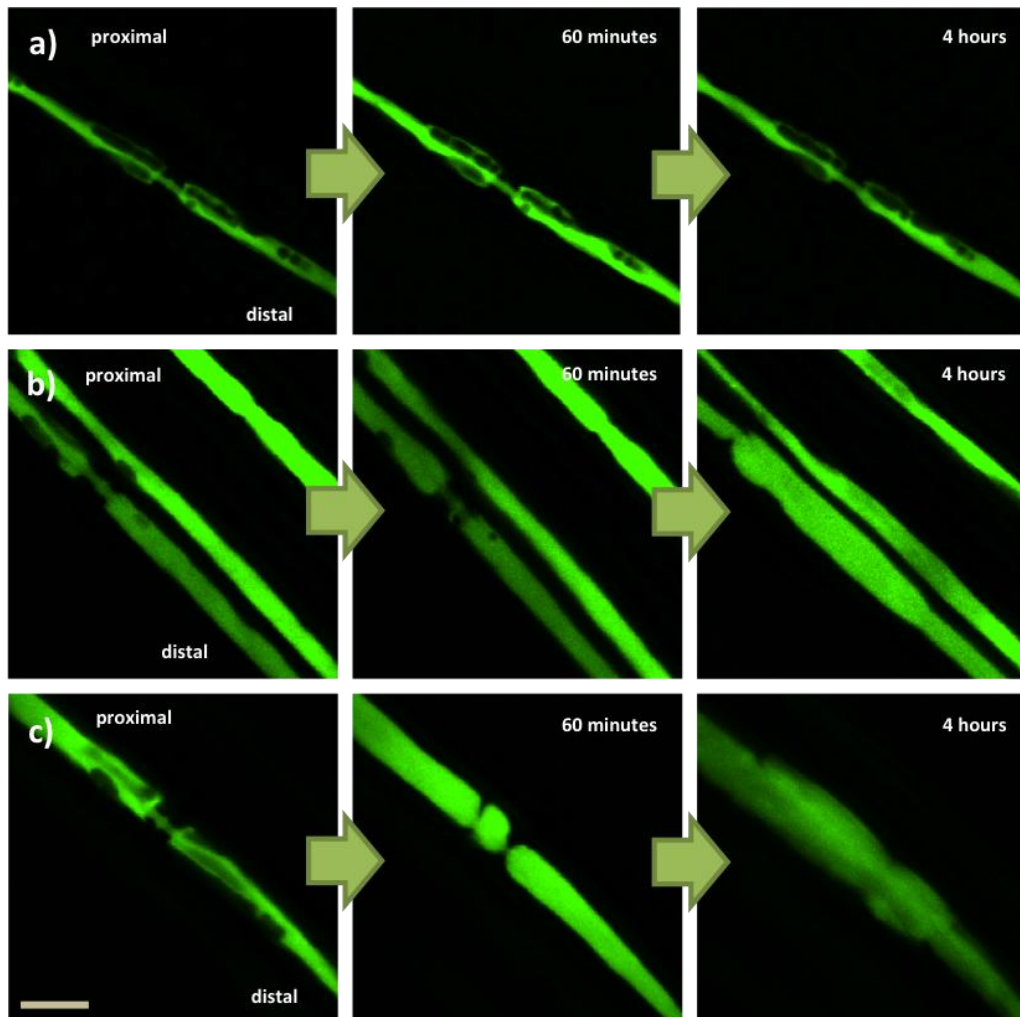
Figure 35a-c – Evolution of the bi-lobed paranodal swelling in veratridine-treated axons.

The paranodal herniation in response to chemical stimulation can start at the distal (**b**, middle panel) or the proximal side of the node (**c**, middle panel). The extension of the expansion can also either be more intense in the distal (**b**, right panel) or at the proximal (**c**, right panel)side. All images refer to axons treated for 10 minutes with veratridine 100 µM except for image **a**, which corresponds to vehicle treated axons. The images on the left panels were taken before treatment. Scale Bar is 10 µm.
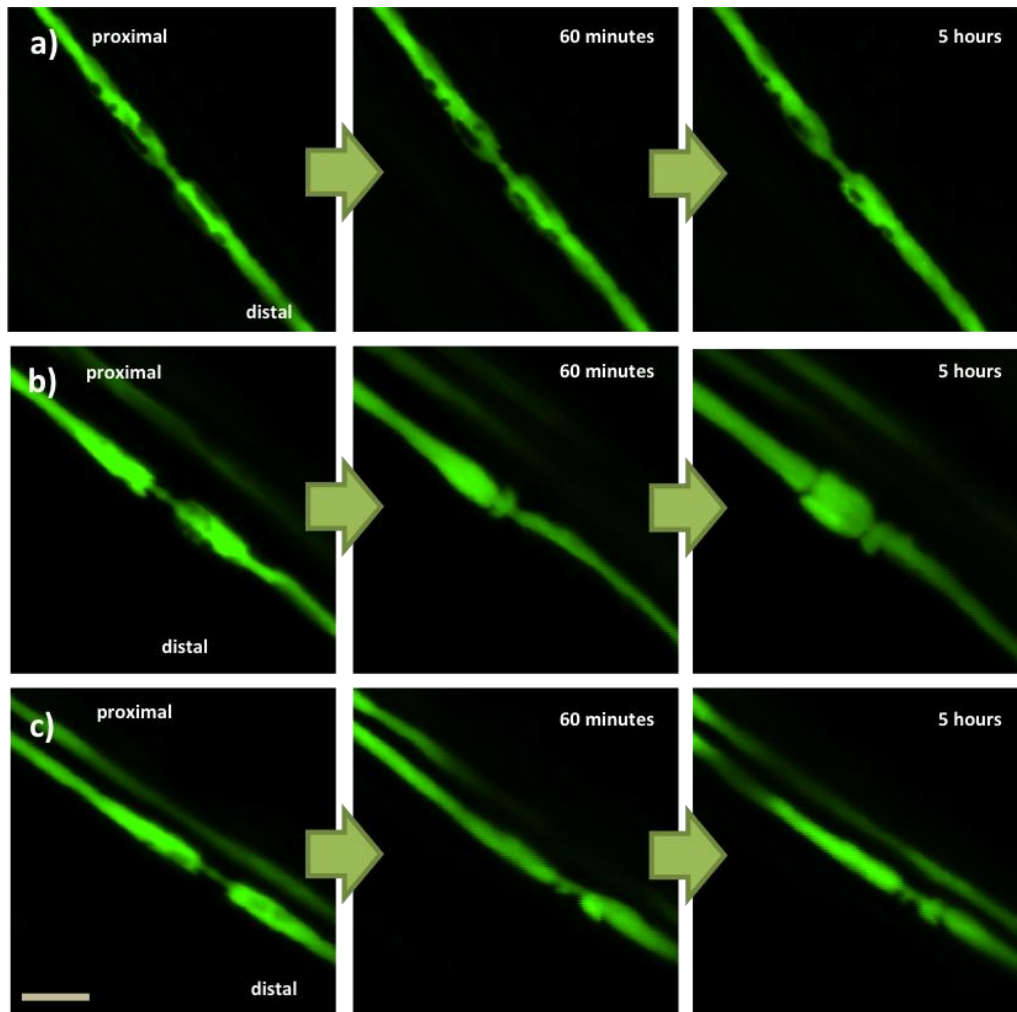
Figure 36a-c – Evolution of the bi-lobed paranodal swelling in electrically stimulated axons.

The paranodal herniation in response to electrical stimulation can start at the distal (**b**, middle panel) or the proximal side of the node (**c**, middle panel). The extension of the expansion can also either be more intense in the distal (**b**, right panel) or at the proximal (**c**, right panel)side. All images refer to axons stimulated for 2hours at 100 Hz except for image **a**, which corresponds to sham treated axons. The images on the left panels were taken before treatment. Scale Bar is 10 µm.
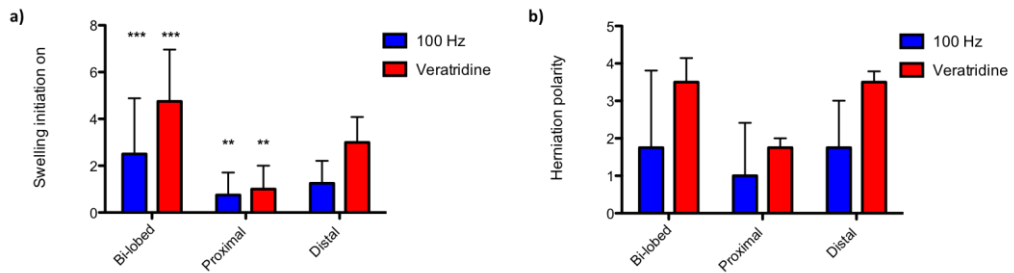
Figure 37a-b – Analysis of the effect of proximal-distal orientation in the bi-lobed paranodal herniation.

Statistical analysis indicates that there is a preference for a bi-lobed swelling initiation, in response to both chemical and electrical stimulation (**a**). There is no statistically significant preference for which side has the greatest magnitude of swelling (**b**) in response to either chemical or electrical stimulation. Statistical test used was chi-square distribution with 2 degrees of freedom, assuming an equal probability of the three outcomes (bi-lobed, proximal or distal preference). **=$p<0.01$, ***=$p<0.001$. N=5 (electrical stimulation) or 9 (chemical stimulation) imaged axons from each of 4 animals/condition.

Excised saphenous nerves are stable in artificial cerebrospinal fluid

Having shown that veratridine treatment mimics the morphological alterations observed following electrical stimulation, we aimed to characterize the mechanisms behind these changes with further pharmacological manipulation of ionic channels. As, for practical reasons, we wished to perform these studies in excised spinal roots, we initially ascertained whether these alterations would be replicated in excised saphenous nerves before moving to excised spinal roots.

Confocal microscopy time lapse imaging of excised Thy1-YFP-16 saphenous nerves showed no visible alterations to the morphology of the axon in an imaging period extending up to 3 hours) (figure 38).
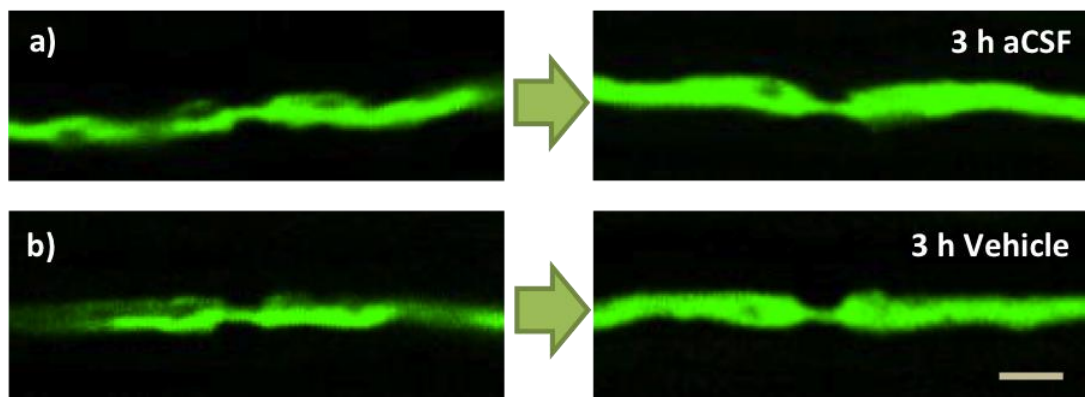
Figure 38 – Excised saphenous nerves are stable in aCSF.

Ex vivo confocal imaging of YFP positive axons in the mouse saphenous nerve immediately (left panel) and 3 hours after (right panel) being excised. The axoplasm of YFP positive axons was not altered during an observation period of 3 hours, either when the roots were incubated with aCSF (**a**) or with vehicle (DMSO in aCSF, **b**). Scale bar is 10 μm.

Treatment of excised saphenous nerves with veratridine induces paranodal axoplasm herniation

For technical reasons, since the excised tissue had to be maintained in artificial CSF, a water-dipping objective was required to perform the imaging. This imaging method did not have high enough resolution to allow the monitoring of the expansion of the periaxonal space with confidence, since the axoplasmic constrictions could not be consistently quantified.

Incubation of excised YFP positive saphenous nerves in aCSF with veratridine (100 µM, applied for 10 minutes) caused swelling of the paranodes in a manner similar to that observed when saphenous nerves were treated *in vivo* with veratridine (or electrically stimulated) (figure 39). These alterations were similar to those observed when *in vivo* saphenous nerves were treated with veratridine.
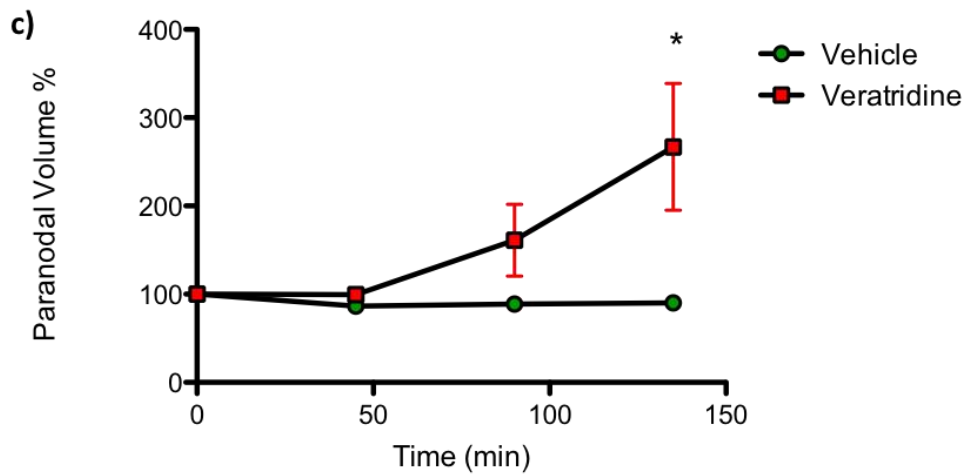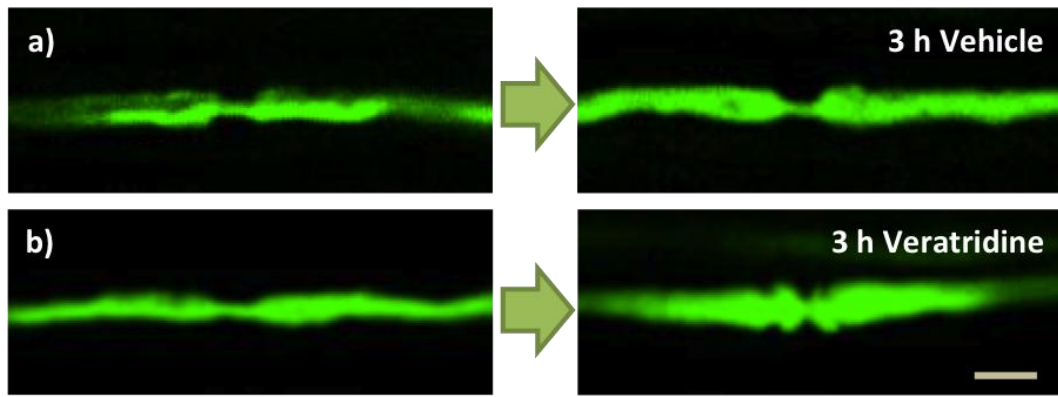
Figure 39a-c – Swelling of the paranodes in excised saphenous nerves treated with veratridine.

Ex vivo confocal imaging of YFP positive axons in the mouse saphenous nerve before (left panel) and after (right panel) treatment with either vehicle (**a**) or veratridine (**b**). While the axoplasm of vehicle treated axons was not altered during an observation period of 3 hours, axons treated with veratridine showed paranodal swelling (quantified in **c**). N= Statistical test used was Student's t-test with two-tailed distribution, two-sample equal variance. *=p<0.05. Scale bar is 10 μm.

Excised spinal roots are stable in artificial cerebrospinal fluid

Having shown that some of the morphological alterations of veratridine treatment of saphenous nerves *in vivo* were maintained *ex vivo*, we then aimed to characterize the mechanisms behind these changes with further pharmacological studies. As we wished to conduct these studies in excised spinal roots, we tried to replicate the effects of veratridine treatment in this model.

Confocal microscopy time lapse imaging of excised YFP positive spinal roots showed no gross alterations to the morphology of the axon in an imaging period extending up to 3 hours (figure 40).
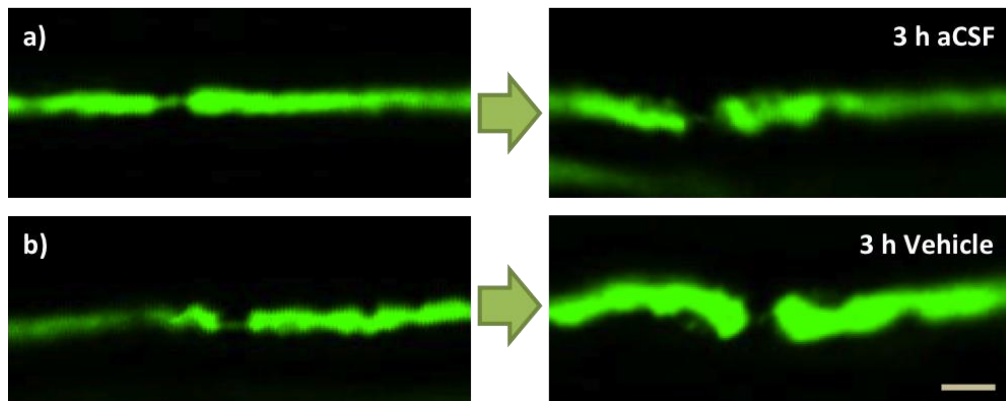
Figure 40a-b – Excised spinal roots are stable in aCSF.

Ex vivo confocal imaging of YFP positive axons in the mouse saphenous nerve immediately (left panel) and 3 hours after being excised (right panel). The spinal roots seem to lose some tension, in both untreated (**a**) and vehicle treated axons (**b**), but other than that no obvious axoplasmic alterations were observed for an experimental time of 3 hours. Scale bar is 10 man=9 nodes from each of 3 animals.

Treatment of excised spinal roots with veratridine induces paranodal axoplasm herniation

Similarly to what happened with excised saphenous nerves, a water-dipping objective was required to perform the imaging, meaning that the experimental preparation did not have high enough resolution to allow the monitoring of the expansion of the periaxonal space. The quantification of axonal morphological alterations was then obtained by comparing the volume of the nodal/paranodal region.

Incubation of excised YFP positive spinal roots in aCSF with veratridine (100 µM, applied for 10 minutes) caused an axoplasmic herniation at the paranodes, in a manner similar to that observed when saphenous nerves were stimulated *in* and *ex vivo* (figure 41).
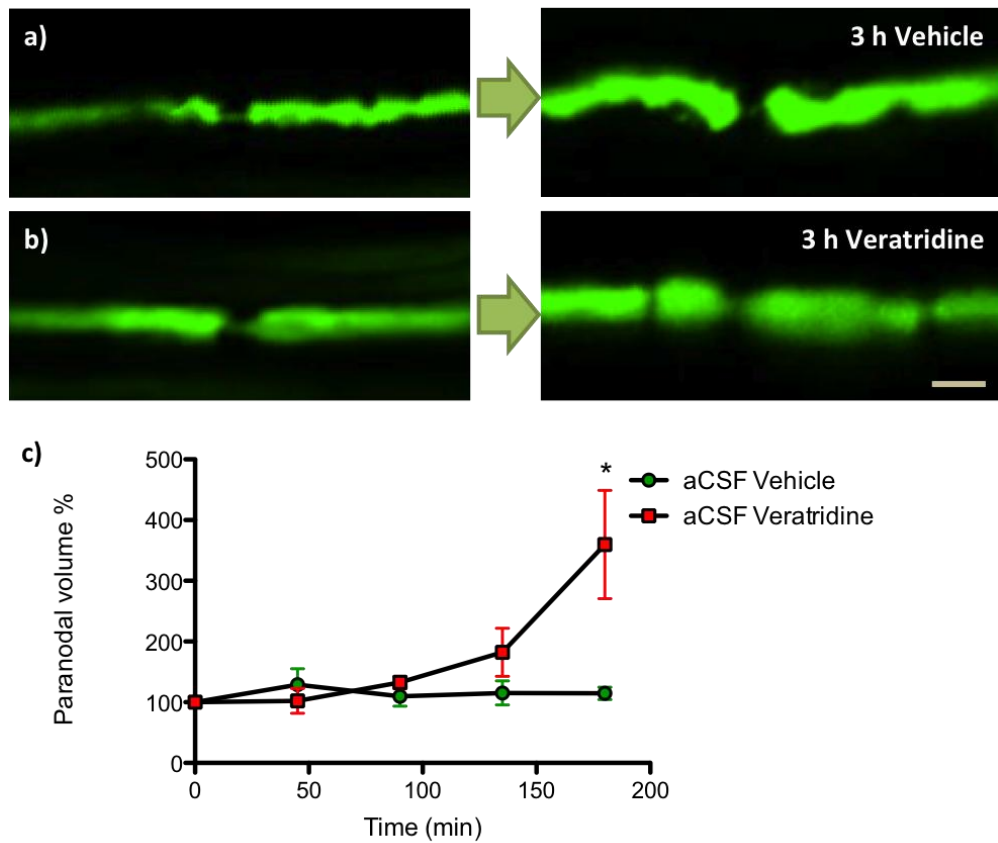
Figure 41a-c – Swelling of the paranodes in excised spinal roots treated with veratridine.

Ex vivo confocal imaging of YFP positive axons in the mouse spinal roots before (left panel) and 3 hours after (right panel) treatment with either vehicle (**a**) or veratridine (**b**). Whilst untreated spinal roots do not appear to be extremely altered, veratridine-treated roots (**b**) show paranodal swelling (quantified in **c**). Scale bar is 10 μm. Statistical test used was Student's t-test with two-tailed distribution, two-sample equal variance. *=$p<0.05$. N=5 nodes from each of 4 animals.

Paranodal herniation in excised spinal roots treated with veratridine depends on the opening of sodium channels

To confirm that the morphological alterations observed after treatment with veratridine resulted from its opening of sodium channels, these were blocked by the drug lidocaine (500 µM, for the duration of the experiment). Lidocaine prevented the herniation of the paranodes observed in excised YFP positive spinal roots incubated with veratridine (figure 42).
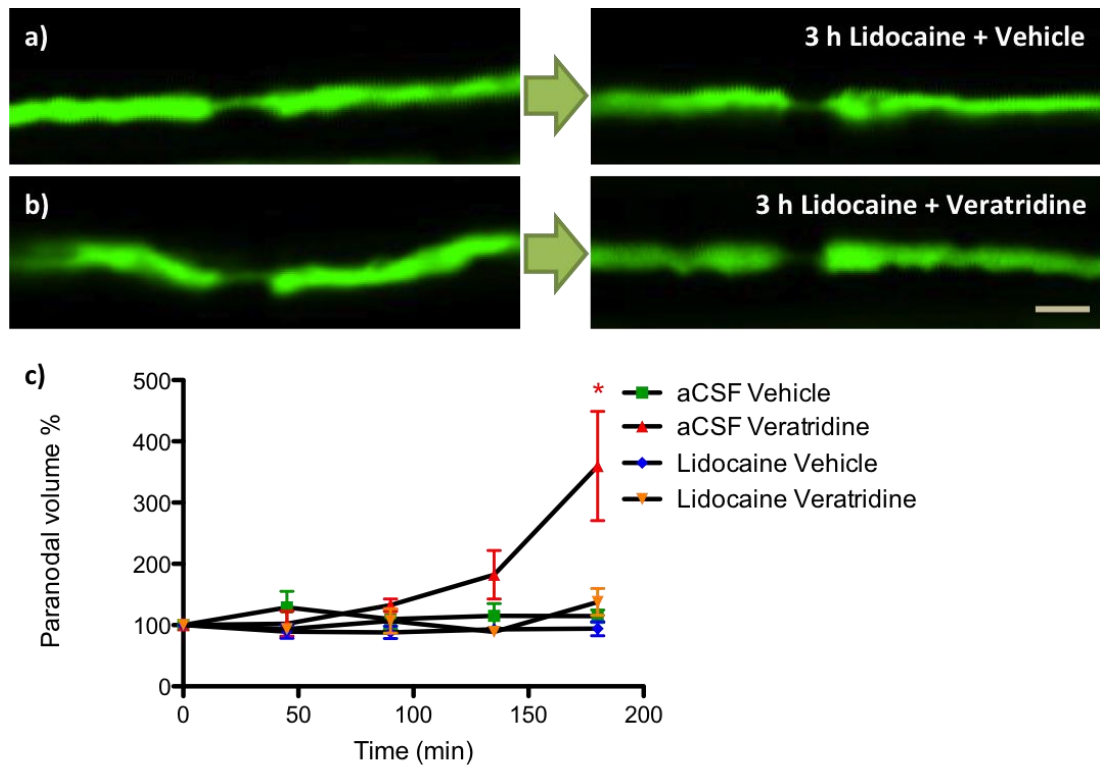
Figure 42a-c – Prevention of the paranodal swelling in axons treated with lidocaine.

Ex vivo confocal imaging of YFP positive axons in the mouse spinal roots incubated with lidocaine, before (left panel) and 3 hours after (right panel) treatment with either vehicle (**a**) or veratridine (**b**). The incubation of the spinal roots with lidocaine did not cause any morphological alterations. Indeed, incubation with lidocaine prevented the

swelling of the paranodes observed in spinal roots treated only with veratridine (quantified in **c**). Scale bar is 10 µm. Statistical test used was Student's t-test with two-tailed distribution, two-sample equal variance. *=p<0.05. N=5 nodes from each of 4 animals.

This finding seems to indicate that the observed effect of axonal morphological alterations following veratridine treatment is due to the opening of sodium channels, and not to an eventual secondary effect of veratridine.

The blocking of potassium channels potentiates paranodal swelling in spinal roots treated with veratridine

The swelling of the paranodes observed in excised YFP positive spinal roots incubated with veratridine was not prevented when incubated with 4-aminopyridine (100 µM, for the duration of the experiment), which blocks potassium channels (figure 43). Actually, while the 4-aminopyridine alone did not cause any obvious morphological alterations, when applied together with veratridine it caused paranodal swelling that was initiated earlier than when spinal roots were treated only with veratridine.

This finding seemingly confirms that the paranodal axoplasm displacement is indeed caused by the movement of ions into and from the axon. The fact that the swelling caused by facilitating the entrance of sodium ions into the axon (by opening sodium channels) is potentiated by preventing potassium ions from leaving the axon (by the blocking of potassium channels) further suggests that these alterations might be caused by osmotic pressure due to imbalanced ionic movements.

Figure 43a-c – Potentiation of the paranodal swelling in axons treated with 4-aminopyridine.

Ex vivo confocal imaging of YFP positive axons in the mouse spinal roots incubated with 4-aminopyridine (4AP), before (left panel) and 3 hours after (right panel) treatment with either vehicle (**a**) or veratridine (**b**). The incubation of the spinal roots with 4-aminopyridine alone did not cause any morphological alterations. However, treatment of spinal roots incubated with 4-aminopyridine with veratridine caused swelling of the paranodes. This swelling was initiated at an earlier time point than when spinal roots were treated only with veratridine (quantified in **c**). Scale bar is 10 μm. Statistical test used was Student's t-test with two-tailed distribution, two-sample equal variance. *=$p<0.05$. N=5 nodes from each of 4 animals.

Hypo-osmotic medium can induce axoplasmic herniation at the paranodes

Having shown that the uncontrolled movement of ions could lead to serious morphological alterations of the axon, we tried to assess the possibility of these alterations being caused by osmotic pressure. To do so, using excised YFP positive spinal roots, we modulated the osmolarity of the aCSF bathing the spinal roots (figure 44).

Hyper-osmotic medium was obtained by adding 200 mM NaCl, while different dilutions of hypo-osmotic aCSF were obtained by diluting iso-osmotic aCSF with dH_2O in 10%, 25% and 50% dilution. When spinal roots were incubated in hyper-osmotic medium, no morphological alterations were obvious. Spinal roots also presented no morphological alterations when incubated with 10% and 25% hypo-osmotic aCSF. However, 50% hypo-osmotic aCSF revealed a series of events consistent with the axonal herniation at the paranodes, forming the same bi-lobed mushroom shape that was observed after electrical and electrical stimulation *in vivo*.
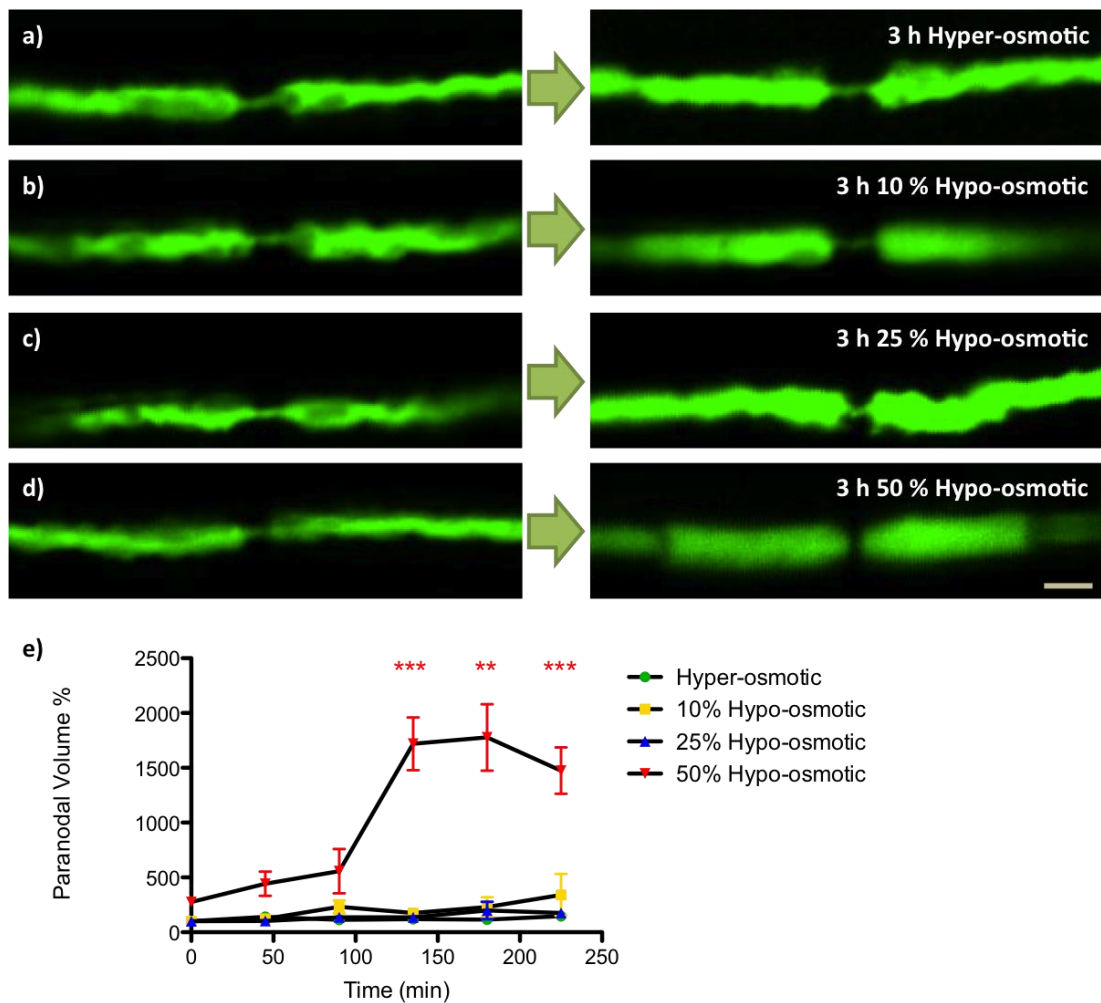
Figure 44a-e – Swelling of the paranodes in axons incubated in hypo-osmotic aCSF.

Ex vivo confocal imaging of YFP positive axons in the mouse spinal roots before (left panel) and 3 hours after (right panel) being incubated with different osmolarities of aCSF. The incubation of the spinal roots with hyper-osmotic aCSF (**a**), or with a 10% (**b**) or 25% (**c**) dilution of aCSF alone did not cause any morphological alterations. However, the incubation of spinal roots with 50% hypo-osmotic aCSF caused axoplasmic herniation at the paranodes (**d**, quantified in **c**). Scale bar is 10 μm. Statistical test used was Student's t-test with two-tailed distribution, two-sample equal variance. **=p<0.01, ***=p<0.001. N=5 nodes from each of 4 animals.
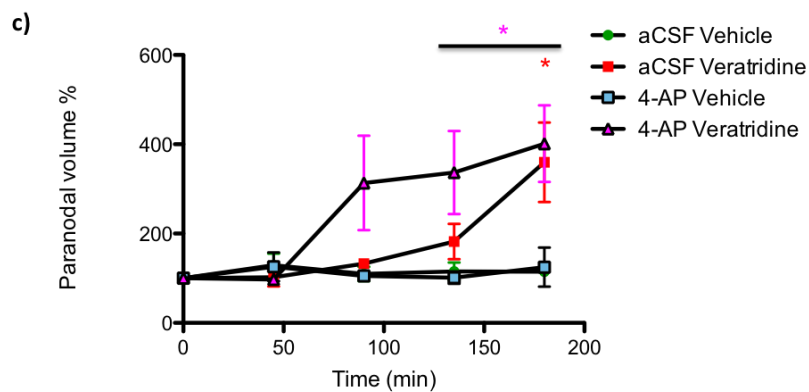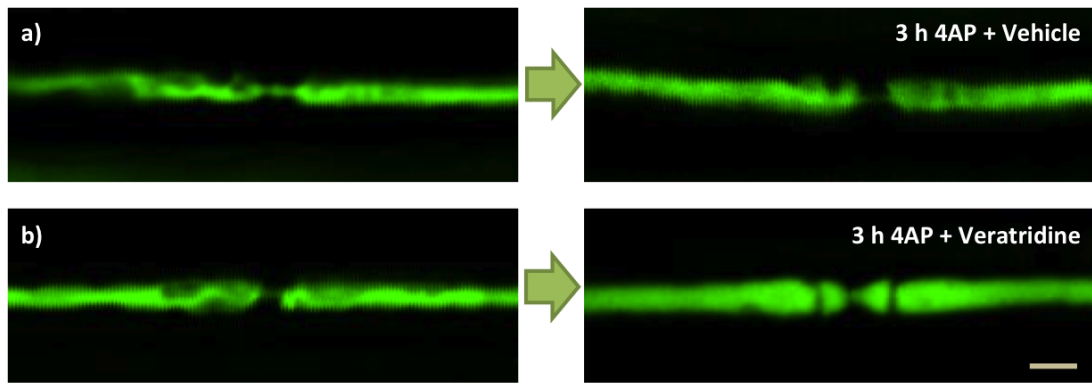
Paranodal swelling in spinal roots treated with veratridine is prevented by blocking the function of the sodium pump

Having shown that the observed axonal morphological alterations were potentiated by the movement of ions, and could possibly be explained by osmotic pressure, we aimed to study a specific ion movement, namely the extrusion of sodium ions and entrance of potassium ions by the sodium pump, presumably taking place at the internode.

To do so, using the same model of excised spinal roots treated with veratridine, these roots were incubated with ouabain, which blocks the sodium pump (figure 45). This resulted in the absence of any morphological alteration, even in the presence of veratridine.
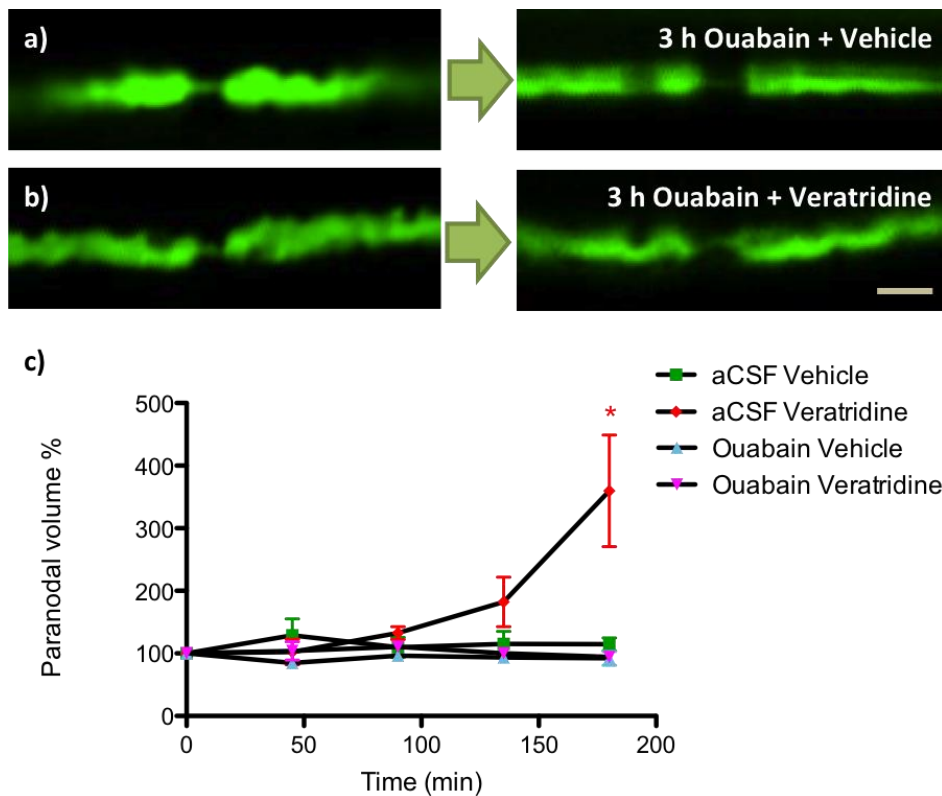
Figure 45a-c – Prevention of the paranodal swelling in axons incubated with ouabain.

Ex vivo confocal imaging of YFP positive axons in the mouse spinal roots incubated with ouabain, before (left panel) and 3 hours after (right panel) treatment with either vehicle (**a**) or veratridine (**b**). The incubation of the spinal roots with ouabain did not cause any morphological alterations. Indeed, incubation with ouabain prevented the swelling of the paranodes observed in spinal roots treated only with veratridine (quantified in **c**). Scale bar is 10 µm. Statistical test used was Student's t-test with two-tailed distribution, two-sample equal variance. *=$p < 0.05$. N=5 nodes from each of 4 animals.

This result raised the issue of whether this was due to ouabain acting downstream on the mechanism triggered by veratridine, or, similarly to what presumably happens with lidocaine, ouabain preventing the action of veratridine (presumably by depolarizing the axons, hence blocking its firing).

To clear this mechanism, the experimental conditions were modified so that ouabain was only applied after veratridine treatment (figure 46).
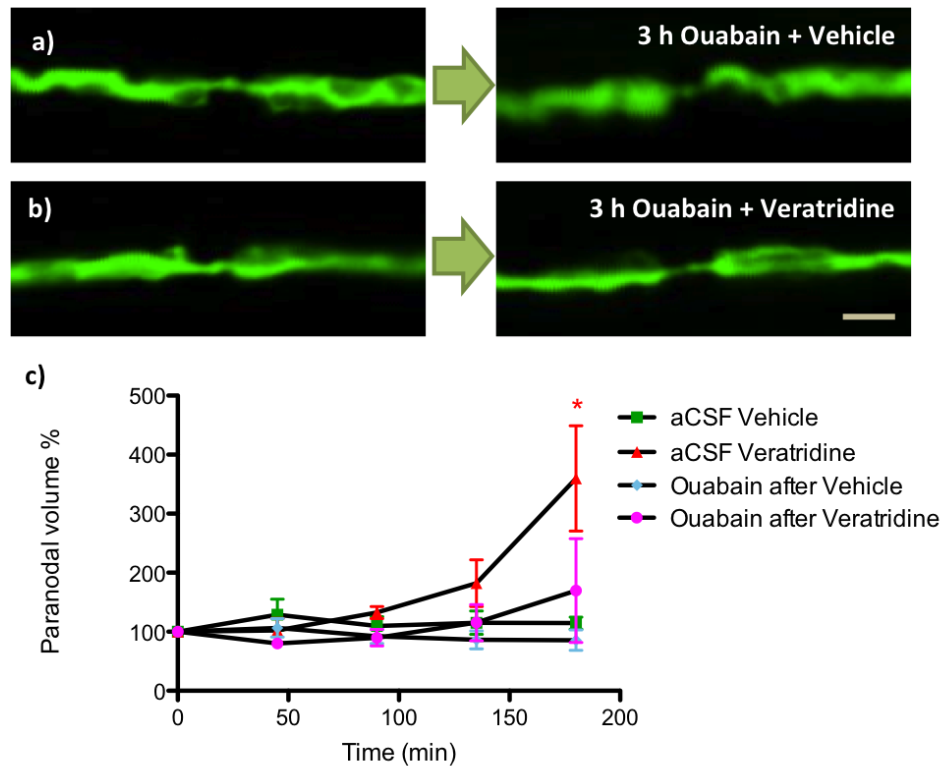
Figure 46a-c – Prevention of the paranodal swelling in axons incubated with ouabain after veratridine treatment.

Ex vivo confocal imaging of YFP positive axons in the mouse spinal roots, before (left panel) and 3 hours after (right panel) treatment with either vehicle (**a**) or veratridine (**b**) followed by incubation with ouabain. The incubation of the spinal roots with ouabain alone did not cause any morphological alterations, and incubation with ouabain after veratridine prevented again the swelling of the paranodes observed in spinal roots treated only with veratridine (quantified in **c**). Scale bar is 10 μm. Statistical test used was Student's t-test with two-tailed distribution, two-sample equal variance. *=$p < 0.05$. N=5 nodes from each of 4 animals.

The incubation of ouabain after treatment with veratridine did not provide us with a definite answer, as it still prevented the paranodal herniation caused

by veratridine treatment alone. Since the duration of action of veratridine is not entirely clear, the opening of sodium channels could likely be prolonged for longer than the 10 minutes of treatment.

We decided to return to the original model of *in vivo* electrical stimulation, to assess the effect of ouabain when applied after 2 hours of electrical stimulation at 100 Hz.

Treatment with ouabain prevented the axoplasmic herniation at the paranodes (figure 47) and the expansion of the periaxonal space (figure 48) normally observed after sustained stimulation. Since in this experiment ouabain was applied only after the stimulation had ceased, this result strongly indicates that these morphological alterations are caused by the activity of the sodium, potassium ATPase after the opening of nodal sodium channels.
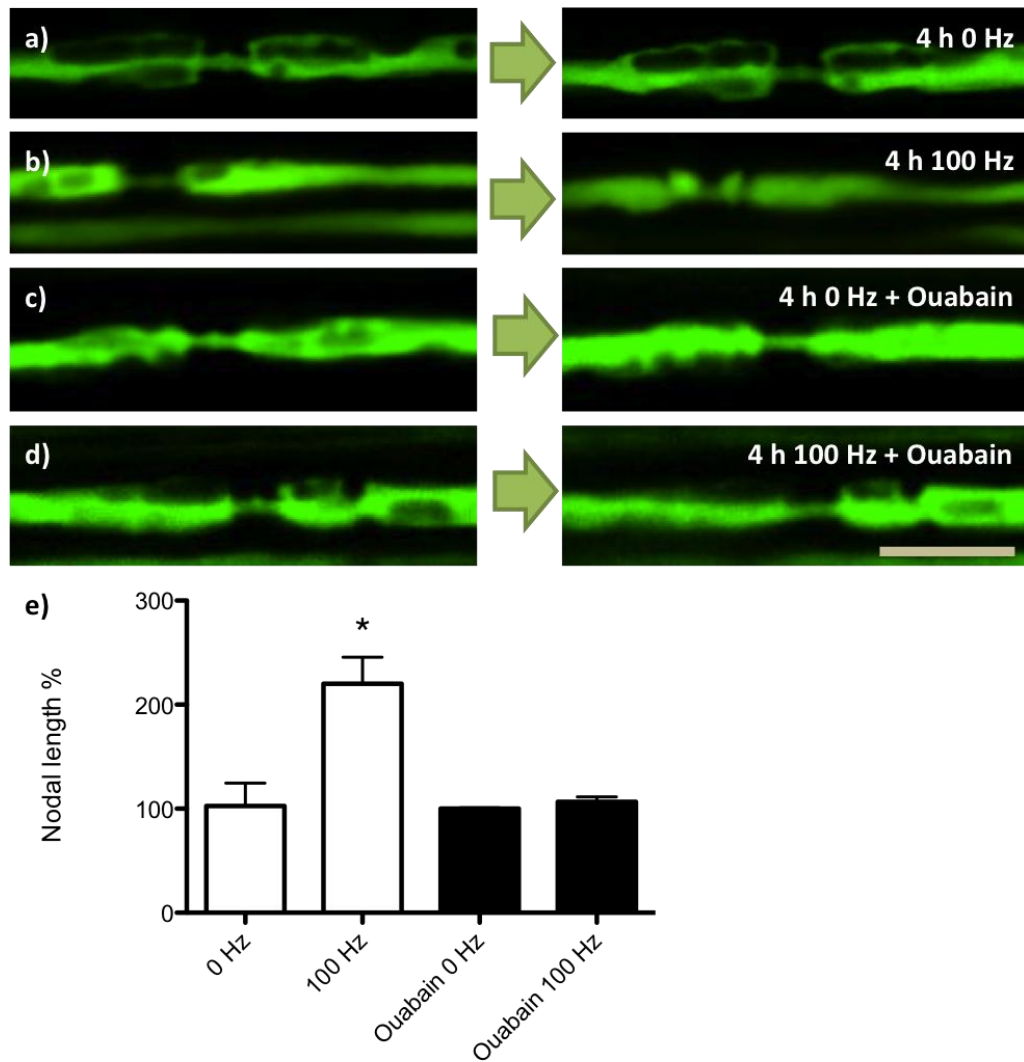
Figure 47a-e – Prevention of the paranodal swelling in axons treated with ouabain.

In vivo confocal imaging of YFP positive axons in the mouse saphenous nerves, before (left panel) and 4 hours after (right panel) stimulation. Similarly to what happened in controls (**a**), treatment with ouabain caused no morphological alterations either when applied alone (**c**) or following electrical stimulation (**d**), preventing the paranodal herniation observed when normal nerves were stimulated (**b**, quantified in **e**). Scale bar is 10 μm. Statistical test used was Student's t-test with two-tailed distribution, two-sample equal variance. *=p<0.05. N=9 nodes from each of 3/4 animals.
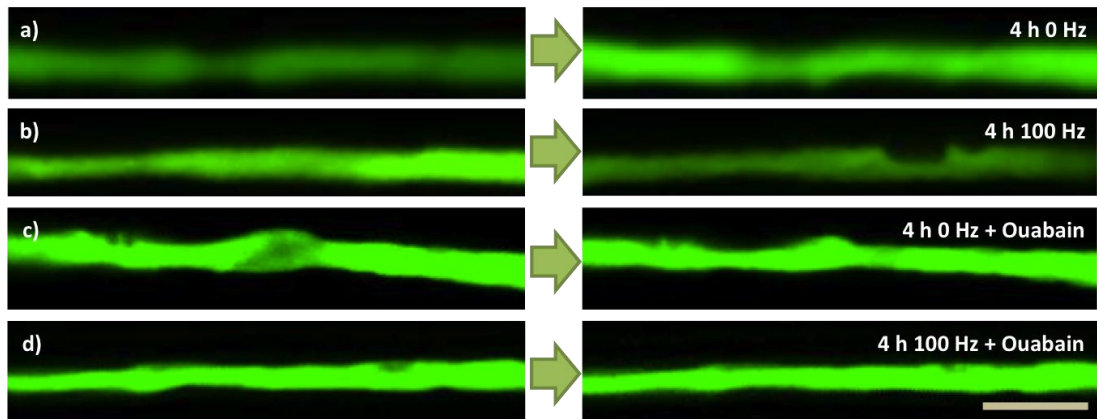
Figure 48a-d – Prevention of the periaxonal space expansion in axons treated with ouabain.

In vivo confocal imaging of YFP positive axons in the mouse saphenous nerves, before (left panel) and 4 hours after (right panel) stimulation. Similarly to controls (**a**), treatment with ouabain caused no morphological alterations either when applied alone (**c**) or following electrical stimulation (**d**), preventing the expansion of the periaxonal space observed when normal nerves were stimulated. Scale bar is 10 µm.

3.4 Discussion

In this chapter the experiments have reproduced the morphological effects of sustained electrical stimulation *in vivo,* but using chemical stimulation, both *in vivo* and in excised tissue. The timing of the two most obvious morphological alterations (expansion of the periaxonal space and paranodal herniation), raises the possibility that they are physically correlated, i.e. negative axonal pressure due to a nodal expansion being resolved by an expansion of the PAS, or, perhaps more likely, positive axonal pressure caused by the PAS expansion leading to the paranodal swelling.

The fact that these observations could be replicated in excised tissue indicated that these morphological alterations relate exclusively to the axon, independent of the cell body and possibly of cellular transport.

Time-lapse studies revealed that the fluid accumulated in the periaxonal space appeared to be relieved, at least in part, by droplets that travel towards the node, where they presumably escape to the nodal gap by parting the attachment of the paranodal loops of myelin to the axolemma. This suggests that the paranodal herniation results from a rise in intraxonal pressure arising from the expanding periaxonal space.

The analysis of electron micrographs revealed the presence of expanded vesicles in the axoplasm, some of which were in close proximity to the axolemma: this is a particular feature of paranodal and juxtaparanodal axoplasm. This observation is consistent with the notion of paranodal plasticity, in which the remodelling of the paranodal loops creates debris that

needs to be removed by a local mechanism. These vesicles, especially if they belong to the axon-Schwann cell network (Gatzinsky, et al. 1988), could be such a mechanism.

We have provided clear evidence that the morphological alterations are dependent on the movement of ions, presumably into and from the axon. Ablation of sodium movement, either by preventing it from entering the axon through nodal channels, or, notably, from leaving through the internodal sodium-potassium ATPase, prevented any of the observed morphological alterations in response to sustained stimulation. The fact that blocking the sodium pump, both *in* and *ex vivo,* resulted in no morphological alterations following either electrical or chemical stimulation strongly suggests that the expansion of the periaxonal space is dependent on the transport of sodium ions, presumably to the periaxonal space. The time course of the expansion of the periaxonal space, lasting up to hours, is consistent with the time course of action of the sodium pump in response to high frequency stimulation (Bostock and Bergmans, 1994).

In a resting state, water is in a thermodynamic equilibrium across the axonal membrane. The dilution of either the axonal or extracellular solutions would cause the diffusion of water driven by the osmotic pressure difference. Experimentally, we observed that dilution of the solution bathing spinal root nerves resulted in a similar process of paranodal herniation as observed after sustained stimulation. Although the mechanisms in the two cases will be different (osmotic compression of the axon vs. osmotic swelling of the axon), both protocols result in an increase in axonal hydrostatic pressure that

results in the herniation of axoplasm at an apparent weak point in the nodal/paranodal membrane.

The expansion of the periaxonal space may thus be due to raised osmotic pressure caused by an accumulation of sodium ions. The sodium pump extrudes three sodium ions per two potassium ions transported into the axon, increasing the periaxonal osmolarity (Rakowski, et al. 1989). Additionally, the atomic structure of the smaller sodium ions causes it to have higher charge density, inducing a stronger electrostatic ordering of nearby water molecules. This means that it has a stronger interaction with its hydration shell, compared with the potassium ions (Carrillo-Tripp, et al. 2003), resulting in a larger osmotic pressure.

The axon would then be compressed beneath the myelin sheath as a consequence of the expansion of the periaxonal space osmotic accumulation of fluid, in turn a consequence of an increased concentration of sodium ions in the periaxonal space due to the action of the internodal sodium pump. This compression would be relieved intermittently by rupture of part of the axolemmal/paranodal loop junctional complex, allowing the system to reset, the paranodal loop/axolemmal junction to reseal, and the axoplasm to return to its original disposition.

These observations may indicate the normal pathway taken by sodium ions to return to the extracellular milieu (first to the periaxonal space, then beneath the paranodal folds of myelin), or a 'storm overflow' pathway activated when impulse activity is excessive. The changes may be an overlooked part of the normal physiological repertoire of nerve fibres.

4 Mitochondria and axonal ionic homeostasis

4.1 Introduction

The fact that impairment of blood supply to the saphenous nerve caused a worsening of the morphological alterations in axons stimulated at lower frequencies (20 Hz) raised the issue of the metabolic component in axonal ionic homeostasis. Indeed, ischaemia is known to affect axonal excitability (Bostock, et al. 1991, Bostock and Bergmans, 1994), meaning that impairment of blood supply, by limiting the delivery of both oxygen and nutrients to the axon, will predictably also affect axonal function. Since axonal transport is known to be ATP-dependent (Hua, et al. 1997), one can predict that transport will be affected by the depletion of ATP.

In addition to axonal transport, the activity of the sodium pump also depends on the hydrolysis of ATP to function (Skou 1957, Koester and Siegelbaum, 1991) and so its role will presumably also be particularly affected by alterations to metabolism. Thus it would be interesting to study the role and behaviour of mitochondria in situations in which the ATP demand is increased, as occurs with sustained high frequency stimulation, and to determine whether the increased ATP requirement affects mitochondrial behaviour.

To study the effects of decreased ATP availability in the axon, we used two methods: in one we treated excised spinal roots with sodium azide (NaN_3), a component that specifically inhibits cytochrome c oxidase, namely complex IV, of the mitochondrial respiratory chain by binding irreversibly to the heme

cofactor (in a manner similar to that of carbon monoxide), hence exhausting the ATP axonal content. In the second, knowing that nitric oxide (NO) can inhibit axonal mitochondrial respiration (Duchen, 2004), causing temporary conduction block (Redford, et al. 1995), we studied the effect of nitric oxide on axons subjected to sustained stimulation. We used the nitric oxide donor DETA-NONOate, which spontaneously dissociates to liberate NO to the medium constantly.

This experiment will allow us to discriminate the roles of mitochondria and energy availability in the axonal response to sustained stimulation. A situation of axonal energy deficit can occur not only specifically in 'neuroinflammatory' pathologies but also in other situations, such as ischaemia, anoxia or mitochondria-related neuronal diseases.

By incorporating a fluorescent marker of mitochondrial membrane potential (i.e. TMRM), which labels polarized mitochondria, the experiments will also allow us to examine mitochondrial function in a simple model of inflammation (i.e. NO exposure) with the activity of ionic pumps (which are energy dependent) and ion channels. .

In addition to the function of mitochondria, their availability along the axon is also likely to play a role in homeostasis. Previous studies of mitochondrial dynamics have suggested that their transport along the axon slows down upon reaching the nodal region (Misgeld, et al. 2007), where mitochondrial density peaks (Berthold, et al. 1993, Fabricius, et al. 1993, Perkins and Ellisman, 2011). It has been suggested that this slowing down could be caused by either a checkpoint mechanism at this location, or by an active

recruitment of mitochondria to the node, perhaps by a high metabolic demand due to the activity of the sodium pump (Edgar, et al. 2008), which in some works has been identified in this region (Vorbrodt, et al. 1982, Mrsulja, et al. 1985, Gerbi, et al. 1999).

This explanation would however be inconsistent with more recent works that locate the sodium pump in the internode (McGrail, et al. 1991, Mata, et al. 1991, Alberti, et al. 2007, Young, et al. 2008), and by our own finding that the sodium pump indeed appears to be located beneath the myelin (chapters 2 and 3).

Additionally, it should be noted that the majority of these studies on mitochondrial movement were performed *in vitro*, typically in excised axons, often unmyelinated. Excised axons lack cell bodies, meaning that they are mandatorily undergoing degeneration, and obviously have no perfused vasculature to provide them with a balanced supply of oxygen and nutrients.

We then proceeded to examine in an *in vivo* preparation whether mitochondria accumulate in stimulated axons near the nodes of Ranvier, and whether electrical impulse activity along the axon alters the pattern of axonal mitochondrial distribution and transport.

4.2 Material and methods

In the experiments that required a visual indication of axonal morphological alterations, continued using transgenic mice (Thy1-YFP-16)(Feng, et al. 2000) in which some axons are labelled with yellow fluorescent protein (YFP. In the experiments in which other fluorescent markers were required, the animals used were Thy1-YFP-16 negative littermates or C57Bl/6 mice.

The role of mitochondrial function in the axonal morphological alterations in response to sustained stimulation was studied using excised saphenous nerves or spinal roots, as previously described.

Using confocal microscopy *in vivo*, we have also studied mitochondrial motility along resting and electrically active axons in the mouse. The saphenous nerve was exposed *in situ* and labelled using tetramethylrhodamine methyl ester (TMRM), which is accumulated by polarised mitochondria.

Myelinated fibres were stimulated using electrodes positioned at the groin, with an 'active' recording electrode at the ankle, an 'indifferent' electrode on the fifth toe and a ground electrode in the abdominal muscle. Supramaximal stimuli were delivered at 1Hz or 50Hz and the evoked compound action potentials (CAPs) averaged (n=10) and stored every 30 seconds. We used stimulation at 1 and 50 Hz because the goal of the experiment was to study mitochondrial distribution and movement behaviour in the axons with electrical conduction at different frequencies, while not inducing any morphological alterations.

For the *in vivo* chemical stimulation studies of mitochondria behaviour in axons morphologically altered by sustained stimulation, the saphenous nerve was exposed in the mid-thigh and labelled using TMRM. Following an initial imaging period, veratridine (100 µM) or vehicle (0.67% DMSO in saline solution, the same concentration of the veratridine treatment) was applied topically with cotton balls immersed in the solution. After drug treatment, a coverslip was placed on the saphenous nerve and it was imaged, *in vivo*, using a confocal laser-scanning microscope. At least 9 different nodes of Ranvier in different axons were imaged in an individual preparation, and either a single image was recorded every 10 minutes, or a z-stack was recorded every 20 minutes, for a period varying between 5 and 10 hours after stimulation.

Time-lapse images of axonal mitochondrial movement were assessed blindly using 'Difference Tracker' plug-in for ImageJ. First, the number of all mitochondrial "tracks" (defined as one mitochondrial profile moving continuously for ≥6 frames, i.e. 11.8s) was recorded over 50 frames (i.e. 98.5 s).

Electron microscopy analysis of mitochondrial distribution in axons subjected to sustained stimulation was performed in the preparations previously obtained and examined in chapters 2 and 3. Briefly, after the saphenous nerve was stimulated either electrically or chemically and imaged in vivo for a period around 6 hours, the nerves were fixed in glutaraldehyde for at least 24 hours and the central 5 mm length of each fixed nerve was excised. The nerves were post-fixed in osmium tetroxide, dehydrated and embedded in

resin. Sections 0.7 µm thick were cut and collected onto slides, stained with thionin acetate and acridine orange, and then examined at light microscopy. Ultrathin sections were also cut and examined in an electron microscope.

4.3 Results

Expansion of the paranode depends on the activity of mitochondria

In view of the observations described above we next aimed to study the role of mitochondria in the axonal morphological alterations following sustained stimulation. To do so, mitochondrial activity was first blocked with sodium azide (1 mM), which inhibits the mitochondrial cytochrome oxidase. Sodium azide alone caused no alterations when it was added to the aCSF incubating the excised spinal roots. Interestingly, it also showed no morphological alterations when the excised spinal roots were treated also with veratridine (100 µM, 10 minutes), contrary to what had been previously observed in spinal roots simply treated with veratridine (figure 49).
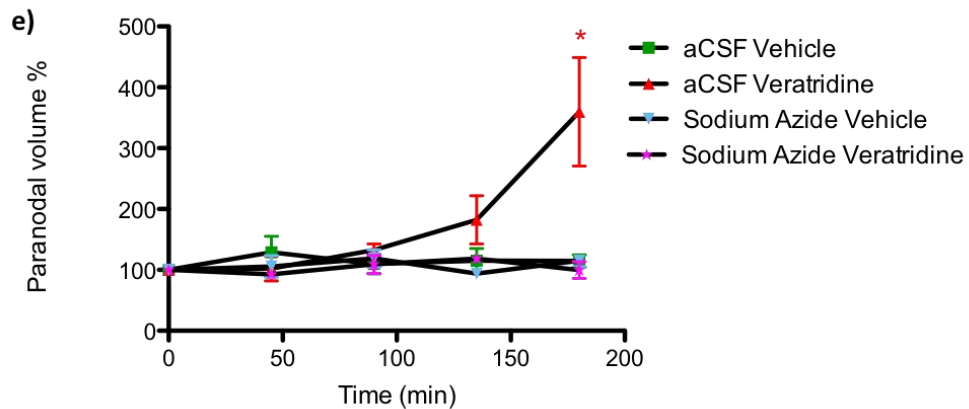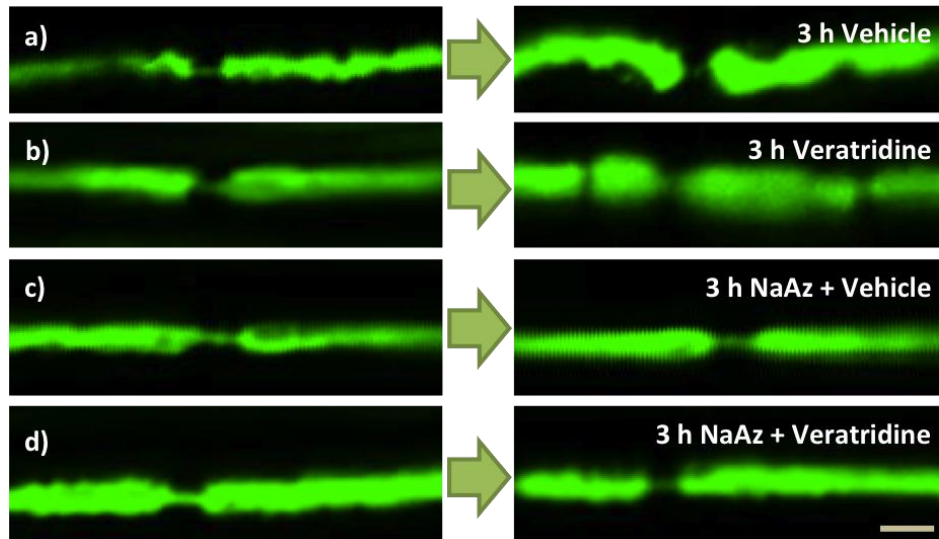
Figure 49a-e– Swelling of the paranodes caused by veratridine is prevented in axons treated with sodium azide.

Ex vivo confocal imaging of YFP positive axons in mouse spinal roots incubated with aCSF (**a**, **b**) or sodium azide (**NaAz**, **c**, **d**), before (left panel) and 3 hours after (right panel) treatment with either vehicle (**a**, **c**) or veratridine (**b**, **d**). Incubation of the spinal roots with sodium azide did not cause any morphological alterations. Indeed, incubation with sodium azide prevented the swelling of the paranodes observed in spinal roots treated only with veratridine (quantified in **e**). Scale bar is 10 µm. Statistical test used was Student's t-test with two-tailed distribution, two-sample equal variance. *=$p<0.05$. N=5 nodes from each of 4 animals.

This result suggests that blocking mitochondrial activity prevents the morphological alterations observed following sustained stimulation. However, considering that this observation could theoretically result from a different mode of action of the sodium azide, we tried to replicate it by impairing mitochondrial function by an alternative method, namely by repeating the experiment using the nitric oxide donor DETA NONOate (6 mM) instead of sodium azide (figure 50).

When DETA NONOate was added to the aCSF, similar results were obtained to those obtained with sodium azide: treatment with both vehicle and veratridine together with DETA NONOate resulted in no morphological alterations, contrary to what happens with axons treated with veratridine alone.

Since nitric oxide inhibits mitochondrial metabolism, thus inhibiting the production of ATP, this result strengthens that obtained with sodium azide, strongly indicating that the observed morphological alterations depend on the normal functioning of the mitochondria.
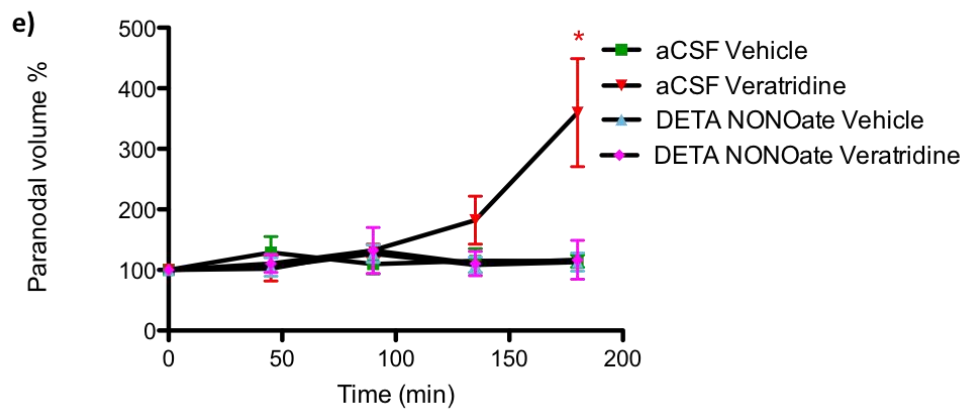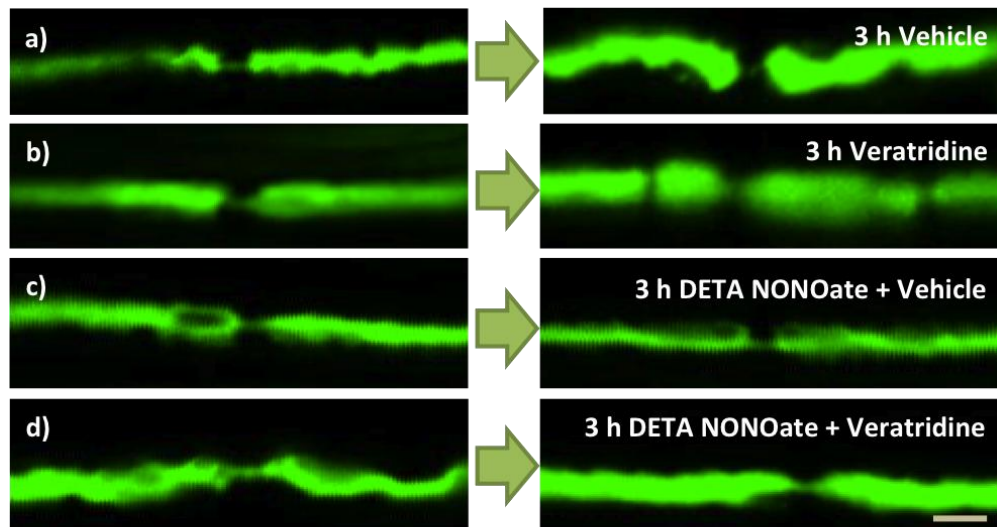
Figure 50a-e– Swelling of the paranodes caused by veratridine is prevented in axons treated with DETA NONOate.

Ex vivo confocal imaging of YFP positive axons in the mouse spinal roots incubated with aCSF (**a**, **b**) or DETA NONOate (**c**, **d**), before (left panel) and 3 hours after (right panel) treatment with either vehicle (**a**, **c**) or veratridine (**b**, **d**). The incubation of the spinal roots with DETA NONOate did not cause any morphological alterations. Indeed, incubation with DETA NONOate prevented the swelling of the paranodes observed in spinal roots treated only with veratridine (quantified in **e**). Scale bar is 10 μm. Statistical test used was Student's t-test with two-tailed distribution, two-sample equal variance. *=p<0.05. N=5 nodes from each of 4 animals.

Mitochondria distribution is not altered in stimulated axons

Given that the previous observations focused attention on energy provision within the axons, experiments were conducted to examine the potential effects on axonal mitochondria of sustained impulse conduction. In particular we studied the distribution of mitochondria along the axon with respect to the node of Ranvier. To do so, electrically conducting saphenous nerves were labelled with TMRM (figure 51), which identifies polarized mitochondria with membrane potential, and real time confocal imaging *in vivo* was used to track mitochondrial movement.
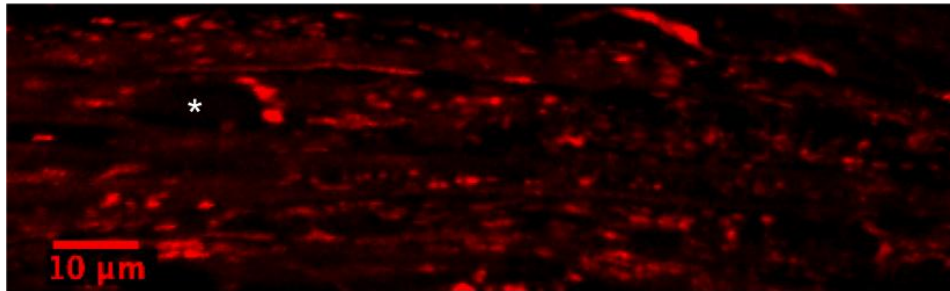
Figure 51 – Mitochondrial trafficking during impulse conduction.

Typical confocal image of *in vivo* saphenous fibres exposed in an anaesthetised mouse, labelled with TMRM. Asterisk denotes Schwann cell nuclei.

Electrical activity did not alter the overall distribution of mitochondria along the axons, although high frequency stimulation resulted in a more even distribution along the axon/internode (figure 52).

These results suggest that even under high frequency stimulation, there is no preferential mitochondria recruitment to any specific axon domain, seemingly indicating the absence of a checkpoints or their recruitment to specific-location in electrically conducting axons.

a)

b)
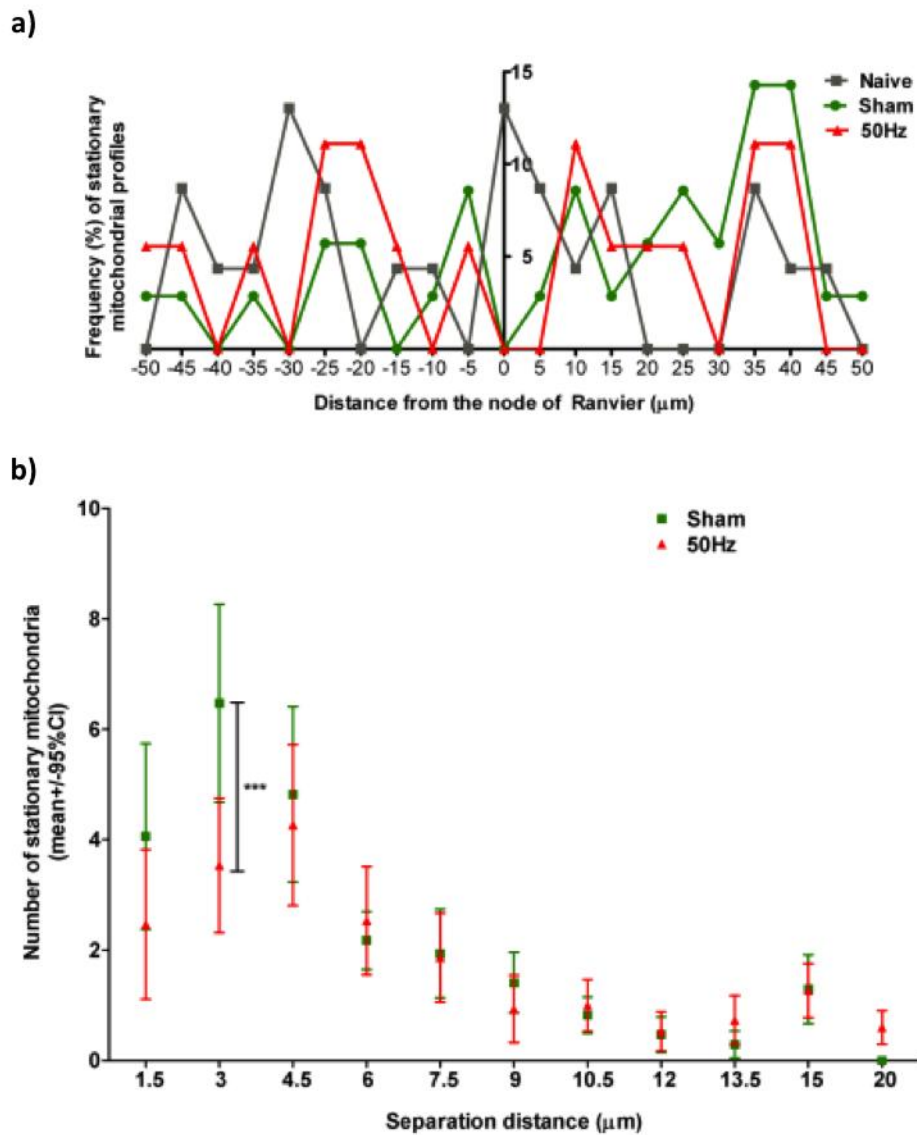
Figure 52a-b – Distribution of mitochondria does not change, but the distance between stationary mitochondria increases in axons conducting at 50 Hz.

No accumulation of mitochondria was detected in the nodal/paranodal region in stimulated axons (**a**). The number of mitochondria separated by 1.5 µm (measured between their mid-points) decreased in axons conducting at 50Hz, and was significantly lower for mitochondria separated by 3µm, i.e. mitochondria were less clustered in stimulated axons (**b**). ***=$P<0.001$. (Data in figure 52 gathered by Dr. Marija Sajic from tissue similar to that generated by the author).

Electrical stimulation does not significantly alter mitochondrial distribution at the nodal/paranodal region

Following the observation that mitochondrial function is essential to the morphological alterations observed under sustained electrical stimulation, and that electrical conduction appears to alter mitochondrial movement, we decided to examine the behaviour of mitochondria following sustained stimulation.

Firstly, we examined whether mitochondria in stimulated axons accumulated near nodes of Ranvier (within 15 μm of the nodal gap), as has been suggested. Although we previously showed that electrical stimulation increased the number of mobile mitochondria, electron microscopic imaging of tissue fixed around six hours after 2 hours of either sham surgery or 100 Hz stimulation, showed no nodal accumulation of mitochondria, or any other obvious difference in their distribution in the nodal/paranodal region (figure 53).

This analysis was conducted in tissue fixed up to 6 hours after electrical stimulation, which included some axons with an expanded nodal gap. As a result, the various axons imaged after stimulation at 100 Hz were in different stages of the previously described morphological alterations resulting from sustained electrical stimulation. This fact caused an increase in the variability in the node/paranode morphology, and, as such, in mitochondrial distribution.
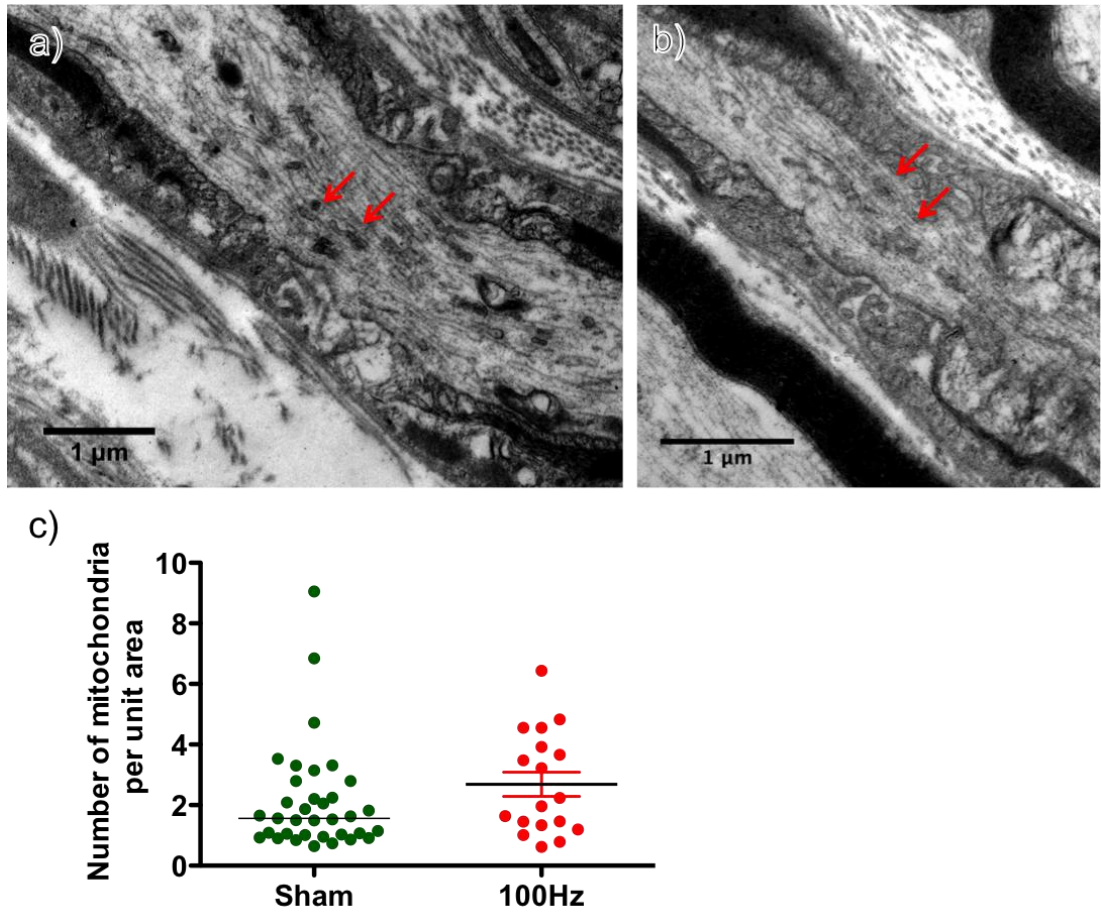
Figure 53a-c – Mitochondrial distribution following electrical stimulation activity.

Mitochondria in axons sham (**a**), and electrically stimulated for 2 hours at 100 Hz (**b**), appeared similar upon ultrastructural examination, and the number of mitochondria (**red arrows**) present in the nodal/paranodal region was similar in both situations (**c**). Statistical test used was Student's t-test with two-tailed distribution, two-sample equal variance's=0.27.N>4 nodes from each of 4 animals.

Chemical stimulation resulted in a lower presence of mitochondria in the nodal region

Due to the variability of timing in the morphological alterations in electrically stimulated axons, we repeated the analysis using veratridine-treated axons in which the timing of the morphological alterations was more homogeneous. The increased homogeneity of the observations was expected to result in greater statistical power (figure 54).

Electron microscopic imaging of mitochondria in axons six hours after treatment (10 minutes) with either vehicle (0.67% DMSO in saline solution) or veratridine (100 μM) showed a decreased number of mitochondria in the nodal/paranodal region (p=0.053). Compared with control, the cytoskeleton in veratridine-treated axons appeared disorganized, losing its characteristic longitudinal orientation. Specifically, in the herniated portions, the cytoskeleton appeared very disrupted.

This result is not particularly surprising nor contrary to that obtained with electrical stimulation, as while some of the electrically stimulated axons had regained their original nodal morphology by the time of fixation and electron microscopy imaging, most of the veratridine-treated axons maintained the herniated paranode for longer time periods. Because the number of mitochondria per node was not altered, it follows that the increase in axoplasmic volume at the paranodal region is not matched by a similar increase in mitochondrial mass.
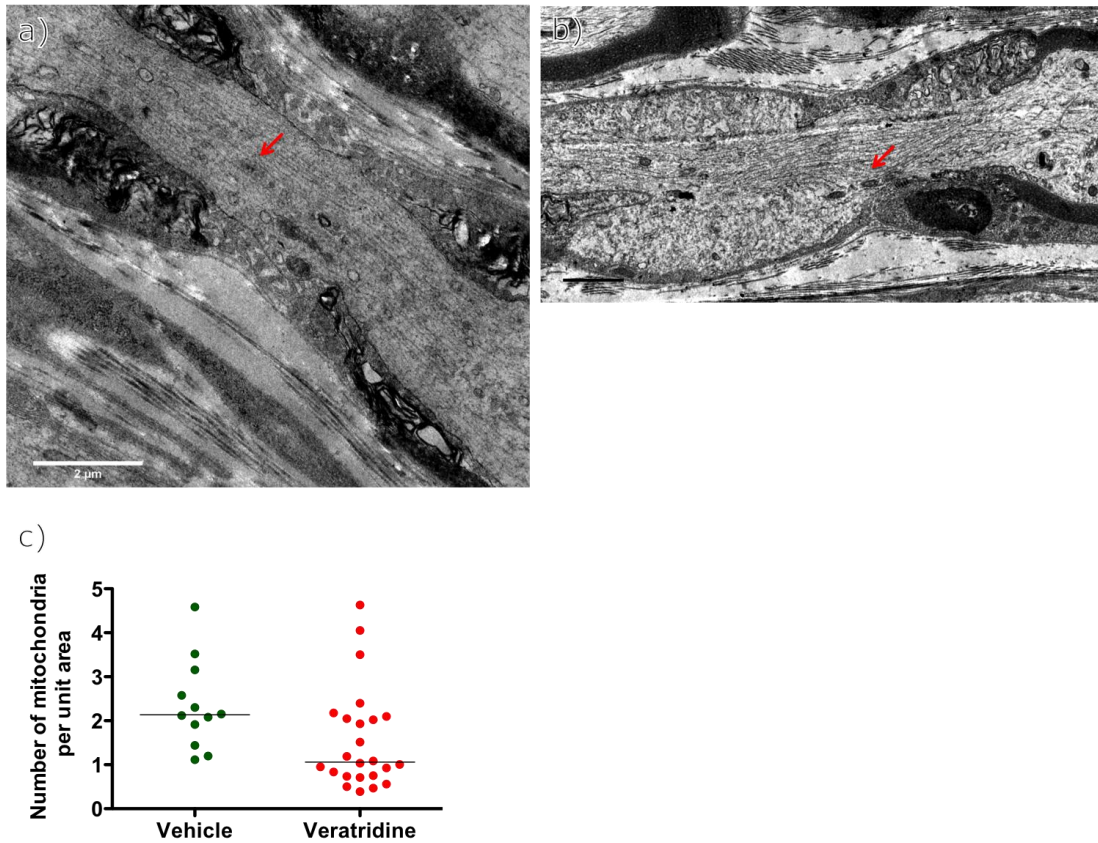
Figure 54a-c – Mitochondrial distribution following treatment with veratridine.

Mitochondria in axons treated with vehicle (**a**) or veratridine (**b**) appeared similar upon ultrastructural examination. The veratridine-treated axons tended to have fewer mitochondria (**red arrows**) per unit area ($p=0.053$) when compared with vehicle-treated controls (quantified in **c**). Statistical test used was Student's t-test with two-tailed distribution, two-sample equal variance. N>4 nodes from each of 4 animals. Scale bar is 2 μm.

Moreover, examination of the distribution of mitochondria at the elongated node/paranode region of stimulated axons showed that mitochondria tended to maintain their distribution along the original outline of the axon, i.e., most of the mitochondria did not follow the herniated axoplasm (figure 55). Indeed, mitochondria appear to maintain not only their location, but also their orientation along the disrupted cytoskeleton orientation. One could argue that

the transient nature of the axoplasmic herniation would not allow sufficient time for the formation of microtubules to transport mitochondria to this location.
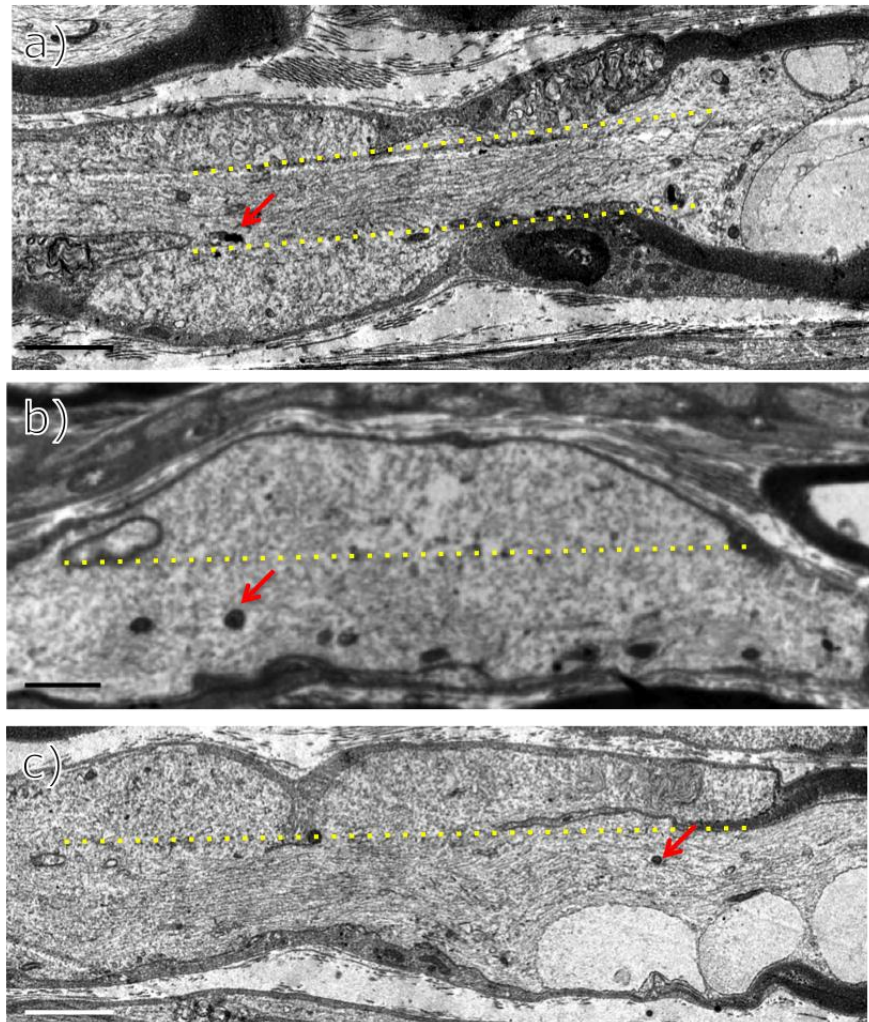
Figure 55a-c–Mitochondria tend to maintain their distribution along the original line of the axoplasm in the expanded nodal gap in veratridine-treated axons.

Mitochondria in veratridine-treated axons tend to maintain their distribution along the original path of the axoplasm (**dashed lines**, as best as can be judged), as best illustrated in a. The mitochondria do not follow the form of the herniation at the nodal/paranodal region and are not seen in the herniated axoplasm. Scale bar is 2 μm.

Treatment of YFP positive axons with TMRM does not seem to affect the morphology of either the axon or the mitochondria

Following the observation that mitochondria do not appear in the herniations of veratridine-treated axons, we decided to study the behaviour of mitochondria treated with veratridine in real time. In order to do so, YFP positive saphenous nerves were labelled with TMRM and imaged *in vivo* under a confocal microscope (figure 56).
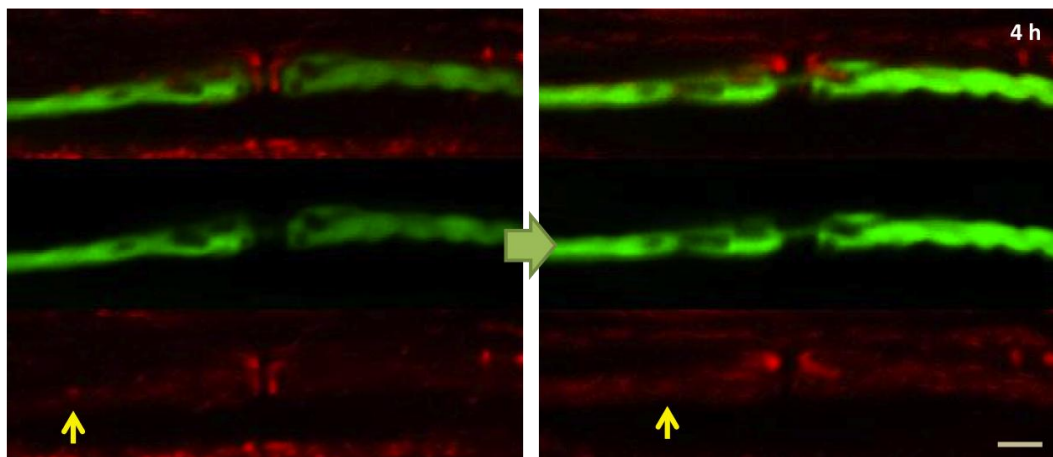
Figure 56 – Imaging of TMRM-labelled, YFP positive axons.

YFP (**green labelling**) saphenous fibres exposed *in vivo* in an anaesthetised mouse, labelled with TMRM (**red labelling**), immediately (left panel) and 4 h after TMRM labelling. Mitochondria are evident in both the axon (**yellow arrows**) and the Schwann cell, and are not grossly altered during the imaging period. Scale bar is 10 μm.

Imaging shows the TMRM signal in YFP positive axons, which confirms that these are axonal mitochondria. At the node of Ranvier there is a concentration of mitochondria in the collar of Schwann cell cytoplasm surrounding the node.

The labelling of TMRM is maintained up to 4 hours into imaging, with no evident loss of signal, which indicates that the mitochondria membrane potential is not grossly altered. Similarly, the labelled mitochondria do not present any obvious morphological alterations during the imaging period.

The motility of mitochondria is affected by axonal morphological alterations

In vivo topical application of veratridine (100 μM, applied for 10 minutes) to the saphenous nerve of Thy1-YFP-16 transgenic mice treated with TMRM allowed the observation of that the herniated axoplasm is directed backwards over the axon, underneath the Schwann cell cytoplasm collar that normally surrounds the node of Ranvier (figure 57).

Imaging reveals that the labelling with TMRM is maintained up to 4 hours into imaging, with no evident loss of signal, indicating that there is no obvious alteration of mitochondrial membrane potential. Similarly, mitochondria do not present any obvious morphological alterations during the imaging period.
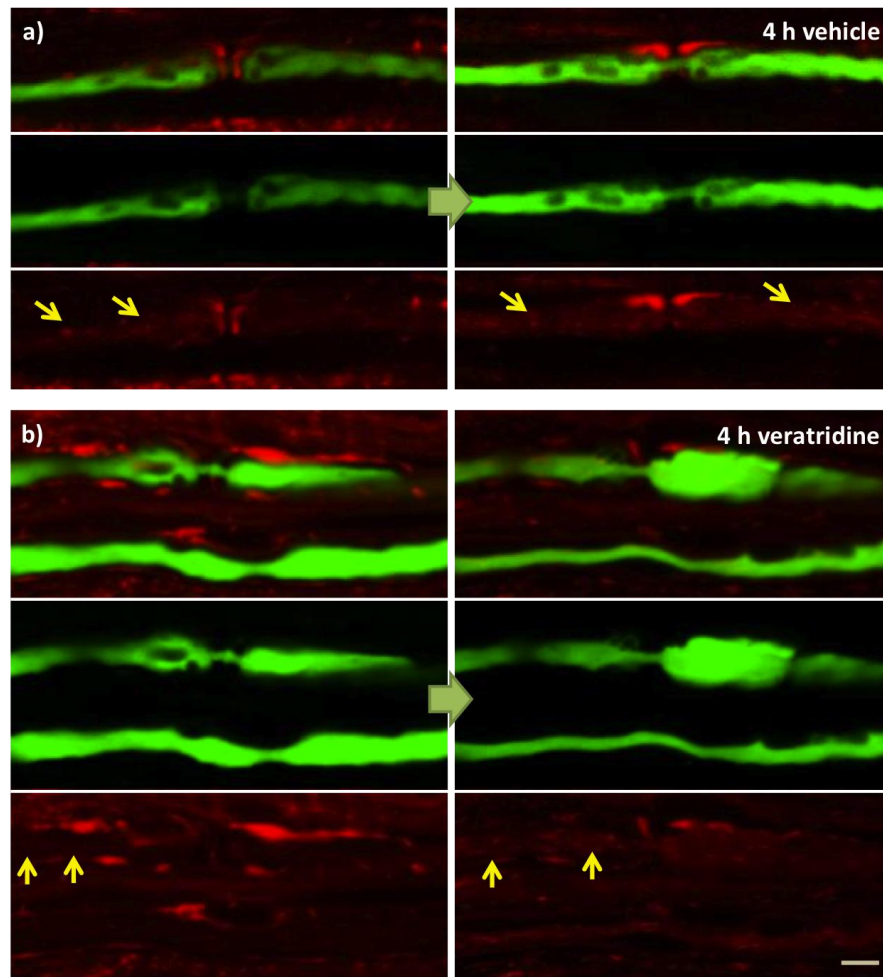
Figure 57a-b–Imaging of TMRM labelled, YFP positive, veratridine-treated axons.

YFP (**green labelling**) saphenous fibres exposed *in vivo* in an anaesthetised mouse, labelled with TMRM (**red labelling**), before (left panel) and 4 h after (right panel) treatment with vehicle (**a**) and veratridine (**b**). Following treatment with veratridine, we can observe the characteristic axoplasmic herniation, that happens underneath the collar of Schwann cell cytoplasm that normally surrounds the node of Ranvier, indicated by the presence of mitochondria surrounding the YFP positive node of Ranvier. Mitochondria are evident in both the axon (**yellow arrows**) and the Schwann cell, and are not altered during the imaging period. Scale bar is 10 µm.

The mitochondria present in the collar of Schwann cell cytoplasm neighbouring the node of Ranvier are also clearly visible, and they appear to be healthy and undisturbed for the duration of the imaging period (figure 57). This result is strengthened by our previous electron microscopic observations showing that sustained stimulation causes no obvious gross alterations of the Schwann cell, other than its adaptation to the form of the axoplasmic herniation. In these images the Schwann cell mitochondria are unaffected by both electrical stimulation and treatment with veratridine.

Quantification of the mitochondria movement in axons treated with veratridine also showed no significant difference from vehicle treated controls. However, when this analysis included exclusively axons undergoing morphological alterations at the node/paranode region, it was clear that moving mitochondria were virtually absent (figure 58), indicating that the morphological alterations may arrest mitochondrial movement.

Even though mitochondrial transport is affected by the morphological alterations elicited by sustained stimulation, there are no other obvious alterations to the mitochondria, either in terms of shape, size, or membrane potential, both in the axons and in the Schwann cells.
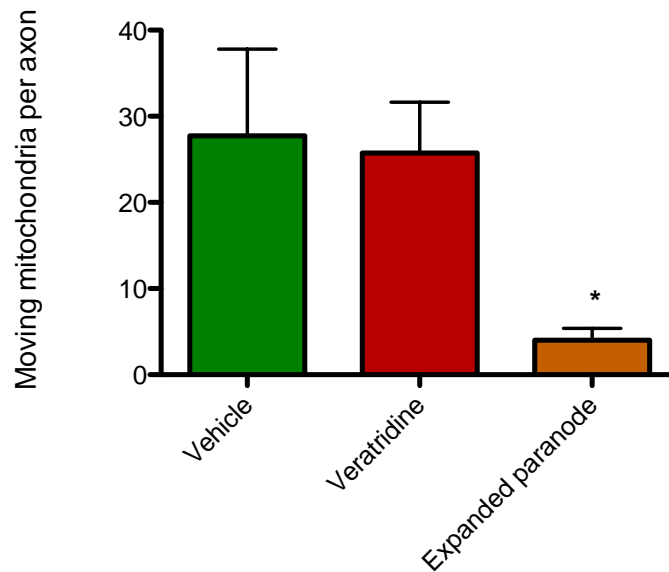
Figure 58–Quantification of mitochondria movement in axons treated with veratridine.

There is no difference in the number of moving mitochondria in YFP positive axons labelled with TMRM, after treatment with vehicle or veratridine. However, when analysis was restricted to those axons with herniated axoplasm (assessed by imaging the YFP positive axoplasm), it was clear that the number of moving mitochondria was greatly decreased. Statistical test used was Student's t-test with two-tailed distribution, two-sample equal variance.*=p<0.05. N>5 axons from each of 4 animals.

4.4 Discussion

Our findings indicate that the morphological alterations of the axon following sustained stimulation are energy dependent, because inhibiting the mitochondrial activity with either sodium azide or a NO donor, in combination with chemical stimulation, resulted in no morphological alteration.

At first glance, this result may seem to contradict a previous observation in this thesis that partial ischaemia after sustained stimulation facilitates the morphological alterations at lower frequencies of stimulation, as both experiments require the axon the axon to cope with sustained stimulation under metabolic deficits. However this superficial interpretation overlooks the fact that the metabolic deficits are applied in different points of the protocol. Whilst the partial ischaemia is applied only after electrical stimulation has ceased, and so the axons are already loaded with sodium, the inhibitors of mitochondrial activity are applied simultaneously with the chemical stimulation. In this latter case the energy depletion will cause axonal depolarisation and this will protect the axons from sodium loading by preventing the sustained impulse activity.

Mitochondrial trafficking along axons is important, but the functional significance of trafficking remains unclear. It has been suggested that mitochondria become distributed to fulfil local energy requirements, or to participate in regulation of the cytosolic calcium concentration (Plucinska, et al. 2012), consistent with observations in vitro in Purkinje cells (Andrews, et al. 2010) and excised frog nerves (Miller and Sheetz, 2004), where activity

leads to mitochondrial accumulation near nodes of Ranvier. However, our observations allow a reconsideration of the notion that mitochondria become distributed along axons to satisfy the local energy demands. The available data on mitochondrial distribution following electrical stimulation are not convincing and they do not really agree with the finding that the sodium potassium ATPase is located along the internode, rather than at the node. We have therefore studied the relationship between the movement and distribution of mitochondria in electrically active axons.

Our findings demonstrate the lack of additional mitochondrial recruitment to nodal/paranodal/juxtaparanodal regions both before and following impulse activity, which suggests that, in these regions, mitochondria are constitutively positioned to maintain the energy demands of sustained impulse activity and so no redistribution is necessary. The overall distribution of mitochondria remained unchanged along the internodes, without accumulation near nodes of Ranvier. Regulation of mitochondrial distribution by impulse activity may provide an effective mechanism to ensure that mitochondrial replenishment is matched to the activity of a particular axon, but sustained impulse conduction does not appear to require additional mitochondrial presence in particular axonal domains.

Time lapse examination of mitochondrial movement revealed that not only were mitochondria absent from the herniated axoplasm, but the mitochondria within the less disrupted portion of the nodal/paranodal axon had also ceased moving. The absence of mitochondria from the herniation can be explained by the paucity of microtubules within this axoplasm, but the cause

of the transport failure remains uncertain, as the data do not clarify whether the mitochondria stopped moving due to active recruitment or due to a checkpoint mechanism in the morphologically altered axon. It is perhaps most likely that the loss of movement may arise from a mechanistic issue resulting from the transient disruption of the microtubule cytoskeleton along which mitochondria are transported (Hollenbeck and Saxton 2005) (indeed, electron microscopy showed that the orientation of the cytoskeleton was disturbed): however, it is also possible that the tissue is depleted of adequate energy to maintain mitochondrial movement, or that the mitochondria are arrested so that they remain in a region of greater energy demand or calcium accumulation. Mitochondrial arrest in association with a rise in cytoplasmic calcium has been reported(MacAskill and Kittler, 2009).

The finding that inhibition of mitochondrial activity with the NO donor or cytochrome oxidase inhibitor prevented the morphological alterations in response to chemical stimulation reinforces our results obtained with sodium azide. These observations are consistent with our hypothesis that the main mechanism behind the morphological alterations is an increase in osmotic pressure in the periaxonal space, caused by the accumulation of sodium ions transported by the sodium pump from the axon to this space, following sustained stimulation (chapter 3). Thus by inhibiting mitochondrial activity there is less ATP available and so less activity of the energy-dependent sodium pump. The osmotic gradient is not established, and so the morphological consequences do not occur.

General Discussion

The results have revealed novel changes in the structure of myelinated axons in response to sustained electrical and chemical stimulation, and the changes may shed light on the mystery regarding the pathway(s) taken by sodium ions in the axon during sustained stimulation. The morphological alterations include a reversible and dramatic expansion of the periaxonal space and a swelling of the axoplasm at the paranodes that culminates with it herniating and greatly expanding the nodal gap. The fluid in the periaxonal space accumulates into droplets that travel down towards the paranode, where they apparently escape to the extracellular space by parting the attachment of the paranodal loops.

The first observed morphological alteration showed an expansion of the periaxonal space, occurring more intensely in the area of the internode. These observations agree with our working hypothesis in which this phenomenon is caused by an osmotic imbalance associated with an increase in ionic circulation.

The cause of nodal herniation appears to be an increase in axoplasmic pressure due to the expansion of the periaxonal space, which compresses the internodal axoplasm. The fact that the voltage-gated sodium channels are located at the nodal membrane, and that the herniation occurred in response to repeated activation of these channels resulting in a high influx of Na^+ into the axon, could suggest that the Na^+ influx would create a local osmotic imbalance that increased fluid pressure, resulting in swelling in this

region where the axon is less rigidly constrained by the physical properties of the myelin sheath and surrounding basal lamina. However, the timing of the swelling, in some nodes initiated only 4 to 6 hours after the stimulation had been terminated, peaked about 4 hours after stimulation. The fact that the swelling was delayed, rather than coincident with the stimulation, narrows the number of possible explanations. Thus presumably the voltage-gated sodium channels were in their closed conformation after stimulation (the axon would be expected to be hyperpolarised due to pump activity once stimulation has finished), and so the influx of sodium would have ceased. We reason that osmosis in response to Na^+ accumulation would be quite a rapid phenomenon, rather than being most apparent hours after stimulation, in which case osmotic swelling due to axoplasmic Na^+ accumulation seems an unsatisfying explanation for the swelling. Events related to pump activity seem a more likely explanation, especially if one considers that the evidence suggests that the pump is active for a period of hours following sustained impulse activity (Bostock and Bergmans, 1994).

Another clue to the mechanism was given by the exaggeration of the structural changes when the blood supply to the nerve was impaired. If the swelling was dependent on metabolic activity, then partial ischaemia would be expected to reduce the swelling, as partial ischaemia would be expected to diminish the ATP availability, but this is not what is observed. Rather, ischaemia makes the swelling worse. We reason that partial ischaemia following stimulation could result in axonal depolarisation, thereby opening sodium channels and increasing the loading of sodium ions to the axon, and

thence to the periaxonal space, so that stimulation at 20 Hz becomes equivalent in terms of sodium loading to stimulation at 100 Hz.

As described above, sustained impulse activity at 20, and even at 100Hz is within the physiological range for many axons, although we found that with 100Hz frequency the amplitude of the compound action potential diminished over the stimulation period indicating that many fibres were not able to follow faithfully at this frequency for the whole stimulation period, or that conduction block developed in some fibres. Notably, the conduction deficits developed during the period of stimulation, and recovered largely back to normal within 30 minutes afterwards, and before or during the period when the herniation occurred. The lack of fidelity during the stimulation could be explained by the leakage of K^+ ions into the periaxonal space during axonal repolarization, since this is aided by the activation of delayed rectifier potassium channels in the internode and the subsequent release of K^+ into the periaxonal space (Baker, et al. 1985, Baker and Bostock 1998, Altevogt, et al. 2002).

To ensure that the morphological observations were not merely artefacts resulting from, for example, the placement of electrodes on the nerve, pharmacological stimulation with veratridine was employed because it causes the same effect of activation of sodium channels and membrane depolarization, but by totally different mechanisms. This approach also allowed imaging of the nerve during the period of supposed impulse activity. In confirmation of the findings with electrical stimulation, pharmacological modulation of voltage-gated sodium channels caused a similar expansion of the periaxonal space, thereby increasing our confidence that the widened

periaxonal space is indeed a direct or indirect consequence of Na$^+$ entry through voltage-gated sodium channels. This expansion also reproduced the herniation of axoplasm in the paranodes, and in fact this axoplasmic extrusion was both faster and more intense than with electrical stimulation. These differences might be due to the mechanism of action of veratridine, which opens Na$^+$ channels persistently, and almost irreversibly (Wang and Wang 2003). Thus whereas Na$^+$ channels in electrically stimulated axons are only open for a small percentage of time, in pharmacologically treated axons the open time may be much greater. It was also observed in both experimental conditions that the periaxonal fluid accumulated into droplets that travelled towards the paranodes, apparently escaping to the extracellular space by parting the attachment of the paranodal loops to the axolemma, indicating that this morphological change was also due to sodium entry rather than resulting from issues such as electrode placement.

It was interesting to find that even extreme morphological alterations of the node of Ranvier and the PAS were nonetheless entirely reversible, and axonal conduction continued throughout. Thus the paranodal herniation had recovered by one day, and the expansion of the PAS by one to two weeks. Both unmyelinated fibres and the Schwann cells appeared largely unaffected by sustained stimulation and the axonal morphological alteration in myelinated axons. It seems clear that degeneration does not occur, as there is no evidence of ovoid formation or axonal loss one week following the stimulation. Imaging of transverse sections one week later also indicates the absence of degeneration or demyelination. This degree of resilience is perhaps greater than might have been expected, and it encourages a view

that the changes may be within the physiological range of changes that can be expressed by axons, representing a mechanism employed to restore homeostasis during sustained conduction.

The morphological alterations appear to be caused by the movement of ions, more specifically sodium ions, as pharmacological blocking of both the entry of sodium ions into the axon and their transport to the periaxonal space prevented the morphological alterations. Interestingly, blocking the potassium channels, preventing potassium from leaving the axon during sustained stimulation, resulted in a faster and more intense paranodal herniation. This result again raised the question of osmotic pressure, since in this experimental condition the increase of osmotic pressure is potentiated both in the axon (due to the accumulation of potassium ions) and the periaxonal space (due to the accumulation of sodium ions), presumably potentiating water diffusion from the extracellular medium into both the axon and the periaxonal space. This interpretation is favoured given the fact that the increase in axonal (and presumably Schwann cell) hydrostatic pressure resulting from incubation in a hypo-osmotic medium causes morphological alterations in the axon similar to those observed following sustained stimulation. Being so, it is very likely that the morphological alterations observed following sustained stimulation are caused by osmotic pressure due to the ions displaced during signal conduction. Finally, the fact that the expansion of the periaxonal space and the herniation at the paranodes were both prevented by blockade of the sodium pump strongly indicates that it is the movement of ions across the internodal axolemma that is responsible. Moreover, recent studies have suggested that the sodium pump, is located

not in the node of Ranvier, as had been previously believed, but in the internodal region of the axolemma, beneath the myelin sheath (Young, et al. 2008).

The blocking of the morphological alterations by inhibiting ATP production strongly implicates the importance of ATP in its genesis, especially since the 'Na$^+$ pump' is perhaps the greatest single consumer of ATP in axons, in fact accounting for more than 50% of ATP utilisation (Koester et al, 1991, Scour, 1957). In a situation of high frequency stimulation, the opening of the voltage-gated sodium channels is such that it allows an elevated influx of sodium, leading to an increased need of 'sodium pump' activity, and a consequential increase in the demand of energy. If this energy requirement is not met, the activity of the pump is compromised, jeopardizing homeostasis by limiting the extrusion of Na$^+$ ions from within the axoplasm to the periaxonal space. Being so, inhibiting the production of ATP limited the activity of the sodium pump, and as a result the sodium ions did not accumulate in the periaxonal space, hence preventing the morphological alterations resulting from this accumulation.

With the critical role that one can assume that mitochondria play in axonal homeostasis, it is perhaps noteworthy to observe that their distribution and morphology were not altered in electrically stimulated axons. The only apparent alteration in mitochondrial distribution was observed with chemical stimulation, which resulted in a paucity of mitochondria in the nodal region, perhaps related to the marked disruption in axoplasmic organisation in the herniated region. Indeed, when the sections were analysed at electron

microscopy most of the axons exhibited a herniated paranodal morphology. The microtubules in the displaced axoplasm were disorganized, and mitochondria were virtually absent from this portion of axoplasm. We presume that mitochondria are absent from the herniated axoplasm because of the lack of an organized microtubule structure in this portion of the axoplasm.

This explanation is strengthened by the *in vivo* observation that the motility of axonal mitochondria is impaired at herniated nodes. In fact, while there is no significant difference in mitochondria movement between stimulated and control axons, there were nonetheless virtually no mitochondria moving when the analysis was limited to those axons with herniated axoplasm in the paranode.

Given the paucity of mitochondria, the resilience of the axon is even more astonishing: not only are the axons able to cope with the morphological alterations both in terms of biology (the alterations are reversible and cause no degeneration) or function (axons keep conducting while the alterations take place), but they do so while their energy homeostasis is apparently disrupted.

A recruitment of mitochondria to the node upon sustained stimulation might have been expected on the basis of some previously published observations (Berthold, et al. 1993, Fabricius, et al. 1993, Perkins and Ellisman, 2011), but the observed lack of recruitment agrees with our view that the sodium pump is not located preferentially at the node, in which case impulse activity does not result in an increased energy demand at the nodes. The mitochondria

are presumably optimally distributed along the axons prior to the experiment, due to the ongoing impulse activity encountered during normal life prior to anaesthesia, in which case no re-distribution is required by the impulse activity imposed during the experiment.

Conclusion

The results show that axons can undergo a hitherto unrecognised, but profound, sequence of morphological changes in response to sustained opening of sodium channels. The changes start with an expansion of the periaxonal space, which separates the axolemma from the Schwann cell and appears to compress the axoplasm. The supposed increase in axoplasmic pressure causes the paranodal herniation of the axoplasm, displacing the paranodes and greatly widening the nodal gap. Concurrently, the fluid in the expanded periaxonal space becomes organised into droplets that travel to the paranode where they escape to the endoneurium by apparently parting the attachment of the paranodal loops. These alterations occurred in virtually all axons (verified using electron microscopy), and were prevented by sodium channel or sodium pump inhibitors. Our interpretation is that the sodium ions entering the axon during impulse activity are pumped into the periaxonal space, which then swells osmotically, compressing the axon. The pressure causes an inflation of the axon at the paranodes and an extrusion of the axoplasm. The sodium rich periaxonal fluid then escapes to the extracellular space through the nodal gap.

The changes are remarkable in that they are entirely reversible, and cause no degeneration, which seems to suggest that they may be part of the normal axonal repertoire, revealing that axons have an extraordinary degree of morphological plasticity. Importantly, the phenomena that are here starting to be unveiled are not 'merely' a laboratory curiosity, but rather they appear to shed light on the mechanisms of axonal ion homeostasis. Indeed, the

changes may provide a visual and quantifiable picture indicating the pathways of ion circulation following sustained activity.

Understanding how axons react to high frequency firing in physiological circumstances may prove valuable in understanding how axons behave under pathological conditions, and indeed we have found that pathological conditions, mimicked here by partial ischaemia and exposure to nitric oxide, exacerbate the morphological changes. It seems reasonable to suggest that the morphologically stressed axons may be more vulnerable to degeneration under adverse conditions that may be tolerated by normal axons. In this case the observations made here may contribute to our understanding of why axons degenerate in neurological disease.

The most obvious shortcoming of this work is that even though we have presented evidence that seems to indicate that the periaxonal space-paranode pathway works at least as a 'storm-overflow' mechanism, restoring homeostasis in the axon, we have not clearly demonstrated that this is the prefered pathway taken by sodium ions during physiological conduction. Further work would necessarily focus on this aspect, trying to demonstrate whether or not this pathway is the exclusive one, and also to clarify which of the three different possible routes the ions take upon reaching the paranode (across the transverse bands, along the spaces between the transverse bands or between the paranodal loops) (Mierzwa, et al. 2010). It would also be interesting to try to replicate these results in a more physiological setup, namely by using a mechanical stimulation of the nerve at the sensory terminals instead of an electrical or chemical one.

Bibliography

Abram's, C K, S Oh, Y Ri, and T A Bargiello. "Mutations in connexin 32: the molecular and biophysical bases for the X-linked form of Charcot-Marie-Tooth disease." Brain Research Reviews 32, no. 1 (2000): 203-14.

Adelman, W J, and Y Palti. "The effects of external potassium and long duration voltage conditioning on the amplitude of sodium currents in the giant axon of the squid, Loligopealei." The Journal of General Physiology 54, no. 5 (1969): 589-606.

Adelman, W J, Y Palti, and J P Senft. "Potassium ion accumulation in a periaxonal space and its effect on the measurement of membrane potassium ion conductance." The Journal of Membrane Biology 13, no. 4 (1973): 387-410.

Aguayo, A J, G M Bray, and S C Perkins. "Axon-Schwann cell relationships in neuropathies of mutant mice." Annals of the New York Academy of Sciences 317 (1979): 512-31.

Alberti, S, Gr, C T Spadella, and C Cojocel. "Localization and irregular distribution of Na,K-ATPase in myelin sheath from rat sciatic nerve." Tissue &Cell 39, no. 3 (2007): 195-201.

Altevogt, B M, K A Kleopa, F R Postma, S S Scherer, and D L Paul. "Connexin29 is uniquely distributed within myelinating glial cells of the central and peripheral nervous systems." Journal of Neuroscience 22, no. 15 (2002): 6458-70.

Andrews, S, J Gilley, and M P Coleman. "Difference Tracker: ImageJ plugins for fully automated analysis of multiple axonal transport parameters." Journal of Neuroscience Methods 193, no. 2 (2010): 281-287.

Angelides, K J, L W Elmer, D Loftus, and Elson E. "Distribution and lateral mobility of voltage-dependent sodium channels in neurons." The Journal of Cell Biology 106, no. 6 (1988): 1911-25.

Armstrong, R, A D Toews, and P Morell. "Axonal transport through nodes of Ranvier." Brain Research 412, no. 1 (1987): 196-9.

Arroyo, E J, Y Xu, L Zhou, A Messing, E Peles, S Y Chiu and S S Scherer. "Myelinating Schwann cells determine the internodal localization of Kv1. 1, Kv1. 2, Kvβ2, and Caspr." Journal of Neurocytology 28, no. 4 (1999): 333-347.

Baker, M D. "Electrophysiology of mammalian Schwann cells." Progress in Biophysics and Molecular Biology 78, no. 2-3 (2002): 83-103.

Baker, M, H Bostock, G A Brook, and S Love. "Phoneutria and Leiurus venoms induce spontaneous compound action potentials in rat spinal roots." Journal of Physiology (1985): 63 P.

Baker, M D. "Axonal flip-flops and oscillators." Trends in Neurosciences 23, no. 11 (2000): 514-9.

Baker, M D, and H Bostock. "Inactivation of macroscopic late Na+ current and characteristics of unitary late Na+ currents in sensory neurons." Journal of Neurophysiology 80, no. 5 (1998): 2538-49.

Balice-Gordon, R J, L J Bone, and S S Scherer. "Functional gap junctions in the Schwann cell myelin sheath." The Journal of Cell Biology 142, no. 4 (1998): 1095-104.

Ballin, R H, and P K Thomas. "Electron microscope observations on demyelination and remyelination in experimental allergic neuritis. I. Demyelination." Journal of the Neurological Sciences 8, no. 1 (1969): 1-18.

Baranauskas, G. "Sodium Currents Activate without a Hodgkin and Huxley-Type Delay in Central Mammalian Neurons." Journal of Neuroscience 26, no. 2 (2006): 671-684.

Barres, B A, and M C Raff. "Axonal control of oligodendrocyte development." The Journal of Cell Biology 147, no. 6 (1999): 1123-8.

Barrett, E F, and J N Barrett. "Intracellular recording from vertebrate myelinated axons: mechanism of the depolarizing afterpotential." Journal of Physiology 323 (1982): 117-44.

Béguin, P, U Hassler, A Beggah, JD Horisberger, and K Geering. "Membrane integration of Na,K-ATPase alpha-subunits and beta-subunit assembly." Journal of Biological Chemistry 273 (38) (1998): 24921-31.

Bennett, V, S Lambert, J Q Davis, and X Zhang. "Molecular architecture of the specialized axonal membrane at the node of Ranvier." Society of General Physiologists Series 52 (1997): 107-20.

Benoit E, P Juzans, A M Legrand, J Molgo. "Nodal swelling produced by ciguatoxin-induced selective activation of sodium channels in myelinated nerve fibers." Neuroscience (1996) 71: 1121-1131

Bergman, C. "Increase of sodium concentration near the inner surface of the nodal membrane." PflügersArchiv: European Journal of Physiology 317, no. 4 (1970): 287-302.

Bergoffen, J, S S Scherer, S Wang, M O Scott, L J Bone, D L Paul, K Chen, M W Lensch, P F Chance, and K H Fischbeck. "Connexin mutations in X-linked Charcot-Marie-Tooth disease." Science 262, no. 5142 (1993): 2039-42.

Berthold, C H, and A Mellström. "Distribution of peroxidase activity at nodes of Ranvier after intramuscular administration of horseradish peroxidase in the cat." Neuroscience 7, no. 1 (1982): 45-54.

Berthold, C H, C Fabricius, M Rydmark, and B Andersén. "Axoplasmic organelles at nodes of Ranvier. I. Occurrence and distribution in large myelinated spinal root axons of the adult cat." Journal of Neurocytology 22, no. 11 (1993): 925-40.

Bezanilla, F. "The action potential: from voltage-gated conductances to molecular structures." Biological Research 39, no. 3 (2006): 425-35.

Bhat, M A. "Molecular organization of axo-glial junctions." Current Opinion in Neurobiology 13, no. 5 (2003): 552-9.

Bhat, M A, J C Rios, Y Lu, G P Garcia-Fresco, W Ching, M St. Martin, J Li, S Einheber, M Chesler, J Rosenbluth, J L Salzer, and H J Bellen. "Axon-glia interactions and the domain organization of myelinated axons requires neurexin IV/Caspr/Paranodin." Neuron 30, no. 2 (2001): 369-83.

Black, J A, B Friedman, S G Waxman, L W Elmer, and K J Angelides. "Immuno-ultrastructural localization of sodium channels at nodes of Ranvier and perinodal astrocytes in rat optic nerve." Proceedings of the Royal Society of London 238, no. 1290 (1989): 39-51.

Black, J A, S G Waxman, and R E Foster. "Spatial heterogeneity of the axolemma of non-myelinated fibers in the optic disc of the adult rat. Freeze-fracture observations." Cell and Tissue Research 224, no. 2 (1982): 239-46.

Blair, N T, and B P Bean. "Role of tetrodotoxin-resistant Na+ current slow inactivation in adaptation of action potential firing in small-diameter dorsal root ganglion neurons." The Journal of Neuroscience 23, no. 32 (2003): 10338-50.

Boiko, T, M N Rasband, S R Levinson, J H Caldwell, G Mandel, J S Trimmer, and G Matthews. "Compact myelin dictates the differential targeting of two sodium channel isoforms in the same axon." Neuron 30, no. 1 (2001): 91-104.

Bostock, H, and J Bergmans. "Post-tetanic excitability changes and ectopic discharges in a human motor axon." Brain 117 (Pt 5) (1994): 913-28.

Bostock, H, M Baker, and G Reid. "Changes in excitability of human motor axons underlying post-ischaemic fasciculations: evidence for two stable states." Journal of Physiology 441 (1991): 537-57.

Boyle, M E, E O Berglund, K K Murai, L Weber, E Peles, and B Ranscht. "Contactin orchestrates assembly of the septate-like junctions at the paranode in myelinated peripheral nerve." Neuron 30, no. 2 (2001): 385-97.

Brazhe, A R, G V Maksimov, E Mosekilde, and O V Sosnovtseva. "Excitation block in a nerve fibre model owing to potassium-dependent changes in myelin resistance." Interface Focus 1, no. 1 (2011): 86-100.

Brismar, T. "Potential clamp analysis of membrane currents in rat myelinated nerve fibres." Journal of Physiology 298 (1980): 171-84.

Brown, A M, P C Schwindt, and W E Crill. "Different voltage dependence of transient and persistent Na+ currents is compatible with modal-gating hypothesis for sodium channels." Journal of Neurophysiology 71, no. 6 (1994): 2562-5.

Brown, E R, and N J Abbott. "Ultrastructure and permeability of the Schwann cell layer surrounding the giant axon of the squid." Journal of Neurocytology 22, no. 4 (1993): 283-98.

Brunder, D G, and E M Lieberman. "Studies of axon-glial cell interactions and periaxonal K- homeostasis--I. The influence of Na+, K+, Cl- and cholinergic agents on the membrane potential of the adaxonal glia of the crayfish medial giant axon." Neuroscience 25, no. 3 (1988): 951-9.

Bunge, R P. "Glial cells and the central myelin sheath." Physiological Reviews 48, no. 1 (1968): 197-251.

Bunge, R P, M B Bunge, and C F Eldridge. "Linkage between axonal ensheathment and basal lamina production by Schwann cells." Annual Review of Neuroscience 9 (1986): 305-28.

Bunge, R P, M B Bunge, and M Bates. "Movements of the Schwann cell nucleus implicate progression of the inner (axon-related) Schwann cell process during myelination." The Journal of Cell Biology 109, no. 1 (1989): 273-84.

Burg, M B, J D Ferraris, and N I Dmitrieva. "Cellular response to hyperosmotic stresses." Physiological Reviews 87, no. 4 (2007): 1441-74.

Butt, A M, and M Berry. "Oligodendrocytes and the control of myelination in vivo: new insights from the rat anterior medullary velum." Journal of Neuroscience Research 59, no. 4 (2000): 477-88.

Butt, A M, A Dunca, M F Hornby, S L Kirvell, A Hunter, J M Levine, and M Berry. "Cells expressing the NG2 antigen contact nodes of Ranvier in adult CNS white matter." Glia 26, no. 1 (1999): 84-91.

Caldwell, J H, K L Schaller, R S Lasher, E Peles, and S R Levinson. "Sodium channel Na(v)1.6 is localized at nodes of ranvier, dendrites, and synapses." Proceedings of the National Academy of Sciences 97, no. 10 (2000): 5616-20.

Carpenter, S. "An ultrastructural study of an acute fatal case of the Guillain-Barré syndrome." Journal of the Neurological Sciences 15, no. 2 (1972): 125-40.

Carrillo-Tripp, M, H Saint-Martin, and I Ortega-Blake. "A comparative study of the hydration of Na and K with refined polarizable model potentials." The Journal of Chemical Physics 118 (2003): 7062.

Cavanagh, J B. "The pattern of recovery of axons in the nervous system of rats following 2,5-hexanediol intoxication: a question of rheology?" Neuropathology and Applied Neurobiology 8, no. 1 (1982): 19-34.

Chávez, E, C Bravo, and J A Holguin. "Metabolite transport in mitochondria as a function of osmolarity." Archives of Biochemistry and Biophysics 253, no. 1 (1987): 94-9.

Chad, S R, and P J Hollenbeck. "Mitochondrial movement and positioning in axons: the role of growth factor signaling." The Journal of Experimental Biology 206, no. Pt 12 (2003): 1985-92.

Chan, J R, C Jolicoeur, J Yamauchi, J Elliott, J P Fawcett, B K Ng, and M Cayouette. "The polarity protein Par-3 directly interacts with p75NTR to regulate myelination." Science 314, no. 5800 (2006): 832-6.

Chance, P F, and D Pleasure. "Charcot-Marie-Tooth syndrome." Archives of Neurology 50, no. 11 (1993): 1180-4.

Chiba, A, S Kusunoki, H Obata, R Machinami, and I Kanazawa. "Serum anti-GQ1b IgG antibody is associated with ophthalmoplegia in Miller Fisher

syndrome and Guillain-Barre syndrome: Clinical and immunohistochemical studies." Neurology 43, no. 10 (1993): 1911-1911.

Chiu, S Y. "Functions and distribution of voltage-gated sodium and potassium channels in mammalian Schwann cells." Glia 4, no. 6 (1991): 541-58.

Chiu, S Y, and J M Ritchie. "Evidence for the presence of potassium channels in the internode of frog myelinated nerve fibres." Journal of Physiology 322, no. 1 (1982): 485-501.

Chiu, S Y, and W Schwarz. "Sodium and potassium currents in acutely demyelinated internodes of rabbit sciatic nerves." Journal of Physiology 391 (1987): 631-49.

Chiu, S Y, S S Scherer, M Blonski, S S Kang, and A Messing. "Axons regulate the expression of Shaker-like potassium channel genes in Schwann cells in peripheral nerve." Glia 12, no. 1 (1994): 1-11.

Colognato, H, and C ffrench-Constant. "Mechanisms of glial development." Current Opinion in Neurobiology 14, no. 1 (2004): 37-44.

Compston A, and A Coles. "Multiple sclerosis." Lancet 359, no. 9313 (2002): 1221-31.

Coombs, J, D Curtis, and J Eccles. "The generation of impulses in motoneurones." Journal of Physiology139, no. 2 (1957): 232-49.

Court, Felipe A, Lawrence Wrabetz, and M Laura Feltri. "Basal lamina: Schwann cells wrap to the rhythm of space-time." Current Opinion in Neurobiology 16, no. 5 (2006): 501-7.

Cruz-Höfling, M A, S Love, G Brook, and L W Duchen. "Effects of Phoneutrianigriventer spider venom on mouse peripheral nerve." Quarterly Journal of Experimental Physiology 70, no. 4 (1985): 623-40.

Culp, W J, and J L Ochoa. "Abnormal nerves and muscles as impulse generators. "Cell and Tissue Research (1982): 750.

Cummings, J F, and D C Haas. "Coonhound paralysis. An acute idiopathic polyradiculoneuritis in dogs resembling the Landry-Guillain-Barré syndrome." Journal of the Neurological Sciences 4, no. 1 (1966): 51-81.

Daniloff, J K, K L Crossin, M Pinçon-Raymond, M Murawsky, F Rieger, and G M Edelman. "Expression of cytotactin in the normal and regenerating neuromuscular system." The Journal of Cell Biology 108, no. 2 (1989): 625-35.

Davis, J Q, and V Bennett. "Ankyrin binding activity shared by the neurofascin/L1/NrCAM family of nervous system cell adhesion molecules." The Journal of Biological Chemistry 269, no. 44 (1994): 27163-6.

Davis, J Q, S Lambert, and V Bennett. "Molecular composition of the node of Ranvier: identification of ankyrin-binding cell adhesion molecules neurofascin (mucin+/third FNIII domain-) and NrCAM at nodal axon segments." The Journal of Cell Biology 135, no. 5 (1996): 1355-67.

Davison, A N, and M L Cuzner. "Immunochemistry and biochemistry of myelin." British Medical Bulletin 33, no. 1 (1977): 60-6.

deWaegh, S, and S T Brady. "Altered slow axonal transport and regeneration in a myelin-deficient mutant mouse: the trembler as an in vivo model for Schwann cell-axon interactions." The Journal of Neuroscience 10, no. 6 (1990): 1855-65.

Deber, C M, and S J Reynolds. "Central nervous system myelin: structure, function, and pathology." Clinical Biochemistry 24, no. 2 (1991): 113-34.

Devaux, J J, K A Kleopa, E C Cooper, and S S Scherer. "KCNQ2 is a nodal K+ channel." Journal of Neuroscience 24, no. 5 (2004): 1236-44.

Doyle, K P, R P Simon, and M P Stenzel-Poore. "Mechanisms of ischemic brain damage." Neuropharmacology 55, no. 3 (2008): 310-8.

Duchen, M R. "Roles of mitochondria in health and disease." Diabetes 53 Suppl 1 (2004): S96-102.

Dupree, J L, J A Girault, and B Popko. "Axo-glial interactions regulate the localization of axonal paranodal proteins." The Journal of Cell Biology 147, no. 6 (1999): 1145-52.

D'Urso, D, P Ehrhardt, and H W Müller. "Peripheral myelin protein 22 and protein zero: a novel association in peripheral nervous system myelin." The Journal of Neuroscience 19, no. 9 (1999): 3396-403.

Edgar, J M, and J Garbern. "The myelinated axon is dependent on the myelinating cell for support and maintenance: molecules involved." Journal of Neuroscience Research 76, no. 5 (2004): 593-8.

Edgar, J M, M C Mcculloch, C E Thomson, and I R Griffiths. "Distribution of mitochondria along small-diameter myelinated central nervous system axons." Journal of Neuroscience Research 86, no. 10 (2008): 2250-7.

Ehrig, K, I Leivo, and E Engvall. "Merosin and laminin. Molecular relationship and role in nerve-muscle development." Annals of the New York Academy of Sciences 580 (1990): 276-80.

Einheber, S, G Zanazzi, W Ching, S Scherer, T A Milner, E Peles, and J L Salzer. "The axonal membrane protein Caspr, a homologue of neurexin IV, is a component of the septate-like paranodal junctions that assemble during myelination." The Journal of Cell Biology 139, no. 6 (1997): 1495-506.

Ellisman, M H, and K R Porter. "Microtrabecular structure of the axoplasmic matrix: visualization of cross-linking structures and their distribution." The Journal of Cell Biology 87, no. 2 Pt 1 (1980): 464-79.

Elmer, L W, J A Black, S G Waxman, and K J Angelides. "The voltage-dependent sodium channel in mammalian CNS and PNS: antibody characterization and immunocytochemical localization." Brain research 532, no. 1-2 (1990): 222-31.

Eng, D L, T R Gordon, J D Kocsis, and S G Waxman. "Development of 4-AP and TEA sensitivities in mammalian myelinated nerve fibers." Journal of Neurophysiology 60, no. 6 (1988): 2168-79.

Ernst, S A. "Transport adenosine triphosphatase cytochemistry. II. Cytochemical localization of ouabain-sensitive, potassium-dependent phosphatase activity in the secretory epithelium of the avian salt gland." The Journal of Histochemistry and Cytochemistry 20, no. 1 (1972): 23-38.

Fabricius, C, C H Berthold, and M Rydmark. "Axoplasmic organelles at nodes of Ranvier. II. Occurrence and distribution in large myelinated spinal cord axons of the adult cat." Journal of Neurocytology 22, no. 11 (1993): 941-54.

Fannon, A M, D L Sherman, G Ilyina-Gragerova, P J Brophy, V L Friedrich, and D R Colman. "Novel E-cadherin-mediated adhesion in peripheral nerve: Schwann cell architecture is stabilized by autotypic adherens junctions." The Journal of Cell Biology 129, no. 1 (1995): 189-202.

Farquhar, M, and G Palade. "Junctional complexes in various epithelia." The Journal of Cell Biology 17 (1963): 375-412.

Fatt, P. "Sequence of events in synaptic activation of a motoneurone." Journal of Neurophysiology 20, no. 1 (1957): 61-80.

Feng, G, R H Mellor, M Bernstein, C Keller-Peck, Q T Nguyen, M Wallace, J M Nerbonne, J W Lichtman, and J R Sanes. "Imaging neuronal subsets in

transgenic mice expressing multiple spectral variants of GFP." Neuron 28, no. 1 (2000): 41-51.

Flores, J, D R DiBona, N Frega, and A Leaf. "Cell volume regulation and ischemic tissue damage." The Journal of Membrane Biology 10, no. 3 (1972): 331-43.

Foster, R E, B W Connors, and S G Waxman. "Rat optic nerve: electrophysiological, pharmacological and anatomical studies during development." Brain Research 255, no. 3 (1982): 371-86.

Frankenhauser, B, and A L Hodgkin. "The after-effects of impulses in the giant nerve fibres of Loligo." Journal of Physiology 131, no. 2 (1956): 341-76.

Friede, R L, and A J Martinez. "Analysis of the process of sheath expansion in swollen nerve fibers." Brain Research 19, no. 2 (1970): 165-82.

Friede, R L, and R Bischhausen. "The precise geometry of large internodes." Journal of the Neurological Sciences 48, no. 3 (1980): 367-81.

Friede, R L, and T Miyagishi. "Adjustment of the myelin sheath to changes in axon caliber." The Anatomical Record 172, no. 1 (1972): 1-14.

Fuortes, M, H Frank, and M Becker. "Steps in the production of motoneuron spikes." The Journal of General Physiology 40, no. 5 (1957): 735-52.

Gatzinsky, K P, and C H Berthold. "Lysosomal activity at nodes of Ranvier during retrograde axonal transport of horseradish peroxidase in alpha-motor neurons of the cat." Journal of Neurocytology 19, no. 6 (1990): 989-1002.

Gatzinsky, K P, C H Berthold, and M Rydmark. "Axon-Schwann cell networks are regular components of nodal regions in normal large nerve fibres of cat spinal roots." Neuroscience Letters 124, no. 2 (1991): 264-8.

Gatzinsky, K P, C H Berthold, and O Cornelius on. "Acid phosphatase activity at nodes of Ranvier in alpha-motor and dorsal root ganglion neurons of the cat." Journal of Neurocytology 17, no. 4 (1988): 531-44.

Gerbi, A, S Sennoune, S Pierre, J Sampol, D Raccah, P Vague, and J-M Maixent. "Localization of Na, K- ATPase α/β Isoforms in Rat Sciatic Nerves: Effect of Diabetes and Fish Oil Treatment." Journal of Neurochemistry73, no. 2 (1999): 719-726.

Goldin, A L. "Resurgence of sodium channel research." Annual Review of Physiology 63 (2001): 871-94.

Gow, A, C M Southwood, J S Li, M Pariali, G P Riordan, S E Brodie, J Danias, J M Bronstein, B Kachar, and R A Lazzarini. "CNS myelin and sertolicell tight junction strands are absent in Osp/claudin-11 null mice." Cell 99, no. 6 (1999): 649-59.

Griffin, J W, C Y Li, C Macko, T W Ho, S T Hsieh, P Xue, F A Wang, D R Cornblath, G M McKhann, and A K Asbury. "Early nodal changes in the acute motor axonal neuropathy pattern of the Guillain-Barré syndrome." Journal of Neurocytology 25, no. 1 (1996): 33-51.

Griffin, J W, C Y Li,T W Ho, M Tian, C Y Gao, P Xue, B Mishu, D R Cornblath, C Macko, G M McKhann, and A K Asbury. "Pathology of the

motor-sensory axonal Guillain-Barré syndrome." Annals of Neurology 39, no. 1 (1996): 17-28.

Grossman, Y, I Parnas, and M E Spira. "Mechanisms involved in differential conduction of potentials at high frequency in a branching axon." Journal of Physiology 295 (1979): 307-22.

Gumbiner, B M. "Regulation of cadherin adhesive activity." The Journal of Cell Biology 148, no. 3 (2000): 399-404.

Hall, S M, and P L Williams. "Studies on the "incisures" of Schmidt and Lanterman." Journal of Cell Science 6, no. 3 (1970): 767-91.

Hall, S M, and P L Williams. "The distribution of electron-dense tracers in peripheral nerve fibres." Journal of Cell Science 8, no. 2 (1971): 541-55.

Hamill, O P, A Marty, E Neher, B Sakmann, and F J Sigworth. "Improved patch-clamp techniques for high-resolution current recording from cells and cell-free membrane patches." PflügersArchiv : European Journal of Physiology 391, no. 2 (1981): 85-100.

Hammarström, A K, and P W Gage. "Nitric oxide increases persistent sodium current in rat hippocampal neurons." Journal of Physiology 520 Pt 2 (1999): 451-61.

Hedstrom, K L, and M N Rasband. "Intrinsic and extrinsic determinants of ion channel localization in neurons." Journal of Neurochemistry 98, no. 5 (2006): 1345-52.

Hess, A, and J Z Young. "The nodes of Ranvier." Proceedings of the Royal Society of London 140, no. 900 (1952): 301-20.

Hirano, A. "The permeability of the extracellular spaces at the Schmidt-Lanterman clefts and paranodes in peripheral myelin sheaths." Acta neuropathologica 58, no. 1 (1982): 34-8.

Hirano, A, and H M Dembitzer. "The periaxonal space in an experimental model of neuropathy: the mutant Syrian hamster with hindleg paralysis." Journal of Neurocytology 10, no. 2 (1981): 261-9.

Hirano, A, and H M Dembitzer. "The transverse bands as a means of access to the periaxonal space of the central myelinated nerve fiber." Journal of Ultrastructure Research 28, no. 1 (1969): 141-9.

Hodgkin, A L. "The relation between conduction velocity and the electrical resistance outside a nerve fibre." Journal of Physiology 94, no. 4 (1939): 560-70.

Hodgkin, A L, A F Huxley, and B Katz. "Measurement of current-voltage relations in the membrane of the giant axon of Loligo." Journal of Physiology 116, no. 4 (1952): 424-48.

Hodgkin, A L, and A F Huxley. "Action potentials recorded from inside a nerve fibre." Nature 144, no. 3651 (1939): 710-711.

Hodgkin, AL, and AF Huxley. "Propagation of electrical signals along giant nerve fibres." Proceedings of the Royal Society of London 140, no. 899 (1952, a): 177-183.

Hodgkin, A L, and A F Huxley. "Currents carried by sodium and potassium ions through the membrane of the giant axon of Loligo." Journal of Physiology 116, no. 4 (1952, b): 449-72.

Hodgkin, A L, and A F Huxley. "The components of membrane conductance in the giant axon of Loligo." Journal of Physiology 116, no. 4 (1952, c): 473-96.

Hodgkin, A L, and A F Huxley. "The dual effect of membrane potential on sodium conductance in the giant axon of Loligo." Journal of Physiology 116, no. 4 (1952, d): 497-506.

Hodgkin, A L, and B Katz. "The effect of sodium ions on the electrical activity of giant axon of the squid Journal of Physiology 108, no. 1 (1949): 37-77.

Hodgkin, A. "The optimum density of sodium channels in an unmyelinated nerve." Philosophical transactions of the Royal Society of London 270, no. 908 (1975): 297-300.

Hollenbeck, P J, and W M Saxton. "The axonal transport of mitochondria." Journal of Cell Science 118, not 23 (2005): 5411-9.

Howe, J R, and J M Ritchie. "Sodium currents in Schwann cells from myelinated and non-myelinated nerves of neonatal and adult rabbits." Journal of Physiology425 (1990): 169-210.

Howell, O W, A Palser, A Polito, S Melrose, B Zonta, C Scheiermann, A J Vora, P J Brophy, and R Reynolds. "Disruption of neurofascin localization

reveals early changes preceding demyelination and remyelination in multiple sclerosis." Brain 129, Pt 12 (2006): 3173-85.

Howell, O W, J L Rundle, A Garg, M Komada, P J Brophy, and R Reynolds. "Activated Microglia Mediate Axoglial Disruption That Contributes to Axonal Injury in Multiple Sclerosis." Journal of Neuropathology & Experimental Neurology 69, no. 10 (2010): 1017.

Hua, W, E C Young, M L Fleming, and J Gelles. "Coupling of kinesin steps to ATP hydrolysis." Nature 388, no. 6640 (1997): 390-3.

Hughes, R A C, R D M Hadden, N A Gregson, and K J Smith. "Pathogenesis of Guillain-Barré syndrome." Journal of Neuroimmunology 100, no. 1-2 (1999): 74-97.

Hunter, L Y, D S Louis, J R Ricciardi, and G A O'Connor. "The saphenous nerve: its course and importance in medial arthrotomy." The American Journal of Sports Medicine 7, no. 4 (1979): 227-30.

Ichimura, T, and M H Ellisman. "Three-dimensional fine structure of cytoskeletal-membrane interactions at nodes of Ranvier." Journal of Neurocytology 20, no. 8 (1991): 667-81.

Iitake, K, T Kimura, K Ota, M Shoji, M Inoue, M Ohta, K Sato, T Yamamoto, M Yasujima, and K Abe. "Responses of vasopressin, atrial natriuretic peptide, and blood pressure to central osmotic stimulation." The American Journal of Physiology 257, no. 4 Pt 1 (1989): E611-6.

Ishibashi, T, J L Dupree, K Ikenaka, Y Hirahara, K Honke, E Peles, B Popko, K Susuki, H Nishino, and H Baba. "A myelin galactolipid, sulfatide, is essential for maintenance of ion channels on myelinated axon but not essential for initial cluster formation." Journal of Neuroscience 22, no. 15 (2002): 6507-14.

Jessen, K R, and R Mirsky. "Signals that determine Schwann cell identity." Journal of Anatomy 200, no. 4 (2002): 367-76.

Jones, H B, and J B Cavanagh. "Distortions of the nodes of Ranvier from axonal distension by filamentous masses in hexacarbon intoxication." Journal of Neurocytology 12, no. 3 (1983): 439-58.

Kapoor, R, K J Smith, P A Felts, and M Davies. "Internodal potassium currents can generate ectopic impulses in mammalian myelinated axons." Brain Research 611, no. 1 (1993): 165-9.

Kidd, G J, S B Andrews, and B D Trapp. "Organization of microtubules in myelinating Schwann cells." Journal of Neurocytology 23, no. 12 (1994): 801-10.

Kidd, G, S B Andrews, and B D Trapp. "Axons regulate the distribution of Schwann cell microtubules." The Journal of Neuroscience16, no. 3 (1996): 946-54.

Kiernan, M C, I Mogyoros, J P Hales, J M Gracies, and D Burke. "Excitability changes in human cutaneous afferents induced by prolonged repetitive axonal activity." Journal of Physiology 500 (Pt 1) (1997): 255-64.

Kirby, B B, N Takada, A J Latimer, J Shin, T J Carney, R N Kelsh, and B Appel. "In vivo time-lapse imaging shows dynamic oligodendrocyte progenitor behavior during zebrafish development." Nature Neuroscience 9, no. 12 (2006): 1506-11.

Kirkpatrick, L L, A S Witt, H R Payne, H D Shine, and S T Brady. "Changes in microtubule stability and density in myelin-deficient shiverer mouse CNS axons." Journal of Neuroscience 21, no. 7 (2001): 2288-97.

Koch, P J, and W W Franke. "Desmosomal cadherins: another growing multigene family of adhesion molecules." Current Opinion in Cell Biology 6, no. 5 (1994): 682-7.

Kocsis, J D, D L Eng, T R Gordon, and S G Waxman. "Functional differences between 4-aminopyridine and tetraethylammonium-sensitive potassium channels in myelinated axons." Neuroscience Letters 75, no. 2 (1987): 193-8.

Kocsis, J D, S G Waxman, C Hildebrand, and J A Ruiz. "Regenerating mammalian nerve fibres: changes in action potential waveform and firing characteristics following blockage of potassium conductance." Proceedings of the Royal Society of London 217, no. 1206 (1982): 77-87.

Koenig, E, and E Repasky. "A regional analysis of alpha-spectrin in the isolated Mauthner neuron and in isolated axons of the goldfish and rabbit." The Journal of Neuroscience 5, no. 3 (1985): 705-14.

Koester, J, and S A Siegelbaum. "Membrane potential." Principles of neural science, 1991: 81–94.

Kofuji, P, and E A Newman. "Potassium buffering in the central nervous system." Neuroscience 129, no. 4 (2004): 1045-56.

Kole, M H P, S U Ilschner, B M Kampa, S R Williams, P C Ruben, and G J Stuart. "Action potential generation requires a high sodium channel density in the axon initial segment." Nature Neuroscience 11, no. 2 (2008): 178-86.

Konishi, T. "Voltage-gated potassium currents in myelinating Schwann cells in the mouse." Journal of Physiology431 (1990): 123-39.

Kordeli, E, J Davis, B Trapp, and V Bennett. "An isoform of ankyrin is localized at nodes of Ranvier in myelinated axons of central and peripheral nerves." The Journal of Cell Biology 110, no. 4 (1990): 1341-52.

Kordeli, E, S Lambert, and V Bennett. "AnkyrinG. A new ankyrin gene with neural-specific isoforms localized at the axonal initial segment and node of Ranvier." The Journal of Biological Chemistry 270, no. 5 (1995): 2352-9.

Korobkin, R, A K Asbury, A J Sumner, and S L Nielsen. "Glue-sniffing neuropathy." Archives of neurology 32, no. 3 (1975): 158-62.

Kress, G J, and S Mennerick. "Action potential initiation and propagation: upstream influences on neurotransmission." Neuroscience 158, no. 1 (2009): 211-22.

Kristol, C, C Sandri, and K Akert. "Intramembranous particles at the nodes of Ranvier of the cat spinal cord: a morphometric study." Brain Research 142, no. 3 (1978): 391-400.

Kukita, F. "K(+) Channels of Squid Giant Axons Open by an Osmotic Stress in Hypertonic Solutions Containing Nonelectrolytes." The Journal of Membrane Biology, Jul 2011.

Kusunoki, S, A Chiba, T Tai, and I Kanazawa. "Localization of GM1 and GD1b antigens in the human peripheral nervous system." Muscle &Nerve 16, no. 7 (1993): 752-6.

Lai, H C, and L Y Jan. "The distribution and targeting of neuronal voltage-gated ion channels." Nature Reviews Neuroscience no. 7 (2006): 548-62.

Lambert, S, J Q Davis, and V Bennett. "Morphogenesis of the node of Ranvier: co-clusters of ankyrin and ankyrin-binding integral proteins define early developmental intermediates." The Journal of Neuroscience17, no. 18 (1997): 7025-36.

Lee, S M, J A Olzmann, L-S Chin, and L Li. "Mutations associated with Charcot-Marie-Tooth disease cause SIMPLE protein mislocalization and degradation by the proteasome and aggresome-autophagy pathways." Journal of Cell Science 124, Pt 19 (2011): 3319-31.

Lehninger, A L. "Water uptake and extrusion by mitochondria in relation to oxidative phosphorylation." Physiological reviews 42 (1962): 467-517.

Leibowitz, M D, J B Sutro, and B Hille. "Voltage-dependent gating of veratridine-modified Na channels." The Journal of General Physiology 87, no. 1 (1986): 25.

Lemke, G, and R Axel. "Isolation and sequence of a cDNA encoding the major structural protein of peripheral myelin." Cell 40, no. 3 (1985): 501-8.

Lorimier, P, P Mezin, F Labat Moleur, N Pinel, S Peyrol, and P Stoebner. "Ultrastructural localization of the major components of the extracellular matrix in normal rat nerve." Journal of Histochemistry & Cytochemistry 40, no. 6 (1992): 859-868.

Love, S, and M A Cruz-Höfling. "Acute swelling of nodes of Ranvier caused by venoms which slow inactivation of sodium channels." Acta Neuropathologica 70, no. 1 (1986): 1-9.

Love, S, M A Cruz-Höfling, and L W Duchen. "Morphological abnormalities in myelinated nerve fibres caused by Leiurus, Centruroides and Phoneutria venoms and their prevention by tetrodotoxin." Quarterly Journal of Experimental Physiology 71, no. 1 (1986): 115-22.

MacAskill, AF, and JT Kittler. "Miro1 is a calcium sensor for glutamate receptor-dependent localization of mitochondria at synapses." Neuron 61(4) (2009): 541-55.

Macknight, A D, and A Leaf. "Regulation of cellular volume." Physiological Reviews 57, no. 3 (1977): 510-73.

Magnani, P, P V Cherian, G W Gould, D A Greene, A A Sima, and F C Brosius. "Glucose transporters in rat peripheral nerve: paranodal expression of GLUT1 and GLUT3." Metabolism: Clinical and Experimental 45, no. 12 (1996): 1466-73.

Martini, R, and M Schachner. "Immunoelectron microscopic localization of neural cell adhesion molecules (L1, N-CAM, and MAG) and their shared carbohydrate epitope and myelin basic protein in developing sciatic nerve." The Journal of Cell Biology 103, no. 6 Pt 1 (1986): 2439-48.

Martini, R, Y Xin, and M Schachner. "Restricted localization of L1 and N-CAM at sites of contact between Schwann cells and neurites in culture." Glia 10, no. 1 (1994): 70-4.

Mata, M, D J Fink, S A Ernst, and G J Siegel. "Immunocytochemical demonstration of Na+,K(+)-ATPase in internodal axolemma of myelinated fibers of rat sciatic and optic nerves." Journal of Neurochemistry 57, no. 1 (1991): 184-92.

Maurel, P, S Einheber, J Galinska, P Thaker, I Lam, M B Rubin, S S Scherer, Y Murakami, D H Gutmann, and J L Salzer. "Nectin-like proteins mediate axon Schwann cell interactions along the internode and are essential for myelination." The Journal of Cell Biology 178, no. 5 (2007): 861-74.

McGrail, K M, J M Phillips, and K J Sweadner. "Immunofluorescent localization of three Na,K-ATPase isozymes in the rat central nervous system: both neurons and glia can express more than one Na,K-ATPase." The Journal of Neuroscience11, no. 2 (1991): 381-91.

Mege, R M, D Goudou, C Diaz, M Nicolet, L Garcia, G Geraud, and F Rieger. "N-cadherin and N-CAM in myoblast fusion: compared localisation and effect of blockade by peptides and antibodies." Journal of Cell Science 103 (Pt 4) (1992): 897-906.

Mi, F, J S Peters, and G A Berkowitz. "Characterization of a chloroplast inner envelope K+ channel." Plant Physiology 105, no. 3 (1994): 955-64.

Mierzwa, A J, J-C Arevalo, R Schiff, M V Chao, and J Rosenbluth. "Role of transverse bands in maintaining paranodal structure and axolemmal domain organization in myelinated nerve fibers: effect on longevity in dysmyelinated mutant mice." The Journal of Comparative Neurology 518, no. 14 (2010): 2841-53.

Mierzwa, A, S Shroff, and J Rosenbluth. "Permeability of the Paranodal Junction of Myelinated Nerve Fibers." Journal of Neuroscience 30, no. 47 (2010): 15962-15968.

Miller, C. "An overview of the potassium channel family." Genome Biology 1(4) (2000).

Miller, K E, and M P Sheetz. "Axonal mitochondrial transport and potential are correlated." Journal of Cell Science 117, no.Pt 13 (2004): 2791-804.

Mirsky, R, K R Jessen, A Brennan, D Parkinson, Z Dong, C Meier, E Parmantier, and D Lawson. "Schwann cells as regulators of nerve development." Journal of Physiology, Paris 96, no. 1-2 (2002): 17-24.

Misgeld, T, M Kerschensteiner, F M Bareyre, R W Burgess, and J W Lichtman. "Imaging axonal transport of mitochondria in vivo." Nature Methods 4, no. 7 (2007): 559-61.

Mitic, L L, and J M Anderson. "Molecular architecture of tight junctions." Annual Review of Physiology 60 (1998): 121-42.

Mizisin, A P, and A Weerasuriya. "Homeostatic regulation of the endoneurial microenvironment during development, aging and in response to trauma, disease and toxic insult." Acta Neuropathologica 121, no. 3 (2011): 291-312.

Mizisin, A P, H C Powell, and R R Myers. "Edema and increased endoneurial sodium in galactose neuropathy. Reversal with an aldose reductase inhibitor." Journal of the Neurological Sciences 74, no. 1 (1986): 35-43.

Mizisin, A P, R R Myers, and H C Powell. "Endoneurial sodium accumulation in galactosemic rat nerves." Muscle &Nerve 9, no. 5 (1986): 440-4.

Mizisin, A P, R R Myers, H M Heckman, and H C Powell. "Dose-dependence of endoneurial fluid sodium and chloride accumulation in galactose intoxication." Journal of the Neurological Sciences 86, no. 2-3 (1988): 113-24.

Montag, D, K P Giese, U Bartsch, R Martini, Y Lang, H Bluthmann, J Karthigasan, D A Kirschner, E S Wintergerst, and K A Nave. "Mice deficient for the myelin-associated glycoprotein show subtle abnormalities in myelin." Neuron 13, no. 1 (1994): 229-46.

Moore, GR, R.J Boegman, D.M Robertson, and C.S Raine. "Acute stages of batrachotoxin-induced neuropathy: a morphologic study of a sodium-channel toxin." Journal of Neurocytology 15, no. 5 (1986): 573.

Mrsulja, B J, A A Zalewski, and G Coping. "Ultracytochemical localization of ouabain-sensitive K+-dependent, p-nitrophenyl phosphatase in myelin." Brain Research 343, no. 1 (1985): 154-8.

Mugnaini, E, and B Schnapp. "Possible role of zonula occludens of the myelin sheath in demyelinating conditions." Nature 251, no. 5477 (1974): 725-7.

Nagafuchi, A, S Tsukita, and M Takeichi. "Transmembrane control of cadherin-mediated cell-cell adhesion." Seminars in Cell Biology 4, no. 3 (1993): 175-81.

Neher, E, and B Sakmann. "Single-channel currents recorded from membrane of denervated frog muscle fibres." Nature 260, no. 5554 (1976): 799-802.

Neumcke, B, and R Stämpfli. "Sodium currents and sodium-current fluctuations in rat myelinated nerve fibres." Journal of Physiology329 (1982): 163-84.

Olivera, B M, G P Miljanich, J Ramachandran, and M E Adams. "Calcium channel diversity and neurotransmitter release: the omega-conotoxins and omega-agatoxins." Annual Review of Biochemistry 63 (1994): 823-67.

Orkand, R K, J G Nicholls, and S W Kuffler. "Effect of nerve impulses on the membrane potential of glial cells in the central nervous system of amphibia." Journal of Neurophysiology 29, no. 4 (1966): 788-806.

Packer, L, J K Pollak, E A Munn, and G D Greville. "Effect of high sucrose concentrations on mitochondria: analysis of mitochondrial populations by density-gradient centrifugation after fixation with glutaraldehyde." Journal of Bioenergetics 2, no. 5 (1971): 305-16.

Pan, Z. "A Common Ankyrin-G-Based Mechanism Retains KCNQ and NaV Channels at Electrically Active Domains of the Axon." Journal of Neuroscience 26, no. 10 (2006): 2599-2613.

Payer, A F. "An ultrastructural study of Schwann cell response to axonal degeneration." The Journal of Comparative Neurology 183, no. 2 (1979): 365-83.

Peles, E, and J L Salzer. "Molecular domains of myelinated axons." Current Opinion in Neurobiology 10, no. 5 (2000): 558-65.

Peles, E, M Nativ, M Lustic, M Grumet, J Schiling, R Martinez, G plowman, and J Schlessinger. "Identification of a novel contactin-associated transmembrane receptor with multiple domains implicated in protein–protein interactions." The EMBO journal 16, no. 5 (1997): 978-988.

Pellegrino, R G, P S Spencer, and J M Ritchie. "Sodium channels in the axolemma of unmyelinated axons: a new estimate." Brain Research 305, no. 2 (1984): 357-60.

Perkins, G A, and M H Ellisman. "Mitochondrial configurations in peripheral nerve suggest differential ATP production." Journal of Structural Biology 173, no. 1 (2011): 117-127.

Perkins, G A, G E Sosinsky, S Ghassemzadeh, A Perez, Y Jones, and M H Ellisman. "Electron tomographic analysis of cytoskeletal cross-bridges in the paranodal region of the node of Ranvier in peripheral nerves." Journal of Structural Biology 161, no. 3 (2008): 469-80.

Peters, A. "The node of Ranvier in the central nervous system." Quarterly Journal of Experimental Physiology and Cognate Medical Sciences 51, no. 3 (1966): 229-36.

Pham, K, and R Gupta. "Understanding the mechanisms of entrapment neuropathies. Review article." Neurosurgical FOCUS 26, no. 2 (2009): E7.

Pillai, A M, C Thaxton, A L Pribisko, J Cheng, J L Dupree, and M A Bhat. "Spatiotemporal ablation of myelinating glia-specific neurofascin (Nfasc NF155) in mice reveals gradual loss of paranodal axoglial junctions and concomitant disorganization of axonal domains." Journal of Neuroscience Research 87, no. 8 (2009): 1773-93.

Piret, G, M-T Perez, and C N Prinz. "Neurite outgrowth and synaptophysin expression of postnatal CNS neurons on GaP nanowire arrays in long-term retinal cell culture." Biomaterials 34, no. 4 (2013): 875-87.

Plucinska, G, D Paquet, A Hruscha, L Godinho, C Haass, B Schmid, and T Misgeld. "In Vivo Imaging of Disease-Related Mitochondrial Dynamics in a

Vertebrate Model System." Journal of Neuroscience 32, no. 46 (2012): 16203-16212.

Poliak, S, L Gollan, R Martinez, A Custer, S Einheber, J L Salzer, J S Trimmer, P Shrager and E Peles. "Caspr2, a new member of the neurexin superfamily, is localized at the juxtaparanodes of myelinated axons and associates with K+ channels." Neuron 24, no. 4 (1999): 1037-47.

Previtali, S C, M L Feltri, J J Archelos, A Quattrini, L Wrabetz, and H Hartung. "Role of integrins in the peripheral nervous system." Progress in Neurobiology 64, no. 1 (2001): 35-49.

Prochazka, A, and M Gorassini. "Ensemble firing of muscle afferents recorded during normal locomotion in cats." Journal of Physiology507 (Pt 1) (1998): 293-304.

Pullarkat, P A, P Dommersnes, P Fernández, J Joanny, and A Ott. "Osmotically driven shape transformations in axons." Physical Review Letters 96, no. 4 (2006): 048104.

Quick, D C, and S G Waxman. "Ferric ion, ferrocyanide, and inorganic phosphate as cytochemical reactants at peripheral nodes of Ranvier." Journal of Neurocytology 6, no. 5 (1977): 555-70.

Rakowski, R F, D C Gadsby, and P De Weer. "Stoichiometry and voltage dependence of the sodium pump in voltage-clamped, internally dialyzed squid giant axon." Journal of General Physiology 93(5) (1989): 903-41.

Raman, I M, and B P Bean. "Resurgent sodium current and action potential formation in dissociated cerebellar Purkinje neurons." The Journal of Neuroscience17, no. 12 (1997): 4517-26.

Rasband, M N, and J S Trimmer. "Subunit composition and novel localization of K+ channels in spinal cord." The Journal of Comparative Neurology 429, no. 1 (2001): 166-76.

Rasband, M N, Epees, J S Trimmer, S R Levinson, S E Lux, and P Shrager. "Dependence of nodal sodium channel clustering on paranodal axoglial contact in the developing CNS." Journal of Neuroscience 19, no. 17 (1999): 7516-28.

Rash, J E. "Molecular disruptions of the panglial syncytium block potassium siphoning and axonal saltatory conduction: pertinence to neuromyelitis optica and other demyelinating diseases of the central nervous system." Neuroscience (2010): 1-27.

Redford, E J, S M Hall, and K J Smith. "Vascular changes and demyelination induced by the intraneural injection of tumour necrosis factor." Brain 118 (Pt 4) (1995): 869-78.

Rios, J C, C V Melendez-Vasquez, S Einheber, M Lustig, M Grumet, J Hemperly, E Peles and J L Salzer. "Contactin-associated protein (Caspr) and contactin form a complex that is targeted to the paranodal junctions during myelination." Journal of Neuroscience 20, no. 22 (2000): 8354-64.

Ritchie, J M. "Sodium and potassium channels in regenerating and developing mammalian myelinated nerves." Proceedings of the Royal Society of London 215, no. 1200 (1982): 273-87.

Ritchie, J M. "Sodium-channel turnover in rabbit cultured Schwann cells." Proceedings of the Royal Society of London 233, no. 1273 (1988): 423-30.

Ritchie, J M. "Voltage-gated ion channels in Schwann cells and glia." Trends in Neurosciences 15, no. 9 (1992): 345-51.

Ritchie, J M, and R B Rogart. "Density of sodium channels in mammalian myelinated nerve fibers and nature of the axonal membrane under the myelin sheath." Proceedings of the National Academy of Sciences 74, no. 1 (1977): 211-5.

Ritchie, J M, J A Black, S G Waxman, and K J Angelides. "Sodium channels in the cytoplasm of Schwann cells." Proceedings of the National Academy of Sciences 87, no. 23 (1990): 9290-4.

Robertson, J D. "Preliminary observations on the ultrastructure of nodes of Ranvier." Cell and Tissue Research 50, no. 4 (1959): 553-560.

Robertson, J D. "The ultrastructure of cell membranes and their derivatives." Biochemical Society Symposium 16 (1959): 3-43.

Roper, J, and JR Schwarz. "Heterogeneous distribution of fast and slow potassium channels in myelinated rat nerve fibres." Journal of Physiology416 (1989): 93-110.

Rosenbluth, J. "A brief history of myelinated nerve fibers: one hundred and fifty years of controversy." Journal of Neurocytology 28, no. 4-5 (1999): 251-62.

Rosenbluth, J. "Intramembranous particle distribution at the node of Ranvier and adjacent axolemma in myelinated axons of the frog brain." Journal of Neurocytology 5, no. 6 (1976): 731-45.

Rosenbluth, J. "Multiple functions of the paranodal junction of myelinated nerve fibers." Journal of Neuroscience Research, 2009.

Rosenbluth, J, K-A Nave, A Mierzwa, and R Schiff. "Subtle myelin defects in PLP-null mice." Glia 54, no. 3 (2006): 172-82.

Rothenberg, M. "Studies on permeability in relation to nerve function, ionic movements across axonal membranes." Biochimica et Biophysica Acta 4, no. 1-3 (1950): 96-114.

Rushton, W A. "A theory of the effects of fibre size in medullated nerve. "Journal of Physiology115, no. 1 (1951): 101-22.

Ruts, H P. "Hydrodynamic consequences of glycolysis: thermodynamic basis and clinical relevance." Cancer Biology &Therapy 3, no. 9 (2004): 812-5.

Rydmark, M, and C.H Berthold. "Electron microscopic serial section analysis of nodes of Ranvier in lumbar spinal roots of the cat: a morphometric study of nodal compartments in fibres of different sizes." Journal of Neurocytology 12, no. 4 (1983): 537-565.

Rydmark, M, C H Berthold, and K P Gatzinsky. "Paranodal Schwann cell mitochondria in spinal roots of the cat. An ultrastructural morphometric analysis." Journal of Neurocytology 27, no. 2 (1998): 99-108.

Saks, V A, M Vendelin, M K Aliev, T Kekelidze, and J Engelbrecht. "38 Mechanisms and Modeling of Energy Transfer Between Intracellular Compartments." 2006.

Salzer, J L. "Polarized domains of myelinated axons." Neuron 40, no. 2 (2003): 297-318.

Sandri, C, J M Van Buren, and K Akert. "Membrane morphology of the vertebrate nervous system. A study with freeze-etch technique." Progress in Brain Research 46 (1977): 1-384.

Sanes, J R, E Engvall, R Butkowski, and D D Hunter. "Molecular heterogeneity of basal laminae: isoforms of laminin and collagen IV at the neuromuscular junction and elsewhere." The Journal of Cell Biology 111, no. 4 (1990): 1685-99.

Sato, T, Y Kamata, and M Irifune. "Inhibitory effect of several nitric oxide-generating compounds on purified Na+, K+-ATPase activity from porcine cerebral cortex." Journal of Neurochemistry 68, no. 3 (1997): 1312-1318.

Scherer, S S, and E J Arroyo. "Recent progress on the molecular organization of myelinated axons." Journal of the peripheral nervous system 7, no. 1 (2002): 1-12.

Scherer, S S, S M Deschênes, Y T Xu, J B Grinspan, K H Fischbeck, and D L Paul. "Connexin32 is a myelin-related protein in the PNS and CNS." The Journal of Neuroscience15, no. 12 (1995): 8281-94.

Scholz, J, and C J Woolf. "The neuropathic pain triad: neurons, immune cells and glia." Nature Neuroscience 10, no. 11 (2007): 1361-8.

Schwarz, J R, G Glassmeier, E C Cooper, T-C Kao, H Nodera, D Tabuena, R Kaji, and H Bostock. "KCNQ channels mediate IKs, a slow K+ current regulating excitability in the rat node of Ranvier." Journal of Physiology(2006): 17-34.

Seneviratne, K N, O A Peiris, and A Weerasuriya. "Effects of hyperkalaemia on the excitability of peripheral nerve." Journal of Neurology, Neurosurgery & Psychiatry 35, no. 2 (1972): 149-155.

Sheikh, K A, T J Deerinck, M H Ellisman, and J W Griffin. "The distribution of ganglioside-like moieties in peripheral nerves." Brain 122 (Pt 3) (1999): 449-60.

Sherman, D L, and P J Brophy. "Mechanisms of axon ensheathment and myelin growth." Nature Reviews Neuroscience, no. 9 (2005): 683-90.

Shrager, P. "Ionic channels and signal conduction in single remyelinating frog nerve fibres." Journal of Physiology404 (1988): 695-712.

Shrager, P. "The distribution of sodium and potassium channels in single demyelinated axons of the frog." Journal of Physiology392 (1987): 587-602.

Shrager, P, J C Starkus, M V Lo, and C Peracchia. "The periaxonal space of crayfish giant axons." The Journal of General Physiology 82, no. 2 (1983): 221-44.

Sigworth, F J, and E Neher. "Single Na+ channel currents observed in cultured rat muscle cells." Nature 287, no. 5781 (1980): 447-9.

Simons, M, E M Krämer, C Thiele, W Stoffel, and J Trotter. "Assembly of myelin by association of proteolipid protein with cholesterol- and galactosylceramide-rich membrane domains." The Journal of Cell Biology 151, no. 1 (2000): 143-54.

Singer, M, and S V Bryant. "Movements in the myelin Schwann sheath of the vertebrate axon." Nature 221, no. 5186 (1969): 1148-50.

Skou, J C. "The influence of some cations on an adenosine triphosphatase from peripheral nerves." Biochimica et Biophysica Acta 23, no. 2 (1957): 394-401.

Skou, J C, and M Esmann. "The Na,K-ATPase." Journal of Bioenergetics and Biomembranes 24, no. 3 (1992): 249-61.

Smith, K J, and C L Schauf. "Effects of gallaminetriethiodide on membrane currents in amphibian and mammalian peripheral nerve." The Journal of Pharmacology and Experimental Therapeutics 217, no. 3 (1981): 719-26.

Smith, K J, and W I McDonald. "The pathophysiology of multiple sclerosis: the mechanisms underlying the production of symptoms and the natural

history of the disease." Philosophical Transactions of the Royal Society 354, no. 1390 (1999): 1649.

Smith, K J, P A Felts, and R Kapoor. "Axonal Hyperexcitability: Mechanisms and Role in Symptom Production in Demyelinating Diseases." The Neuroscientist 3, no. 4 (1997): 237.

Smith, K J, R Kapoor, S M Hall, and M Davies. "Electrically active axons degenerate when exposed to nitric oxide." Annals of Neurology 49, no. 4 (2001): 470-6.

Smith, K J, W F Blakemore, J A Murray, and R C Patterson. "Internodal myelin volume and axon surface area. A relationship determining myelin thickness?" Journal of the Neurological Sciences 55, no. 2 (1982): 231-46.

Snow, D M, V Lemmon, D A Carrino, A I Caplan, and J Silver. "Sulfated proteoglycans in astroglial barriers inhibit neurite outgrowth in vitro." Experimental Neurology 109, no. 1 (1990): 111-30.

Snyder, R E. "Loss of material from the retrograde axonal transport system in frog sciatic nerve." Journal of Neurobiology 20, no. 2 (1989): 81-94.

Spencer, P S, and P K Thomas. "Ultrastructural studies of the dying-back process. II. The sequestration and removal by Schwann cells and oligodendrocytes of organelles from normal and diseases axons." Journal of Neurocytology 3, no. 6 (1974): 763-83.

Spiegel, I, and E Peles. "Cellular junctions of myelinated nerves (Review)." Molecular Membrane Biology 19, no. 2 (2002): 95-101.

Spiegel, I, K Adamsky, Y Eshed, R Milo, H Sabanay, O Sarig-Nadir, I Horresh, S S Scherer, M N Rasband and E Peles. "A central role for Necl4 (SynCAM4) in Schwann cell-axon interaction and myelination." Nature Neuroscience 10, no. 7 (2007): 861-9.

Srinivasan, Y, L Elmer, J Davis, V Bennett, and K Angelides. "Ankyrin and spectrin associate with voltage-dependent sodium channels in brain." Nature 333, no. 6169 (1988): 177-80.

Sterns, R H, J E Riggs, and S S Schochet. "Osmotic demyelination syndrome following correction of hyponatremia." The New England Journal of Medicine 314, no. 24 (1986): 1535-42.

Stolinski, C, A S Breathnach, P K Thomas, G Gabriel, and R H King. "Distribution of particle aggregates in the internodal axolemma and adaxonal Schwann cell membrane of rodent peripheral nerve." Journal of the Neurological Sciences 67, no. 2 (1985): 213-22.

Stone, T W. "Physiological roles for adenosine and adenosine 5'-triphosphate in the nervous system." Neuroscience 6, no. 4 (1981): 523-55.

Stys, P K, and R M Lopachin. "Mechanisms of calcium and sodium fluxes in anoxic myelinated central nervous system axons." Neuroscience 82, no. 1 (1998): 21-32.

Sunderland, S. "The effect of rupture of the perineurium on the contained nerve-fibres." Brain 69, no. 2 (1946): 149-52.

Suter, U, and G J Snipes. "Biology and genetics of hereditary motor and sensory neuropathies." Annual Review of Neuroscience 18 (1995): 45-75.

Taddese, A, and B P Bean. "Subthreshold sodium current from rapidly inactivating sodium channels drives spontaneous firing of tuberomammillary neurons." Neuron 33, no. 4 (2002): 587-600.

Tait, S, F Gunn-Moore, J M Collinson, J Huang, C Lubetzki, L Pedraza, D L Sherman, D R Colman and P J Brophy. "An oligodendrocyte cell adhesion molecule at the site of assembly of the paranodal axo-glial junction." The Journal of Cell Biology 150, no. 3 (2000): 657-66.

Tetzlaff, W. "Tight junction contact events and temporary gap junctions in the sciatic nerve fibres of the chicken during Wallerian degeneration and subsequent regeneration." Journal of Neurocytology 11, no. 5 (1982): 839-58.

Thaxton, C, A M Pillai, A L Pribisko, J L Dupree, and M A Bhat. "Nodes of Ranvier act as barriers to restrict invasion of flanking paranodal domains in myelinated axons." Neuron 69, no. 2 (2011): 244-57.

Tokuno, H A, J D Kocsis, and S G Waxman. "Noninactivating, tetrodotoxin-sensitive Na+ conductance in peripheral axons." Muscle &Nerve 28, no. 2 (2003): 212-7.

Tona, A, G Perides, F Rahemtulla, and D Dahl. "Extracellular matrix in regenerating rat sciatic nerve: a comparative study on the localization of laminin, hyaluronic acid, and chondroitin sulfate proteoglycans, including

versican." The Journal of Histochemistry and Cytochemistry 41, no. 4 (1993): 593-9.

Tranum-Jensen, J, M J Janse, W T Fiolet, W J Krieger, C N D'Alnoncourt, and D Durrer. "Tissue osmolality, cell swelling, and reperfusion in acute regional myocardial ischemia in the isolated porcine heart." Circulation Research 49, no. 2 (1981): 364-81.

Trapp, B D. "Myelin-associated glycoprotein. Location and potential functions." Annals of the New York Academy of Sciences 605 (1990): 29-43.

Trapp, B D, and R H Quarles. "Immunocytochemical localization of the myelin-associated glycoprotein. Fact or artifact?" Journal of Neuroimmunology 6, no. 4 (1984): 231-49.

Trapp, B D, S B Andrews, A Wong, M O'Connell, and J W Griffin. "Co-localization of the myelin-associated glycoprotein and the microfilament components, F-actin and spectrin, in Schwann cells of myelinated nerve fibres." Journal of Neurocytology 18, no. 1 (1989): 47-60.

Ulbricht, W. "Effects of veratridine on sodium currents and fluxes." Reviews of Physiology Biochemistry and Pharmacology, Volume 133 (Springer), 1998: 1-54.

Vabnick, I, J S Trimmer, T L Schwarz, S R Levinson, D Risal, and P Shrager. "Dynamic potassium channel distributions during axonal development prevent aberrant firing patterns." The Journal of Neuroscience19, no. 2 (1999): 747-58.

Vabnick, I, S D Novaković, S R Levinson, M Schachner, and P Shrager. "The clustering of axonal sodium channels during development of the peripheral nervous system." The Journal of Neuroscience 16, no. 16 (1996): 4914-22.

Vizoso, A D, and J Z Young. "Internode length and fibre diameter in developing and regenerating nerves." Journal of Anatomy 82, no. Pt 1-2 (1948): 110-134.1.

Vorbrodt, A W, A S Lossinsky, and H M Wisniewski. "Cytochemical localization of ouabain-sensitive, K+-dependent p-nitro-phenylphosphatase (transport ATPase) in the mouse central and peripheral nervous systems." Brain Research 243, no. 2 (1982): 225-34.

Wald, R, B L Jaber, L L Price, A Upadhyay, and N E Madias. "Impact of hospital-associated hyponatremia on selected outcomes." Archives of Internal Medicine 170, no. 3 (2010): 294-302.

Wang, G K, and S-Y Wang. "Veratridine block of rat skeletal muscle Nav1.4 sodium channels in the inner vestibule." The Journal of Physiology 548, no. 3 (2003): 667-675.

Wang, H, D D Kunkel, T M Martin, P A Schwartzkroin, and B L Tempel. "Heteromultimeric K+ channels in terminal and juxtaparanodal regions of neurons." Nature 365, no. 6441 (1993): 75-9.

Waxman, S G. "Sodium channel blockade by antibodies: a new mechanism of neurological disease?" Annals of Neurology 37, no. 4 (1995): 421-3.

Waxman, S G, and D C Quick. "Cytochemical differentiation of the axon membrane in A- and C-fibres." Journal of Neurology, Neurosurgery, and Psychiatry 40, no. 4 (1977): 379-85.

Waxman, S G, and D C Quick. "Intra-axonal ferric ion-ferrocyanide staining of nodes of Ranvier and initial segments in central myelinated fibers." Brain Research 144, no. 1 (1978): 1-10.

Waxman, S G, and J M Ritchie. "Molecular dissection of the myelinated axon." Annals of Neurology 33, no. 2 (1993): 121-36.

Waxman, S G, and M V Bennett. "Relative conduction velocities of small myelinated and non-myelinated fibres in the central nervous system." Nature New Biology 238, no. 85 (1972): 217-9.

Williams, P L, and D Landon. "Paranodal apparatus of peripheral myelinated nerve fibres of mammals." Nature 198 (1963): 670-3.

Williams, P L, and S M Hall. "In vivo observations on mature myelinated nerve fibres of the mouse." Journal of Anatomy 107, no.Pt 1 (1970): 31.

Wilson, G F, and S Y Chiu. "Ion channels in axon and Schwann cell membranes at paranodes of mammalian myelinated fibers studied with patch clamp." The Journal of Neuroscience10, no. 10 (1990): 3263-74.

Wingerchuk, D M, V A Lennon, C F Lucchinetti, S J Pittock, and B G Weinshenker. "The spectrum of neuromyelitis optica." Lancet Neurology 6, no. 9 (2007): 805-15.

Wolswijk, G, and R Balesar. "Changes in the expression and localization of the paranodal protein Caspr on axons in chronic multiple sclerosis." Brain 126, no.Pt 7 (2003): 1638-49.

Wood, P, F Moya, C Eldridge, G Owens, B Ranscht, M Schachner, M Bunge and R Bunge. "Studies of the initiation of myelination by Schwann cells." Annals of the New York Academy of Sciences 605 (1990): 1-14.

Xiao, Z C, D S Ragsdale, J D Malhotra, L N Mattei, P E Braun, M Schachner, L LIsom. "Tenascin-R is a functional modulator of sodium channel beta subunits." The Journal of Biological Chemistry 274, no. 37 (1999): 26511-7.

Yellen, G. "The voltage-gated potassium channels and their relatives." Nature 419 (6902) (2002): 35-42.

Young, E A, C D Fowler, G J Kidd, A Chang, R Rudick, E Fisher and B D Trapp. "Imaging correlates of decreased axonal Na+/K+ ATPase in chronic multiple sclerosis lesions." Annals of Neurology 63, no. 4 (2008): 428-435.

Young, W, J Rosenbluth, J C Wojak, K Sakatani, and H Kim. "Extracellular potassium activity and axonal conduction in spinal cord of the myelin-deficient mutant rat." Experimental Neurology 106, no. 1 (1989): 41-51.

Zhang, X, and V Bennett. "Identification of O-linked N-acetylglucosamine modification of ankyrinG isoforms targeted to nodes of Ranvier." The Journal of Biological Chemistry 271, no. 49 (1996): 31391-8.